



POLITECNICO
MILANO 1863

SCUOLA DI INGEGNERIA INDUSTRIALE
E DELL'INFORMAZIONE

Comparison of Flamelet models for CH₄/O₂ diffusion flame using FINE/Open

TESI DI LAUREA MAGISTRALE IN
SPACE ENGINEERING - INGEGNERIA SPAZIALE

Author: **Alberto Giuseppe Lunghi**

Student ID: 968935

Advisor: Prof. Filippo Maggi

Co-advisors: Andrej Sternin

Academic Year: 2022-23

Abstract

This study presents a comparison of Flamelet models for simulating a methane/oxygen diffusion flame using FINE/Open. Three distinct models were evaluated and compared to DNS results. The first model is the classical adiabatic Flamelet, which employs a tabulation technique for the thermochemical properties as function of a mixing parameter. This technique avoids the need for chemistry integration during run-time, hence decreasing the computational effort. The second model is the Flamelet generated manifold (FGM), typically utilized for partially-premixed combustion, which extends the classical model by incorporating a reactive progress variable. The third is a hybrid technique, which incorporates a reactive progress variable while still utilizing the tabulation approach of the classical Flamelet model. The study found that all three approaches produced consistent and approximately equivalent results. However, the FGM simulation was found to offer a better estimation of species mass fraction fields, as expected due to the inclusion of a further variable that describes the progression of the chemical reaction.

Keywords: Computational Fluid Dynamics, Non-premixed Combustion, Flamelet Model, Flamelet Generated Manifold model, FINE/Open

Abstract in lingua italiana

Questo studio presenta una comparazione di modelli Flamelet per la simulazione di una fiamma diffusiva metano/ossigeno utilizzando FINE/Open. Sono stati valutati e confrontati tre differenti modelli con i risultati DNS. Il primo è il modello Flamelet adiabatico, che utilizza una tecnica di tabulazione per le proprietà termochimiche in funzione di un parametro di mescolamento. Questa tecnica evita la necessità di integrazione delle equazioni di trasporto delle specie chimiche durante la risoluzione del software, riducendo quindi il calcolo computazionale. Il secondo è il modello Flamelet generated manifold (FGM), tipicamente utilizzato per la combustione parzialmente pre-miscelata, che estende il modello classico incorporando una variabile di avanzamento della reazione. Il terzo è una tecnica ibrida, che incorpora una variabile di avanzamento della reazione pur continuando a utilizzare l'approccio di tabulazione del modello Flamelet classico. Lo studio ha riscontrato che tutti e tre gli approcci hanno prodotto risultati coerenti e approssimativamente equivalenti. Tuttavia, la simulazione FGM è risultata offrire una migliore stima dei campi di concentrazione delle specie, come ci si aspetterebbe data l'inclusione di una variabile che descrive la progressione della reazione chimica.

Parole chiave: Fluidodinamica computazionale, Combustione diffusiva, Modello Flamelet, Modello Flamelet Generated Manifold, FINE/Open

Contents

Abstract	i
Abstract in lingua italiana	iii
Contents	v
Introduction	1
1 Literature background	3
1.1 Computational Fluid Dynamics	3
1.2 Turbulence Modeling	5
1.3 Turbulent Combustion	7
1.4 Non-premixed Turbulent Combustion	10
1.4.1 Mixture Fraction Theory	10
1.4.2 Flamelet Model Theory	13
1.4.3 Turbulence-Chemistry Interaction	18
1.5 Partially-premixed Turbulent Combustion	20
1.5.1 Flamelet Generated Manifold Theory	21
2 Mathematical Modeling	23
2.1 k - ϵ Turbulence Model	23
2.2 Flamelet Model Implementation	24
2.2.1 FINE/Open Implementation	26
2.2.2 FLUENT Implementation	27
2.3 FGM Implementation	28
2.4 Hybrid BML/Flamelet Technique	31
2.5 Table Generation - TabGen/Chemistry	32
3 Case Settings	35
3.1 Flamelet Set Up	39

3.2	FGM Set Up	41
3.3	Hybrid BML/Flamelet Set up	43
4	Results and Critical analysis	45
4.1	DNS post-processing	45
4.2	FINE/Open vs FLUENT Flamelet cases	46
4.3	Flamelet results	50
4.4	FGM results	58
4.5	Hybrid results	64
5	Conclusion	67
	Bibliography	69
A	Appendix A	73
B	Appendix B	77
	List of Figures	81
	List of Tables	83
	Acknowledgements	85

Introduction

Motivation

The space industry and research community have shifted their focus towards methane as a potential substitute for hydrogen in liquid rocket engine propulsion systems due to its numerous benefits [7]. Methane is easier and safer to store than hydrogen, which ultimately helps reduce operational costs and also has a positive ecological impact. Additionally, its higher density allows for a more compact stage, thereby providing better containment for the tank volume. Furthermore, methane has better cooling properties for rocket engines due to its higher molar heat capacity compared to hydrogen. However, combustion of CH_4/O_2 at high pressure still remains a field of research, as higher chamber pressure results in improved vehicle performance but also increases heat transfer at the wall. Accurate prediction of the thermal loads during the design phase of a LRE is a critical requirement. To obtain a better understanding of the performance properties of methane, significant efforts are being placed in its experimental characterization and proper modeling of its combustion attributes.

When it comes to designing rocket engines, using experimental methods to measure wall heat loads during firing tests can be quite costly, leading to increased development expenses. To mitigate these costs, there is a need for numerical methods that can accurately describe the combustion and heat transfer processes [13]. However, these methods should not be computationally expensive, as they should allow for fast estimations of performance and heat loads during the early design process. Additionally, using hydrocarbon fuels instead of hydrogen can have an impact on the computational cost required by numerical simulations of turbulent reactive flows. For example, a detailed chemical mechanism for CH_4/O_2 combustion typically involves 53 species and 325 reactions, resulting in a stiff chemical system that is impractical for industrial use due to its high computational cost.

To address the high computational cost of turbulent combustion simulations, efforts have been made to introduce simplified models with fewer equations. One such method is chemistry tabulation, which involves tabulating the thermochemical properties of the reactive flow in advance to remove the chemistry integration step at run-time, thereby accelerat-

ing computation. The assumption of chemical equilibrium is a common method used for the simulation of H₂/O₂ rocket engines due to the high pressure and high temperature combustion environment and fast time-scales of hydrogen combustion [10]. However, it is not valid for hydrocarbon combustion, such as CH₄/O₂, due to the slow time-scales of chemical kinetics that give rise to non-equilibrium effects. To overcome this limitation, the Flamelet model has been widely used in CH₄/O₂ simulations. This model describes the turbulent flame as a collection of laminar flames, called Flamelets, characterized by a mixing parameter and potentially extended to include a reactive progress variable.

Objective

The primary aim of this thesis is to examine the functionality of all the Flamelet models offered in FINE/Open. The purpose of this analysis is to evaluate the quality of non-premixed and partially-premixed combustion models provided by this software. This evaluation is also the foundation of the collaboration between the Space Propulsion Chair of the Technical University of Munich and the software provider NUMECA. The objective of this collaboration is to enhance the software's capabilities by comparing its output with experimental data available to the hosting university. The thesis intends to determine whether the available combustion models are trustworthy or require further development by comparing FINE/Open results with DNS data provided by the university. To provide a more comprehensive overview, another CFD software, FLUENT by Ansys, which is already in use at the institute, is employed. This is done to highlight the differences and benefits of the FINE/Open Flamelet model over FLUENT which is considered a state-of-the-art CFD software.

Thesis outline

The first chapter provides an overview of the theoretical background, starting with the Navier-Stokes equation and continuing with turbulence modeling and turbulence combustion theory. The second chapter details the specific mathematical modeling used in the software, including the turbulence models, Flamelet model implementation, FGM models, and table generation tool. The third chapter discusses the configuration of each computed case, describing the architecture, mathematical models, boundary conditions, numerical parameters, and specific combustion table used. In the fourth chapter a comparison between FINE/Open and FLUENT Flamelet cases with DNS results is given. After that each FINE/Open combustion model's consistency is verified and the outcomes are compared with DNS data. In conclusion an overview of all results and potential model improvements is presented in the last chapter.

1 | Literature background

In the first chapter a complete and synthetic overview of the theoretical background is given. Starting from the general Navier-Stokes equation, the turbulence modeling is described. After that turbulence combustion theory is presented in order to introduce non-premixed and partially-premixed turbulent combustion modeling.

1.1. Computational Fluid Dynamics

In order to solve a fluid mechanics problem utilizing Computational Fluid Dynamics (CFD) it is necessary to portray physical phenomena through suitable models. These models can be expressed as a collection of mathematical equations, which are subsequently solved by softwares. The key objective in selecting the appropriate models is to realistically approximate the physical processes, while minimizing computational requirements to an acceptable degree. In conventional space applications, the characteristic length scales and densities permit the use of the continuum assumption, which enables the characterization of the flow through the Navier-Stokes (NS) equations. The NS equations are a set of coupled nonlinear partial differential equations that accurately describe three-dimensional, compressible and viscous flows. The formulation provided in equation 1.1 is the one given in [16]. In a stationary frame, the integral form of the NS equations in the Euler specification of the flow field can be expressed as follows

$$\frac{\partial}{\partial t} \int_{\Omega} U d\Omega + \int_S \bar{F} \cdot d\bar{S} - \int_S \bar{G} \cdot d\bar{S} = \int_{\Omega} S_T d\Omega \quad (1.1)$$

where Ω is the control volume whose border is represented by the control surface S . The vector of conservative variables U is

$$U = \begin{bmatrix} \rho \\ \rho u \\ \rho v \\ \rho w \\ \rho E \end{bmatrix}$$

where ρ is the density of the fluid, u , v and w are the velocity components and E the total energy per unit volume. The advective \bar{F} and diffusive \bar{G} part of the fluxes are defined as

$$\bar{F} = \begin{bmatrix} \rho u_i \\ \rho w u_i + p \delta_{1i} \\ \rho v u_i + p \delta_{2i} \\ \rho w u_i + p \delta_{3i} \\ (pE + p)u_i \end{bmatrix} \quad \bar{G} = \begin{bmatrix} 0 \\ \tau_{i1} \\ \tau_{i2} \\ \tau_{i3} \\ q_i + u_i \tau_{ij} \end{bmatrix}$$

where τ_{ij} is the stress tensor and q_i is the heat flux vector, typically defined by Fourier's law. In conclusion the source term vector S_T is

$$S_T = \begin{bmatrix} 0 \\ \rho f_{e1} \\ \rho f_{e2} \\ \rho f_{e3} \\ W \end{bmatrix}$$

where \bar{f}_e is the external force vector and W is the work performed by these forces. The system of equations represented by equation 1.1 comprises of five equations, yet it involves seven unknown flow variables, which include pressure, density, temperature, energy, and the three velocity components. Therefore, the system is not closed and requires the implementation of two additional relationships to establish a well-posed problem. For example, the ideal gas equation of state can be considered as an additional relationship, given that the fluid is consistent with ideal assumptions. Another possible option is the use of tables containing thermodynamic properties of the specific fluid examined.

Discretization is a crucial step in solving a CFD problem, as it converts the partial differential equations governing fluid flow into a system of nonlinear algebraic equations. The choice of discretization method can have a significant impact on the efficiency and accuracy of the solution. The three most commonly used methods for discretization in CFD are the Finite Difference Method (FDM), Finite Element Method (FEM), and Finite Volume Method (FVM).

The Navier-Stokes equations are solved in this thesis using FINE/Open, a commercial solver from NUMECA that implements the Finite Volume Method. While various literature sources detail the specifics of the Finite Volume Method, this thesis does not discuss the solution process of the resulting algebraic equations, as it has already been thoroughly covered in [16].

1.2. Turbulence Modeling

The Navier-Stokes equations (NS) can be used to model both laminar and turbulent flow fields. Various models have been developed to effectively simulate turbulent flows, including Direct Numerical Simulation (DNS), Large Eddy Simulation (LES), and Reynolds Averaged Navier-Stokes (RANS).

DNS involves direct calculation of the entire turbulent spectrum, without the need for modeling. However, this approach requires high computational resources, and therefore it is used in simple configurations with small domains.

LES aims to reduce computational cost by separating the turbulent spectrum into large and small scales. Smaller length scales, which are costly to resolve, are ignored via low-pass filtering of the NS equations. The effect of these scales on the flow field is then modeled. While progress is being made in applying LES, it remains computationally expensive for most engineering applications.

RANS is the most widely used approach in industry. The method involves decomposing an instantaneous quantity - such as velocity, pressure, or temperature - into its time-averaged and fluctuating components. The NS equations are then solved only for the time-averaged quantities, and the influence of turbulence is included through modeling the complete turbulence spectrum. This leads to lower computation times, but results are heavily dependent on the chosen turbulence model.

The Reynolds decomposition of an instantaneous variable u_i is expressed as follows

$$u_i = \langle u_i \rangle + u'_i \quad (1.2)$$

where the ensemble-average $\langle u_i \rangle$ is defined in steady state condition as

$$\bar{u}_i = \langle u_i \rangle = \lim_{t \rightarrow \infty} \frac{1}{t} \int_0^t u_i(t') dt' \quad (1.3)$$

and u'_i represents variable fluctuations [23, 25]. Substituting the Reynolds decomposition in NS equations leads to the presence of new terms. In the momentum balance averaged equation a new unknown tensor $\overline{u'_i u'_j}$ is attained.

$$\frac{\partial \bar{u}_i}{\partial t} + \nabla \cdot (\overline{u'_i u'_j}) = -\frac{1}{\rho} \nabla \bar{p} + \frac{1}{\rho} \nabla \cdot \bar{\tau}_{ij} \quad (1.4)$$

It is referred to as the Reynolds stress tensor and it represents fluctuations due to turbu-

lence. To close this system of equations, a suitable turbulence model must be chosen.

The available models for RANS equations closure can be classified into two main categories, Reynolds Stress Models (RSM) and Eddy Viscosity Models (EVM). RSM involve solving a transport equation for the Reynolds stress tensor, which increases computational cost by requiring the solution of at least six additional equations, one per each component of the tensor. RSM is not considered in this thesis due to the lack of availability in the software used.

In the context of EVM, the Reynolds stress tensor is formulated as a viscous stress tensor by retaining the expression for Newtonian fluids. This can be done by considering a similarity between molecular and turbulent processes. Similarly to how the momentum transfer caused by molecular motion in a gas is described through molecular viscosity, the momentum transfer caused by turbulent fluctuations can be modeled through the use of an eddy viscosity ν_t [1]. Therefore, considering the Boussinesq assumption, the Reynolds stress tensor is formulated as

$$\overline{u'_i u'_j} = -2\nu_t S_{ij} + \frac{2}{3}k\delta_{ij} \quad (1.5)$$

where δ_{ij} is the Kronecker function, S_{ij} is the mean rate of the strain tensor defined as $S_{ij} = \frac{1}{2} \left(\frac{\partial \bar{u}_i}{\partial x_j} + \frac{\partial \bar{u}_j}{\partial x_i} \right)$. The last term in equation 1.5 is needed to ensure the right formulation of the turbulent kinetic energy k , which is defined as $k = \frac{1}{2} \langle u'_i u'_i \rangle$.

As a result of this approach, the closure of RANS equations is simplified to the determination of the eddy viscosity, which, unlike the molecular viscosity, is not a characteristic property of the fluid, but rather a feature of the flow field. While this simplification is computationally efficient, it does have the drawback of assuming a proportional relationship between the Reynolds stress tensor and the mean strain rate, potentially resulting in inadequate modeling of anisotropic effects within the flow.

Eddy Viscosity Models can be classified into three categories, namely zero-equation, one-equation, and two-equation models, based on the number of partial differential equations (PDEs) that must be solved in order to calculate the eddy viscosity. In the context of space applications, the most widely employed models are the two-equation models, specifically the $k - \epsilon$ and $k - \omega$ models.

The $k - \epsilon$ model requires the solution of two additional equations, one for the turbulent kinetic energy k and the other for the eddy dissipation rate ϵ . It is based on the assumption that turbulence production and dissipation are in equilibrium. Under the assumption

of isotropic turbulence, the turbulent dynamic viscosity μ_t takes the form of

$$\mu_t = \bar{\rho} C_\mu \frac{k^2}{\epsilon}. \quad (1.6)$$

Considering the Einstein notation and the Favre averaging - which is introduced in the next paragraph - the transport equations for k [Eq.1.7] and ϵ [Eq.1.8] are formulated as follow

$$\frac{\partial \bar{\rho} k}{\partial t} + \frac{\partial}{\partial x_i} (\bar{\rho} \tilde{u}_i k) = \frac{\partial}{\partial x_i} \left[\left(\mu + \frac{\mu_t}{\sigma_k} \right) \frac{\partial k}{\partial x_i} \right] + P_k - \bar{\rho} \epsilon \quad (1.7)$$

$$\frac{\partial \bar{\rho} \epsilon}{\partial t} + \frac{\partial}{\partial x_i} (\bar{\rho} \tilde{u}_i \epsilon) = \frac{\partial}{\partial x_i} \left[\left(\mu + \frac{\mu_t}{\sigma_\epsilon} \right) \frac{\partial \epsilon}{\partial x_i} \right] + C_{\epsilon 1} \frac{\epsilon}{k} P_k - C_{\epsilon 2} \bar{\rho} \frac{\epsilon^2}{k} \quad (1.8)$$

where P_k represents the source term whose formulation is $P_k = -\bar{\rho} \widetilde{u_i'' u_j''} \frac{\partial \tilde{u}_i}{\partial x_j}$. This term connects the mean flow field with the velocity fluctuations, it can be seen as an energy transfer from the mean field to the turbulent kinetic energy. The Reynolds stress tensor $\widetilde{u_i'' u_j''}$ is computed with equation 1.5.

While this model is popular for its simplicity and cost-effectiveness, it does have some known limitations. These include the difficulty in exactly deriving and closing balance equations for k and ϵ without making strong assumptions, such as turbulence isotropy in the boundary layer. This leads to the need for algebraic equations to predict flow fields in the vicinity of walls.

1.3. Turbulent Combustion

Turbulent combustion is a really complex process which is encountered in the majority of rockets combustion chambers. To develop and improve new rocket engines, mathematical modeling of turbulent combustion is crucial. Anyhow the complexity remains also in numerical simulations. A general combustion problem is complicated due to the large range of chemical length and time scales. Moreover, a chemical mechanism can require hundreds of species and thousands of reactions to be fully described. On the other hand, turbulence itself is considered as the most complex phenomenon regarding non-reacting fluid dynamics. Combining these two phenomena leads to a modification of turbulence due to combustion and vice versa.

Fuel and oxidizer must be combined at the molecular level in order to react during combustion. This depends on the turbulent mixing mechanism during turbulent combustion. Once a variety of different-sized vortices have formed, strain and shear at the interface

between eddies improve the mixing. According to the energy cascade of turbulent scales, bigger eddies disrupt, and the smaller eddies that arise inherit their energy [1]. During the process of eddy break-up, strain and shear will rise, amplifying the concentration gradients at the interface between reactants, hence enhancing their molecular interdiffusion. As a requirement for combustion, the molecular mixing of fuel and oxidizer takes place at the interface of tiny eddies.

In order to formulate the problem, balance instantaneous equations for mass, species, momentum and temperature are the starting point [23].

$$\frac{\partial \rho}{\partial t} + \nabla \cdot (\rho \mathbf{u}) = 0 \quad (1.9)$$

$$\rho \frac{\partial (Y_i)}{\partial t} + \rho \mathbf{u} \cdot \nabla T = \nabla \cdot (\rho D_i \nabla Y_i) + \dot{\omega}_i \quad (1.10)$$

$$\frac{\partial (\rho \mathbf{u})}{\partial t} + \nabla \cdot (\rho \mathbf{u} \mathbf{u}) = -\nabla p - \nabla \cdot \underline{\underline{\tau}}} \quad (1.11)$$

$$\rho \frac{\partial (T)}{\partial t} + \rho \mathbf{u} \cdot \nabla T = \nabla \cdot (\rho \alpha_T \nabla T) + \dot{\omega}_T \quad (1.12)$$

These equations are simplified since they are formulated considering equal specific heat capacities and binary diffusivity for all species. Moreover, the pressure is assumed constant.

The species source term $\dot{\omega}_i$ is defined as

$$\dot{\omega}_i = M_i \sum_{j=1}^{N_r} (\nu_{ij}'' - \nu_{ij}') \left[k_{F,j} \prod_{k=1}^K [C_k]^{r_{kj}'} - k_{B,j} \prod_{k=1}^K [C_k]^{r_{kj}''} \right] \quad (1.13)$$

where N_r is the number of reactions considered in the mechanism, ν_{ij}' and ν_{ij}'' are respectively the forward and backward stoichiometric coefficients of species i in reaction j . The forward and backward rate constants $k_{F,j}$ and $k_{B,j}$ are computed with the Arrhenius law.

The temperature source term $\dot{\omega}_T$ is defined as

$$\dot{\omega}_T = -\frac{1}{c_p} \sum_{i=1}^K h_i \dot{\omega}_i \quad (1.14)$$

where h_i is the enthalpy of the i -th species.

In order to consider turbulence an averaging has to be applied to the variables. As a consequence, RANS equations are attained.

In the case of constant density flows, Reynolds averaging is applied. Substituting this formulation in the instantaneous balance equations introduces correlation terms which require modeling. For example, correlations between density fluctuations and other quantities are introduced in case of variable density flows. Therefore, using the Reynolds average for reactive flow is not clever. Due to the presence of large density gradients, mass-weighted Favre average is usually preferred [23]. The decomposition is formulated as follows

$$u = \tilde{u} + u'', \quad (1.15)$$

$$\tilde{u} = \frac{\overline{\rho u}}{\bar{\rho}} \quad (1.16)$$

where u'' represents fluctuations with respect to density averaged mean flow. Once the averaging is applied, the Favre averaged Navier-Stokes equations are computed. Their formulation is formally identical to RANS equations for incompressible flows.

$$\frac{\partial \bar{\rho}}{\partial t} + \nabla \cdot (\bar{\rho} \tilde{\mathbf{u}}) = 0 \quad (1.17)$$

$$\frac{\partial (\bar{\rho} \tilde{\mathbf{u}})}{\partial t} + \nabla \cdot (\bar{\rho} \tilde{\mathbf{u}} \tilde{\mathbf{u}}) = -\nabla \bar{p} - \nabla \cdot \underline{\underline{\tau}} - \nabla \cdot (\bar{\rho} \widetilde{\mathbf{u}'' \mathbf{u}''}) \quad (1.18)$$

$$\bar{\rho} \frac{\partial \tilde{Y}_l}{\partial t} + \bar{\rho} \tilde{\mathbf{u}} \cdot \nabla \tilde{Y}_l = \nabla \cdot (\overline{\rho D_l \nabla Y_l}) - \nabla \cdot (\bar{\rho} \widetilde{\mathbf{u}'' Y_l''}) + \bar{\omega}_l \quad (1.19)$$

$$\bar{\rho} \frac{\partial \tilde{T}}{\partial t} + \bar{\rho} \tilde{\mathbf{u}} \cdot \nabla \tilde{T} = \nabla \cdot (\overline{\rho \alpha_T \nabla T}) - \nabla \cdot (\bar{\rho} \widetilde{\mathbf{u}'' T''}) + \bar{\omega}_T \quad (1.20)$$

The system of equations is not closed since there are many unknown terms due to the averaging process. Therefore it is necessary to use specific mathematical models for each of these terms. The first term taken in consideration is the Reynolds stress tensor $\widetilde{\mathbf{u}'' \mathbf{u}''}$; its closure is a consequence of the turbulence model applied, i.e. 1-equation, 2-equation or RSM.

Other terms that need closure are laminar diffusive fluxes for species and temperature, which in first approximation can be neglected for highly turbulent conditions. Anyway their contribution in the vicinity of the walls is retained and it is usually modeled as follows [25]

$$\overline{\rho D_i \nabla Y_i} \approx \bar{\rho} \overline{D_i \nabla Y_i} \quad (1.21)$$

$$\overline{\rho\alpha_T\nabla T} \approx \frac{\tilde{\lambda}}{c_p}\nabla\tilde{T}. \quad (1.22)$$

Species and temperature turbulent fluxes also need to be modeled. They are usually closed with a first order assumption which consists in using a classical gradient method

$$\overline{\rho\mathbf{u}''\widetilde{Y_i''}} \approx -\frac{\mu_t}{Sc_t}\nabla\tilde{Y}_i \quad (1.23)$$

$$\overline{\rho\mathbf{u}''\widetilde{T''}} \approx -\frac{\mu_t}{Pr_t}\nabla\tilde{T}_i \quad (1.24)$$

where μ_t is the turbulent viscosity retrieved from the turbulence model considered. Moreover turbulent Schmidt number Sc_t and turbulent Prandtl number Pr_t are respectively defined as $Sc_t = \frac{\mu_t}{\bar{\rho}D_t}$ and $Pr_t = \frac{\mu_t c_p}{\lambda_t}$.

1.4. Non-premixed Turbulent Combustion

Most of bipropellants rocket engines have separate injection for fuel and oxidizer. Once they enter in the combustion chamber they need to mix before they can start burning. This kind of combustion is called non-premixed or diffusive. Once the mixing attained is at molecular level, the chemical combustion reaction can take place between the reactants. A possible solution to consider the combustion process is to use a finite-rate chemistry model, which has the drawback of an high computational time depending on the mechanism considered.

In order to reduce the overall computational time it is possible to simplify the problem by considering that the mixing of the reactants defines the combustion time scale. Therefore the problem is reduced to the mixing of the reactants only. To be consistent with this simplification it must be assumed that the chemistry time scale is much lower than the convection and diffusion time scales.

1.4.1. Mixture Fraction Theory

It is useful to introduce a conserved scalar quantity, named mixture fraction Z , when considering non-premixed combustion. The temperature of the gas, as well as the source terms and species mass fraction, can be expressed as function of Z if the mixture fraction is introduced. By doing so, the combustion problem - computation of $T(x, t)$ and $Y_i(x, t)$ - can be reduced to determining the mixture fraction distribution in the reaction zone $Z = Z(x, t)$. Afterward it is possible to calculate the temperature and species concentrations

as $T(x, t) = T(Z(x, t))$ and $Y_i(x, t) = Y_i(Z(x, t))$.

There are different definitions in literature [23, 25] for mixture fraction, typically it is formulated as the local ratio of the mass flux generating from the fuel feed to the sum of both mass fluxes. Thus, its value is zero at the oxidizer inlet and one at the fuel inlet.

$$Z = \frac{\dot{m}_{fu}}{\dot{m}_{fu} + \dot{m}_{ox}} \quad (1.25)$$

Another possible definition is based on elemental mass fraction Z_i . Assuming also that all species have the same diffusion coefficient, the mixture fraction is identical for all elements and it is defined as

$$Z = \frac{Z_i - Z_{i,ox}}{Z_{i,fu} - Z_{i,ox}} \quad (1.26)$$

where $Z_{i,ox}$ and $Z_{i,fu}$ are related respectively to the oxidizer and fuel inlet. These formulations are applicable when the engine configuration comprises only two separate inlet streams, one for the fuel and one for the oxidizer. In case of hydrocarbons combustion it can be useful to consider the formulation given by Bilger in [5].

The species equations can be simplified to a single equation for the mixture fraction under the assumption of equal diffusivities $D_i = D$. The reaction source terms in the species equations cancel out - elements are conserved in chemical reactions - hence Z is a conserved quantity. The conservation equation for the mixing fraction is

$$\frac{\partial \rho Z}{\partial t} + \frac{\partial}{\partial x_j} (\rho u_j Z) = \frac{\partial}{\partial x_j} \left(\rho D \frac{\partial Z}{\partial x_j} \right). \quad (1.27)$$

Whereas the assumption of equal diffusivities is controversial for laminar flows, it is often acceptable for turbulent flows in which turbulent convection predominates over molecular diffusion. Considering the Favre averaged formulation, the mixture fraction transport equation is defined as [25]

$$\frac{\partial}{\partial t} (\bar{\rho} \tilde{Z}) + \frac{\partial \bar{\rho} \tilde{u}_j \tilde{Z}}{\partial x_j} = \frac{\partial}{\partial x_j} \left(\overline{\rho D \frac{\partial Z}{\partial x_j}} - \bar{\rho} \tilde{u}_j'' \tilde{Z}'' \right). \quad (1.28)$$

To account for the turbulence-chemistry interaction, it is necessary to determine the mixture fraction variance $\widetilde{Z''^2}$. In RANS solvers a transport equation for the mixture fraction variance is typically solved. If the reader is interested in the precise derivation of

the transport equation he can refer to section 5.3.7 of [25]. The equation is defined as

$$\begin{aligned} \frac{\partial \overline{\rho Z''^2}}{\partial t} + \frac{\partial}{\partial x_j} \left(\overline{\rho \tilde{u}_j Z''^2} \right) = & - \frac{\partial}{\partial x_j} \left(\overline{\rho u_j'' Z''^2} \right) + \frac{\partial}{\partial x_j} \left(\overline{\rho D \frac{\partial Z''^2}{\partial x_j}} \right) \\ & + 2 \overline{Z'' \frac{\partial}{\partial x_j} \left(\rho D \frac{\partial \tilde{Z}}{\partial x_j} \right)} - 2 \overline{\rho u_j'' Z''} \frac{\partial \tilde{Z}}{\partial x_j} - 2 \overline{\rho D \frac{\partial Z''}{\partial x_j} \frac{\partial Z''}{\partial x_j}} \end{aligned} \quad (1.29)$$

where the first term of the RHS represents transport due to turbulence and it is usually modeled with the gradient assumption. Molecular diffusion, expressed by the second and third term, is typically neglected. The fourth term illustrates the production of scalar fluctuations caused by a gradient in the mean mixture fraction field and it is commonly modeled with the gradient assumption. The fifth term represents the decay of the mixture fraction variance. It is directly proportional to the scalar dissipation rate $\tilde{\chi}_p$ of the fluctuations of the mixture fraction field. Its Favre-averaged expression is generally defined as

$$\tilde{\chi}_p = 2D \overline{\frac{\partial Z''}{\partial x_j} \frac{\partial Z''}{\partial x_j}} \quad (1.30)$$

where the fluctuations of mixture fraction field are considered. The connection between the total mixture fraction Z and its fluctuations Z'' with the global scalar dissipation rate $\tilde{\chi}$ can be found in section 6.4.3 of [25]. This quantity serves the same purpose for the mixture fraction as the dissipation rate of kinetic energy does for the velocity field. This reasoning is frequently used to model this factor as function of turbulent time scale τ_t , whose formulation is strictly related to the turbulence model used.

$$\frac{\overline{Z''^2}}{\tilde{\chi}_p} = \frac{1}{c} \tau_t \quad (1.31)$$

As mentioned previously in this chapter, considering the conservation equations for the mixture fraction and its variance simplify considerably the resolution of non-premixed turbulent flames. Infact, enthalpy and mass fraction conservation equations do not need to be solved and reaction rates do not require additional modeling. The so-called Flamelet model, which is described in the next section, consists in solving mixture fraction transport equation in conjunction with pre-computed and tabulated mass fraction and temperature fields.

1.4.2. Flamelet Model Theory

The Flamelet model, utilized in this thesis, is a unique approach for non-premixed turbulent combustion. It provides a distinctive model that integrates finite rate and non-equilibrium phenomena without solving the computationally costly equations for the mass fraction of the chemical species and the enthalpy [18]. The theory extends the traditional Burke-Schumann model by including non-equilibrium factors [23]. Flow-induced non-equilibrium effects are incorporated into the Flamelet model by the scalar dissipation rate. These non-equilibrium effects are particularly significant when examining the concentrations of minor species, particularly where pollutant production (NO_x , CO, UHC, etc.) is of importance.

The assumption of lower chemical time scales than the turbulence ones is fundamental for the validity of the Flamelet model. This correlates to extremely high values of the Damkohler number Da , which is defined as the ratio of chemical τ_c to turbulent macroscopic time scales τ_t , $Da = \frac{\tau_t}{\tau_c}$. If this assumption is true, then the thickness of the reaction zone is less than the size of the smallest vortex in the flow field, which is in the order of the Kolmogorov length scale [23]. This indicates that the vortices are incapable of entering the reaction zone and extinguishing the flame. In conclusion the flame - laminar or turbulent - may be seen as an ensemble of Flamelets immersed in the flow field and susceptible to flow-induced strain.

These laminar Flamelets can be computed as idealized counter-flow diffusion flames in which fuel and oxidizer are introduced by two opposing nozzles, therefore the flame is placed between the jets as shown in figure 1.1. In this case the computation is performed in the physical space. Moreover it is also possible to use another approach which consists in solving Flamelet equations in the mixture fraction space. Both approaches will be described in the following subsections.

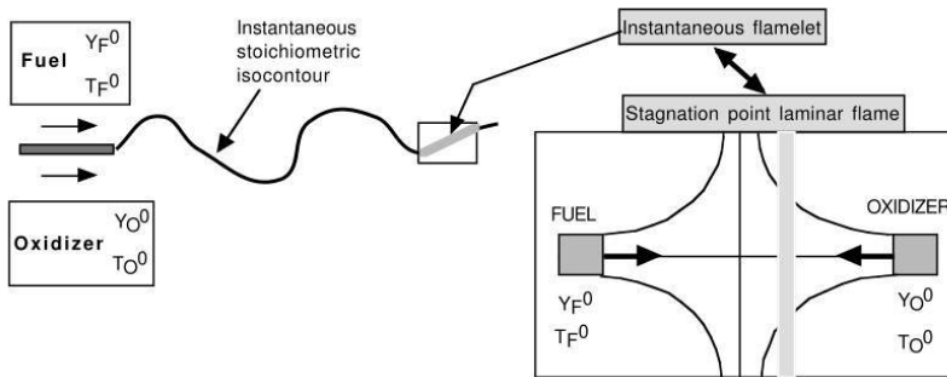


Figure 1.1: Flamelet approach for non-premixed turbulent flames [25].

Counter-flow Diffusion Flame

Counterflow diffusion flames are a form of stagnation flows in which the oxidizer and fuel inlets are opposite one another. Due to inlets configuration, the two streams slow down until a stagnation plane is achieved. This stagnation plane's location is determined by the density and the velocity of the two fluids. The interactions between the fuel and oxidizer produce a stationary flame which is situated where the mixture ratio has its stoichiometric value, i.e. where $Z = Z_{st}$. However, its location does not always coincide with the stagnation plane, as it is shown in Fig.1.2.

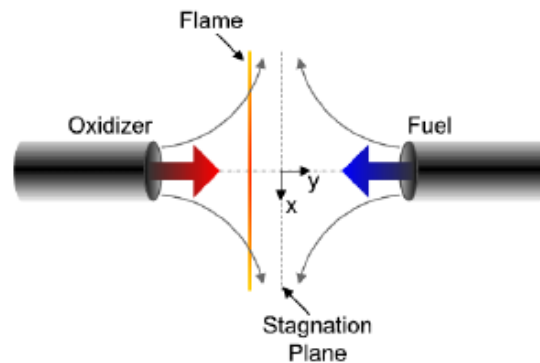


Figure 1.2: Counter-flow diffusion flame configuration.

In the majority of ordinary rocket fuel combinations, the stoichiometric O/F is more than 1, hence $Z_{st} < 0.5$. As a direct consequence, the flame is closer to the oxidizer entrance. Another crucial position is the one with the highest temperature. This position is analogous to the stoichiometric point for quasi-equilibrium flames. When a non-equilibrium flame is investigated, the point of maximum temperature slightly deviates from the position where $Z = Z_{st}$.

Counterflow diffusion flames have the primary advantage of reducing the complicated 3D flow issue to a series of 1D equations that precisely describe the phenomenon. This significantly reduces the processing effort and allows to consider complex reaction processes that would be prohibitively expensive in 2D or 3D simulations. The degree of non-equilibrium is represented by the strain rate a , which represents the time scale¹ of the problem [11, 23].

A comprehensive chemistry program may simulate this setup as a quasi-1D diffusion

¹Various definitions exist for a , such as the maximum or average velocity gradient, the average velocity gradient at the stoichiometric point, or the velocity gradient in the oxidizer-rich side assuming potential flow [23]. However, studies have indicated that these definitions are similar to each other [9].

flame. The simulation consists in the resolution of the conservation equations for mass, momentum, energy and species. A look-up table can be created by tabulating the thermochemical characteristics along the centerline from the oxidizer inlet to the fuel inlet in relation to the mixture fraction.

By modeling counter-diffusion flames for a range of various strain rates, the thermochemical characteristics may be tabulated also as function of the strain rate a . Considering that thermochemical properties naturally depend also on the mixture fraction, tables can be described by the following expressions

$$T = T(Z(x, t), a), Y_i = Y_i(Z(x, t), a). \quad (1.32)$$

By altering the velocity of the fuel/oxidizer streams while maintaining the spacing between the nozzles, the strain in the simulated Flamelets can be modified. As stated previously, the scalar dissipation rate characterizes the influence of the flow field on the flame-structure. It can be shown that the scalar dissipation rate is proportional to the strain rate; for counter-flow diffusion flames in which the oxidizer and fuel streams are far enough apart to assume a potential flow condition, the scalar dissipation rate can be computed, knowing the strain rate, via a power law [25]

$$a = \pi\chi(Z) \left(\exp \left(-2 \left(\operatorname{erfc}^{-1} (2Z) \right)^2 \right) \right)^{-1}. \quad (1.33)$$

Since the strain rate is constant for each individual Flamelet, it is ideal for characterizing different non-equilibrium conditions in a library. As a matter of fact, scalar dissipation rate changes with mixture fraction within a given Flamelet and therefore it is not constant. After calculating the scalar dissipation rate, the local value for the mixture fraction and the strain rate - derived from the scalar dissipation rate - are used to look up the Flamelet tables.

Flamelet equations

The Flamelet equations were formulated by Peters [23],[21] and describe the behavior of the chemical species and temperature or enthalpy in a one-dimensional flame structure. To derive these equations, Peters introduced a coordinate system attached to the Flamelet structure and replaced the spatial coordinate with the mixture fraction². This approach strongly simplifies the equations, as only the gradients perpendicular to the iso-surface of

²The replacement of spatial coordinates with mixture fraction is performed following the Crocco-type transformation.

the mixture fraction are significant, while the gradients on the iso-surface can be ignored. The Flamelet equations assume a unity Lewis number for all chemical species and can be expressed as follows:

$$\frac{\partial Y_k}{\partial t} = \frac{\chi}{2} \frac{\partial^2 Y_k}{\partial Z^2} + \frac{\dot{m}_k}{\rho} \quad (1.34)$$

$$\frac{\partial T}{\partial t} = \frac{\chi}{2} \frac{\partial^2 T}{\partial Z^2} - \frac{1}{\rho c_p} \sum_{k=1}^N \dot{m}_k h_k \quad (1.35)$$

where Y_k , \dot{m}_k and h_k respectively represents the mass fraction, mass source rate and specific enthalpy of species k . Many formulations exist for the temperature Flamelet equation, the one reported in equation 1.35 is derived in [22].

The unity Lewis number assumption is a key hypothesis in the Flamelet approach to attain Flamelet equations and to coherently define the mixture fraction. While this assumption is valid for hydrocarbon combustion due to the proximity to unity Lewis number of the main species involved [25], it can lead to inaccuracies for hydrogen combustion, which has a lower Lewis number. To address this issue, different models have been developed in the past. A typical formulation considering differential diffusion effects was developed by Pitsch and Peters in [24], where new passive scalar variables were introduced for every species with a non-unity Lewis number.

Also in this case, the scalar dissipation rate χ is a measure of the deviation of the local flame structure from chemical equilibrium, and represents the diffusion time scale. Values of scalar dissipation rate close to zero correspond to the equilibrium solution, while higher values result in a larger deviation from equilibrium. This parameter is crucial in the description of non-premixed turbulent combustion and can also indicate the extinction limit of the flame. When the scalar dissipation rate reaches the critical value of χ_q , non-equilibrium effects become dominant and the flame extinguishes. Many formulations for the scalar dissipation rate profile exist, but a typical one is given by the parametric distribution in equation 1.36, proposed by Peters in [23].

$$\chi(Z) = \chi_{st} \exp \left[2 \left(\operatorname{erfc}^{-1} (2Z_{st}) \right)^2 - 2 \left(\operatorname{erfc}^{-1} (2Z) \right)^2 \right] \quad (1.36)$$

The subscript st represents stoichiometry conditions and erfc^{-1} is the inverse of the complementary error function. The boundary value problem described by equations 1.34 and 1.35 can be solved for steady-state conditions for various values of χ_{st} . The solution yields a table of temperature and species mass fractions for the laminar Flamelets, given by

$$T, Y_k = f(Z, \chi_{st}). \quad (1.37)$$

Non-Adiabatic Extension of the Flamelet Model

The Flamelet equations and the governing equations of the counterflow diffusion flame are both adiabatic, meaning that the resulting profiles for species mass fractions and temperature correspond to a specific adiabatic enthalpy profile. Considering the assumption of unity Lewis number, the profile can be formulated as

$$h_{ad}(Z) = h_{ox} + Z(h_{fu} - h_{ox}). \quad (1.38)$$

Hence, it is represented as a linear function between the boundary enthalpy levels of fuel and oxidizer. In practical engineering applications, the flow usually exchanges heat with its surroundings, resulting in non-adiabatic conditions. To address this, the adiabatic Flamelet model is often extended to the concept of a "frozen" Flamelet, where species concentrations are assumed to be constant and equal to their values at adiabatic conditions for all enthalpy levels. This assumes that the change in enthalpy does not affect the reaction chain in the chemical mechanism and does not alter the gas composition. Therefore the only effect of non-adiabatic enthalpy is to change temperature, transport and thermodynamic properties to ensure thermochemical consistency. The mathematical tabulation can be defined as

$$Y_k = f(Z, \chi_{st}, h) = f(Z, \chi_{st}, h_{ad}), \quad (1.39)$$

$$T = f(Z, \chi_{st}, h \neq h_{ad}). \quad (1.40)$$

Typically thrust chamber's walls are cooled to prevent overheating and damage. This introduces a lower enthalpy environment that can cause an increase in recombination reactions, which is not captured by the traditional adiabatic Flamelet model. Therefore, extensions of the Flamelet model to non-adiabatic calculations were developed to accurately describe the heat flux in the wall.

Many different approaches were developed in the past in order to model non-adiabatic effects:

- Reduction by a constant factor of the chemical heat source term in the energy equation of the counterflow diffusion flame. [26]
- Modification of the thermal boundary conditions for the counterflow diffusion flame in the form of a permeable wall. [32]
- Introduction of a convective heat loss term in the unsteady Flamelet equations by

means of a Nusselt-number correlation. [12]

- Adjusting fuel and oxidizer boundaries for radiative losses. [14]
- Introduction of a source term in the temperature equation of the counterflow diffusion flame. [19]
- Replacement of the temperature Flamelet equation with an imposed enthalpy profile as an equality constraint. [19]

The articles cited in the previous list provide detailed information about each approach for non-adiabatic Flamelet model.

1.4.3. Turbulence-Chemistry Interaction

In the vast majority of technical applications involving combustion processes, the combustion flow is turbulent. In turbulent flows spatial and temporal fluctuations in the temperature and concentrations fields are a consequence of a cascade of vortices.

Due to the extremely nonlinear nature of combustion, simple linear averaging of fluctuating variables in the numerical model would result in significant modeling inaccuracy. Given the nonlinear relationship between thermochemical characteristics and mixture fraction, a straight lookup of these values in the combustion tables using the Favre-Reynolds average of the mixture fraction variable is not correct.

Probability density functions (PDF) are employed to account for scalar fluctuations in turbulent flow as well as for the nonlinear relationship between scalars and the mixture fraction. In general, a probability density function $P(Z)$ for the mixture fraction variable describes the possibility that, at a given position, the flow field takes on a particular mixture fraction value. The fluctuating behavior of Z is represented on the right side of figure 1.3. A specific value of Z spends a certain amount of time in a range ΔZ . The PDF - left part of figure 1.3 - is constructed such that the area under its curve in the band ΔZ equals the fraction of time that Z spends in the range ΔZ . The PDF depends on the characteristics of the turbulent fluctuations in Z . However, in practice, the actual PDF is unknown and it is usually approximated by a mathematical function that models experimental PDF shapes.

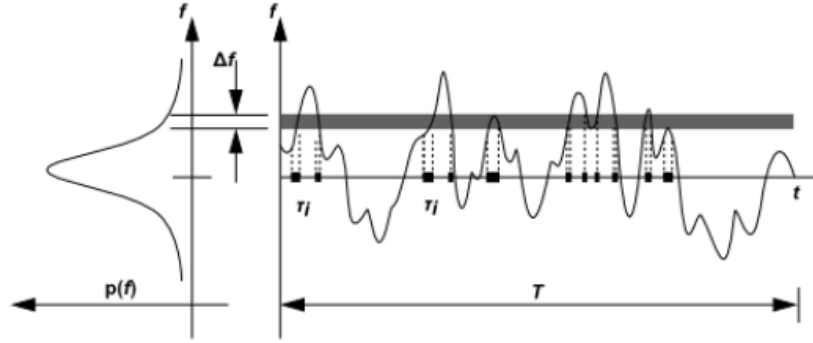


Figure 1.3: Graphical description of the PDF [3].

Since look-up tables [Eq.1.32] depend only on the scalar dissipation rate - through the strain rate [Eq.1.33] - and on the mixture fraction, both their statistical distribution should be considered to calculate the statistical moments of reactive scalars. Therefore a joint Favre PDF $\tilde{P}(Z, \chi)$ is theoretically required. The integration is defined as follows

$$\tilde{\phi} = \int_0^1 \int_0^\infty \phi(Z, \chi) \tilde{P}(Z, \chi) d\chi dZ. \quad (1.41)$$

However, assuming statistical independence between Z and χ and that the fluctuations of the scalar dissipation rate are negligible [2], the only PDF required is the one for the mixture fraction. By solving PDF transport equations, one may obtain the explicit probability density function. This approach employs stochastic methods and is quite computationally intensive. A more computationally efficient PDF-based technique is usually implemented, namely the presumed PDF approach. As the method's name implies, the PDF shape is assumed and the distribution is parameterized using statistical moments of the independent variable. Hence, the probability density function is also a function of the variance $P(Z, Z''^2)$. In this case, the mathematical function representing the PDF is assumed to be a β -functions. The β probability density function is formulated as follows

$$\tilde{P}(Z) = \frac{Z^{\alpha-1} (1-Z)^{\beta-1}}{\Gamma(\alpha)\Gamma(\beta)} \Gamma(\alpha + \beta) \quad (1.42)$$

where

$$\alpha = \tilde{Z}\gamma, \quad \beta = (1 - \tilde{Z})\gamma, \quad \gamma = \frac{\tilde{Z}(1 - \tilde{Z})}{\widetilde{Z''^2}} \quad \text{and} \quad \Gamma(x) = \int_0^{+\infty} e^{-t} t^{x-1} dt.$$

The advantage of the β -PDF is that it can display bimodal behavior for high variations. This indicates that the function can explain the coexistence of fuel and oxidizer in turbulent flows. For intermediate values of the variance, the function resembles a Gaussian distribution, whereas it represents a Dirac function at the limits of vanishing variance. A drawback is the incapability of describing distributions with a singularity at $Z = 0$ or $Z = 1$ with an addition intermediate maximum in the range $0 < Z < 1$ [23]. To overcome this limitation a composite model was developed in [8] thanks experimental observation in jets and shear layers. As this model is not implemented in FINE/Open, the explanation is not provided in this thesis.

Once such a function is determined, it is possible to compute the Favre-averaged thermochemical states. By integrating the state-functions with the probability density function throughout the whole physical range of the mixture fraction, the Favre-averaged temperature and mass fractions can be computed as:

$$\tilde{T}(\tilde{Z}, \widetilde{Z'^2}, \tilde{\chi}) \approx \int_0^1 T(Z, \tilde{\chi}) \tilde{P}(Z) dZ \quad (1.43)$$

$$\tilde{Y}_i(\tilde{Z}, \widetilde{Z'^2}, \tilde{\chi}) \approx \int_0^1 Y_i(Z, \tilde{\chi}) \tilde{P}(Z) dZ \quad (1.44)$$

where the Favre-averaged scalar dissipation rate is calculated as

$$\tilde{\chi} = \int_0^1 \chi(Z) \tilde{P}(Z) dZ. \quad (1.45)$$

1.5. Partially-premixed Turbulent Combustion

The combination of the mixture fraction modeling approach and Flamelet tables is well-known for its accuracy and reliability in the simulation of diffusion flames. The primary advantage of this approach is the efficiency that it provides. The flame-structure is calculated in a preprocessing step, thereby enabling the chemistry calculations to be performed outside the flow solver. Despite this advantage, the method is limited to the simulation of non-premixed flows, due to the assumption of fast chemistry that is only partially relieved by accounting for the effect of strain. In order to comprehend both non-premixed and premixed conditions in a combustion simulation, other methods and approaches might need to be considered as well.

The concept of Flamelet Generated Manifolds (FGM) was initially developed for the simulation of steady, adiabatic, and freely propagating premixed flames. However, subsequent efforts have aimed to integrate the premixed and diffusion Flamelet theories. In practical combustion scenarios, the reactants are not always perfectly premixed or completely separated prior to ignition. Hence, premixed and non-premixed flames can be seen as the two extreme cases of a broad range of flame structures. To attain an accurate representation of combustion chemistry in turbulent flame simulations, it is crucial to choose the appropriate Flamelet type as the basis for the FGM table, consistently resembling the flame characteristics.

1.5.1. Flamelet Generated Manifold Theory

Considering an isobaric reactive system, the physical state is composed by $N_s + 1$ quantities, including the variables Y_i and T . The chemical manifold represents a lower-dimensional subset of this space. As the dimensionality of the manifold increases, it becomes capable of accessing a larger portion of the full composition space. Theoretically, the dimensionality of the manifold can be expanded up to $N_s + 1$ dimensions, resulting in the full recovery of the composition space [27]. However, expanding the amplitude of a database also requires the solution of more differential equations and the implementation of a more complicated look-up procedure, leading to a reduced improvement in computational efficiency.

Defining multiple control variables to parameterize a combustion chemistry table is not a simple task in practice. The ideal control variables should be independent of one another and produce single-valued functions for all dependent variables. When control variables are not fully independent, it is necessary for subsequent control variables to have a monotonous relationship when conditioned on the previous control variables. The FGM model allows for user-defined control variables, which are projected onto the manifold. This is a practical approach as it provides a straightforward physical interpretation of the control variables, which remains identical throughout the manifold.

However, the utilization of fixed control variables can lead to inaccuracies in representing certain subspaces of the manifold. This may happen, for instance, when the control variables remain quasi-constant while the dependent variables exhibit significant changes, or when the control variables do not provide a unique representation of the manifold. The Generalized Coordinates method was introduced to overcome the limitations of fixed control variables in parametrizing a combustion chemistry table [4]. This method adapts the parametrization locally to follow the chemical manifold.

Anyhow instead of the Generalized Coordinates method, the conventional approach, enclosing user-defined control variables, is typically used. The reason for this choice is due to the difficulty in combining the Generalized Coordinates method with the FGM model. Moreover, the loss of the physical meaning of control variables with the use of Generalized Coordinates is disadvantageous. In the case of partially-premixed combustion, two control variables are necessary: the first describes the mixing of fuel and oxidizer and the second represents the progression of chemical reaction. The former is the mixture fraction Z whose theory has been widely explained in section 1.4.1. The latter is the reaction progress variable Y [6] and it is used to quantify the transition from unburnt mixture to chemical equilibrium. This variable must be monotonous from the initial state to chemical equilibrium in both lean and rich regions in order to clearly map the dependent variables. In the next section a brief overview of progress variable theory is provided.

Progress Variable Theory

A linear combination of species mass fractions can serve as the reaction progress variable Y , as it has the desired properties for the transition from unburnt to chemical equilibrium mixture. This linear combination should have a direct connection to the formation of reaction products and be monotonous in both lean and rich regions. Therefore it can be defined as

$$Y = \sum_{i=1}^N \frac{Y_i}{M_i} \quad (1.46)$$

where Y_i represents the mass fraction of the species i and M_i the molar mass of species i . The selection of which species to consider in the summation depends on the atoms contained in the fluid streams. For example, taking into account a methane-air flame, the species usually selected are CO_2 , H_2O and H_2 which ensure the required behavior inside flammability limits.

At this stage Flamelet solutions are computed as function of Z and Y by defining $\phi = \phi(Z, Y)$, where ϕ can be any thermochemical variable. This approach has been already demonstrated to be functioning [31]. Although a two-dimensional space already requires a lot of computer memory, increasing the resolution and dimensionality of the FGM tables can improve accuracy of the solution. Non-adiabatic effects, such as radiative heat transfer or flame stabilization, may not be captured by this parametrization and an additional control variable, is needed to include these effects [30].

2 | Mathematical Modeling

In the second chapter the specific mathematical modeling implemented in the softwares used are reported. The aim of the thesis is to analyse the quality of FINE/Open regarding Flamelet model computations. In order to have another term of comparison, also the Flamelet model implemented in FLUENT is used. The first section is focused on the turbulence models utilized in both softwares. The second section describes the Flamelet model implementation in FINE/Open, highlighting also the differences with respect to FLUENT. The third and fourth sections illustrate the FGM models available on FINE/Open. In the last section an overview of the table generation tool of FINE/Open is given.

2.1. k - ϵ Turbulence Model

The aim of this section is to describe and compare the k - ϵ turbulence model in FINE/Open and Fluent. Firstly, the differences between the software will be highlighted, i.e. how the model is mathematically modelled. It will be shown that the same model contains different definitions within the transport equations depending on the software. Since the thesis is focused on the analysis of FINE/Open, the transport equations of this software only will be reported, highlighting the differences with respect to FLUENT.

The standard k - ϵ transport equations formulated in FINE/Open are

$$\frac{\partial \rho k}{\partial t} + \nabla \cdot \left(\rho \vec{v} k - \left(\mu + \frac{\mu_t}{\sigma_k} \nabla k \right) \right) = P - \rho \frac{k}{T} \quad (2.1)$$

$$\frac{\partial \rho \epsilon}{\partial t} + \nabla \cdot \left(\rho \vec{v} \epsilon - \left(\mu + \frac{\mu_t}{\sigma_\epsilon} \right) \nabla \epsilon \right) = \frac{1}{T} (C_{\epsilon 1} P - C_{\epsilon 2} \rho \epsilon) + E + \rho S_\epsilon. \quad (2.2)$$

In FINE/Open both the transport equations do not include the effects of buoyancy and the possibility of setting an user-defined source with respect to FLUENT. Moreover, in the k equation it is not considered the contribution of the fluctuating dilatation in compressible turbulence. This term is related to the decrease in spreading rate with

increasing Mach number for compressible mixing. Furthermore, the destruction term in FLUENT is proportional to the dissipation rate ϵ , while in FINE/Open it is proportional to $\frac{k}{T}$, where T [Eq.2.6] is defined differently from the typical turbulent time scale. On the other hand, the ϵ equation includes two terms related to the specific standard FINE/Open formulation: the Yang-Shih term E and the Yap correction term ρS_ϵ .

$$E = \nu \mu_t (\vec{\nabla} \cdot \vec{S})^2 \quad (2.3)$$

$$\rho S_\epsilon = 0.83 \rho \frac{\epsilon}{T} \left(\frac{\sqrt{k} T}{0.41 y C_\mu^{-0.75}} - 1 \right) \left(\frac{\sqrt{k} T}{0.41 y C_\mu^{-0.75}} \right)^2. \quad (2.4)$$

Regarding the eddy viscosity definition, in FLUENT it is defined as $\mu_t = \rho C_\mu \frac{k^2}{\epsilon}$ while in FINE/Open it is defined as $\mu_t = \rho C_\mu f_\mu k T$, where f_μ is a damping function depending on the Reynolds number based upon the distance to the wall.

$$f_\mu = \sqrt{1 - \exp(-c_1 Re_y - c_2 Re_y^3 - c_3 Re_y^5)}, Re_y = \frac{\rho \sqrt{k} y}{\mu} \quad (2.5)$$

$$T = \frac{k}{\epsilon} + \left(\frac{\nu}{\epsilon} \right)^{0.5} \quad (2.6)$$

The model constants have the same default values in both the softwares, $C_\mu = 0.09$, $C_{\epsilon 1} = 1.44$, $C_{\epsilon 2} = 1.92$, $\sigma_k = 1.0$ and $\sigma_\epsilon = 1.3$. All the other quantities needed to define the terms in FINE/Open can be found in section 3.1.3 of [16].

2.2. Flamelet Model Implementation

The aim of this section is to present how the Flamelet model is combined with RANS solvers and in particular with FINE/Open. Firstly, the theoretical functioning of a RANS solver combined with the Flamelet approach is presented [Fig.2.1], then the specific steps in FINE/Open are reported. In conclusion the differences with respect to FLUENT are highlighted.

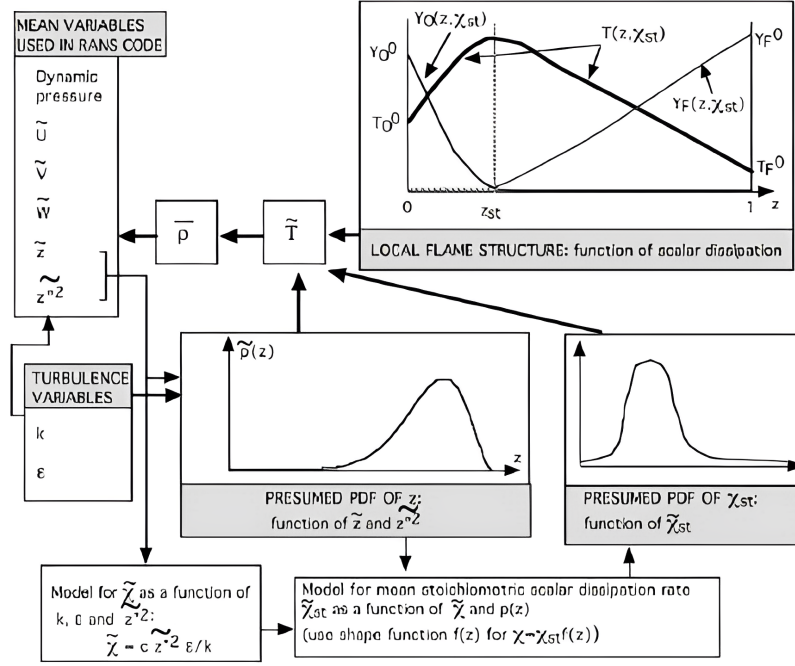


Figure 2.1: Flamelet model solver implementation [25].

The solver [Eq.1.17, Eq.1.18] computes the main flow quantities such as the velocity components but also the mean mixture fraction \tilde{Z} [Eq.1.28] and its variance \tilde{Z}'^2 [Eq.1.29]. Knowing \tilde{Z} and \tilde{Z}'^2 is needed in order to compute the probability density function of the mixture fraction $\tilde{P}(Z)$ using the presumed pdf shape approach [Eq.1.42].

The next step is to evaluate the mean scalar dissipation rate $\tilde{\chi}$ using equation 2.9 where $\tilde{\tau}$ is usually defined as the ratio between turbulent kinetic energy k and dissipation rate ϵ which are computed respectively with equation 1.7 and equation 1.8.

The previous step is needed to subsequently compute the stoichiometric mean scalar dissipation rate $\tilde{\chi}_{st}$, which in turn is used to compute the probability density function of the stoichiometric scalar dissipation rate $P(\chi_{st})$ ¹. Once both the pdfs are computed, they are combined with the Flamelet library - representing the local flame structure - in order to resolve all the remaining flow variables, such as temperature and mass fractions. After that density is retrieved from temperature and given as input to the RANS solver to close the loop.

For the sake of clarity, all mentioned steps are reported in figure 2.2.

¹This PDF is usually neglected in commercial solvers.

OPERATION	RESULTS
STAGNATION POINT FLAMES: Store flame structure in library	$T(z, \chi_{st}) \quad Y_k(z, \chi_{st})$
IN RANS CODE: Solve for mixture fraction and variance Construct β pdf for z using \tilde{z} and \tilde{z}''^2 Evaluate $\tilde{\chi}$ from \tilde{z}''^2 , k and ε Evaluate $\tilde{\chi}_{st}$ from $\tilde{\chi}$ and $\mathcal{F}(\tilde{z}, \tilde{z}''^2)$ Construct log normal pdf for χ_{st} using $\tilde{\chi}_{st}$ Compute mean temperature Compute density from \tilde{T} and send back to RANS code	$\tilde{z} \quad \tilde{z}''^2$ $\tilde{p}(z)$ $\tilde{\chi} = cz''^2 \varepsilon / k$ $\tilde{\chi}_{st} = \tilde{\chi} / \mathcal{F}(\tilde{z}, \tilde{z}''^2)$ $p(\chi_{st})$ $\tilde{T} = \int_0^\infty \int_0^1 T(z, \chi_{st}) \tilde{p}(z) p(\chi_{st}) dz d\chi_{st}$ $\bar{\rho}$

Figure 2.2: Flamelet model implementation steps [25].

Since the aim of the Flamelet approach is to decrease the computation effort needed, it must be highlighted that the integration of Flamelet libraries with PDFs is not performed during the solver computation. Flamelet libraries are tabulated a priori as function of \tilde{Z} , \tilde{Z}''^2 , $\tilde{\chi}$, therefore once these quantities are computed, temperature and the other flow variables are simply recovered from the library.

2.2.1. FINE/Open Implementation

Also in FINE/Open, RANS equations [Eq.1.17,Eq.1.18] are solved together with a transport equation for mixture fraction and its variance. Specifically, the Favre-averaged mixture fraction transport equation is formulated as follows.

$$\frac{\partial \bar{\rho} \tilde{Z}}{\partial t} + \frac{\partial \bar{\rho} u_j \tilde{Z}}{\partial x_j} = \frac{\partial}{\partial x_j} \left(\bar{\rho} (\tilde{D} + D_t) \frac{\partial \tilde{Z}}{\partial x_j} \right) \quad (2.7)$$

where $\tilde{D} = \frac{\nu}{\sigma}$ is the molecular mass diffusivity. ν is the molecular kinematic viscosity and it is retrieved from the combustion table while σ is the molecular Schmidt number considered constant and equal to 0.7. $D_t = \frac{\nu_t}{\sigma_t}$ is the turbulent diffusivity where the turbulent kinematic viscosity ν_t is defined by the turbulence model and the turbulent Schmidt number σ_t is considered constant and equal to 0.7. Despite the fact that the molecular diffusivity of mixture fraction is typically low compared to its turbulent equivalent, it is not ignored because it may have an impact. Notably, the transport coefficients of combusting gaseous fluids often increase by one order of magnitude as the temperature rises during the course of the process.

The Favre-averaged mixture fraction variance transport equation is implemented as fol-

lows

$$\frac{\partial \bar{\rho} \widetilde{Z''^2}}{\partial t} + \frac{\partial \bar{\rho} u_j \widetilde{Z''^2}}{\partial x_j} = \frac{\partial}{\partial x_j} \left(\bar{\rho} \left(\tilde{D} + D_t \right) \frac{\partial \widetilde{Z''^2}}{\partial x_j} \right) - 2 \bar{\rho} D_t \left(\frac{\partial \tilde{Z}}{\partial x_j} \right)^2 - \bar{\rho} \tilde{\chi}. \quad (2.8)$$

where the scalar dissipation rate $\tilde{\chi}$ is modeled as

$$\tilde{\chi} = C_\chi \frac{\widetilde{Z''^2}}{\tilde{\tau}}. \quad (2.9)$$

C_χ is a constant in the order of unity and $\tilde{\tau}$ is the turbulent time scale, defined by equation 2.6. Subsequently the solver is able to compute the scalar dissipation rate with the previous equation and therefore the strain rate a through the equation 1.33. The integration defined in equation 2.10, considering that in FINE/Open the scalar dissipation rate fluctuations are neglected, is not computed during each iteration for each cell.

$$\Phi(Z, Z''^2, a) = \int_0^1 P(Z, Z''^2) \Phi(Z, a) dZ \quad (2.10)$$

The distributions in the look-up tables for laminar combustion are integrated with the β -PDF and stored for discrete values across the whole physical range of the mixture fraction and its variance and for specific discrete values of strain rate. The results is combustion look-up tables which include the mixture fraction variance as a new dimension. The software is equipped with a combustion table reading routine that employs first-order extrapolation when independent parameters are within the table bounds. The strain rate, however, may exceed the table limits, and in such cases, the reading routine resorts to zero-order extrapolation. This approach is necessary due to the possibility of the solver computing a strain rate higher than the maximum value included in the table.

2.2.2. FLUENT Implementation

The implementation scheme used in FLUENT is similar to the one used in FINE/Open. RANS equations are solved together with transport equations for mixture fraction [Eq.2.11] and its variance [Eq.2.12].

$$\frac{\partial \rho \bar{Z}}{\partial t} + \frac{\partial \rho u_j \bar{Z}}{\partial x_j} = \frac{\partial}{\partial x_j} \left(\left(\frac{k}{c_p} + \frac{\mu_t}{\sigma_t} \right) \frac{\partial \bar{Z}}{\partial x_j} \right) + S_m + S_{user} \quad (2.11)$$

$$\frac{\partial \rho \overline{Z''^2}}{\partial t} + \frac{\partial \rho u_j \overline{Z''^2}}{\partial x_j} = \frac{\partial}{\partial x_j} \left(\left(\frac{k}{c_p} + \frac{\mu_t}{\sigma_t} \right) \frac{\partial \overline{Z''^2}}{\partial x_j} \right) - C_g \mu_t \left(\frac{\partial \overline{Z}}{\partial x_j} \right)^2 - C_d \rho \frac{\epsilon}{k} \overline{Z''^2} + S_{user}. \quad (2.12)$$

In this case the transport equations are Reynolds-averaged. The diffusivity coefficient \tilde{D} is substituted by $\frac{k}{c_p}$ thanks to the unity Lewis number assumption. This assumption is still considered in order to be coherent with the formulation of the Flamelet equations. The thermal conductivity k is set as a constant equal to $0.0454 \frac{W}{mK}$ while the specific heat c_p is computed with a mixing law. It is important to note that also the molecular viscosity is constant and it is equal to $1.72e-05 \frac{Kg}{ms}$. These two constant thermochemical properties are not computed in the combustion look-up tables as in FINE/Open. As a matter of fact FLUENT laminar combustion tables only comprehend temperature and species concentrations. Moreover, the reading routine does not require the computation of the strain rate as in FINE/Open.

Considering both transport equations, the turbulent diffusion coefficient is defined as $\frac{\mu_t}{\sigma_t}$ where σ_t is the turbulent Prandtl number - equal to 0.85 - and μ_t is the turbulent dynamic viscosity defined by the turbulence model. S_m represents transfer of mass into the gas phase from liquid fuel droplets or reacting particles while S_{user} is a user defined source term. It can be also shown that the production term in equation 2.12 - second term in the RHS - is modeled in the same way as in FINE/Open. In conclusion the last difference with respect of FINE/Open is the turbulent time scale definition used in the modeling of the scalar dissipation rate. As a matter of fact, it is defined as $\frac{k}{\epsilon}$ differently from equation 2.6 in FINE/Open. These considerations will be used for the critical analysis of FLUENT results in comparison with FINE/Open.

2.3. FGM Implementation

The current methodology in FINE/Open for modeling partially-premixed combustion involves solving RANS equations along with a transport equation for the mixture fraction \tilde{Z} and its variance $\overline{Z''^2}$. A transport equation for the progress variable Y is also solved to model the evolution of the overall reaction. This approach assumes that the variance of the progress variable has a negligible impact on the turbulence-chemistry interaction compared to the variance of the mixture fraction.

The governing equations computed by the solver are the same governing equations as the Flamelet case [Eq.1.17, Eq.1.18, Eq.2.7, Eq.2.8], but with the additional inclusion of

a transport equation for the reaction progress variable [Eq.2.13].

$$\frac{\partial \bar{\rho} \tilde{Y}}{\partial t} + \nabla \cdot (\bar{\rho} \tilde{\mathbf{u}} \tilde{Y} - \bar{\rho} D_e \nabla \tilde{Y}) = \tilde{\omega}_Y \quad (2.13)$$

In this equation $D_e = \tilde{D} + D_t$ is the effective diffusivity coefficient and $\tilde{\omega}_Y$ is the source term of the progress variable. The molecular dynamic viscosity $\bar{\mu}$, density $\bar{\rho}$, and the aforementioned source term $\tilde{\omega}_Y$ are obtained from FGM tables, which can be expressed as

$$\bar{\mu}, \bar{\rho}, \tilde{\omega}_Y = F(\tilde{Z}, \tilde{Z}^{m2}, \tilde{Y}) \quad (2.14)$$

clearly showing the new dependence on \tilde{Y} with respect to Flamelet tables [Eq.2.10]. The Flamelets can encompass a range of combustion scenarios, including non-burning, premixed propagating, and stretched non-premixed burning flames. The FGM tables can be constructed either from a library of premixed or non-premixed Flamelets, depending on the desired simulation outcome.

Premixed FGM tables are constructed using a library of premixed Flamelets, where each Flamelet corresponds to a distinct mixture fraction. The primary stage in generating these manifolds involves mapping the thermochemical conditions of each Flamelet onto a grid that spans the complete physical range of the mixture fraction and the progress variable. Typically, the progress variable is defined as a linear combination of the intermediate species and the products. In FINETM/Open, if the streams contain carbon atoms, the following definition for the progress variable is utilized,

$$Y = \frac{Y_{CO_2}}{M_{CO_2}} + \frac{Y_{CO}}{M_{CO}} \quad (2.15)$$

where Y_i and M_i respectively represent the mass fraction and molar mass of species i . It is important to note that, since the mixture of fuel and oxidizer is usually not flammable for the complete range of physical values of the mixture fraction, an interpolation must be conducted for the states with a mixture fraction lying between the pure oxidizer and the lower flammability limit Z_l as well as for the states with a mixture fraction between the upper flammability limit Z_u and that of the pure fuel.

The creation of Non-premixed FGM tables involves a library of steady-state non-premixed Flamelets, ranging from low to high strain levels, as well as an unsteady extinguishing Flamelet. The steady-state Flamelets form the basis for constructing the non-premixed FGM tables. To fill the state-space between the steady burning Flamelet at the highest

strain and the unburnt mixture of fuel and oxidizer, the thermochemical states of the unsteady Flamelet are utilized. This unsteady Flamelet is generated by using the steady Flamelet at the highest strain as initial solution. After that, a strain rate slightly above the quenching limit is imposed, causing the flame to progressively extinguish. Once the progress variable is determined from the transport equation [Eq.2.13], the Flamelet library is then mapped onto a two-dimensional grid that is spanned by the mixture fraction and the progress variable. The inclusion of the solution of an unsteady Flamelet to fill the non-equilibrium part of the reaction domain results in a non-smooth manifold. However, this approach has the advantage of predicting intermediate species and slow chemistry effectively, as unsteady Flamelets are known to do. It is worth noting that compared to the set of Flamelets used for the construction of a non-premixed FGM, a library of premixed Flamelets generally covers a smaller portion of the state space. In conclusion it can be stated that both types of table can be used in both types of combustion simulations. Obviously, using a non-premixed FGM table for a non-premixed combustion case would provide slightly better results than using a premixed FGM table. However, due to convergence problems in the table generation tool a premixed FGM is used. Further details will be provided in section 2.5.

Also in this approach the turbulence-chemistry interaction is accounted for using the presumed PDF approach. To facilitate the pre-integration of combustion look-up tables, they must be transformed into a square domain of independent variables. This is done by re-mapping the Flamelets onto the normalized progress variable which is defined as

$$\widetilde{Y}^*(Z, Y) = \frac{\widetilde{Y} - \widetilde{Y}_{min}(Z)}{\widetilde{Y}_{max}(Z) - \widetilde{Y}_{min}(Z)}. \quad (2.16)$$

The mixture fraction and the normalized progress variable serve as independent parameterizing variables, both ranging from zero to unity throughout the physical domain. It is assumed that there is statistical independence between the mixture fraction and the normalized progress variable and that fluctuations in the latter are negligible. Therefore the pre-integrated tables [Eq.2.17] depend on the mixture fraction \widetilde{Z} , its variance \widetilde{Z}''^2 , and the normalized progress variable \widetilde{Y}^* .

$$\widetilde{\mu}, \widetilde{\rho}, \widetilde{\omega}_Y = F(\widetilde{Z}, \widetilde{Z}''^2, \widetilde{Y}^*) \quad (2.17)$$

Nevertheless, the transport equations are still solved for the non-normalized progress variable Y , so a normalization of the latter is performed before accessing the combustion tables. The table reading routine used in the FGM model is similar to the one used in the Flamelet approach, with the difference that the strain rate dependency is replaced by

the normalized progress variable. This approach ensures that the independent parameters used for table interpolation are within the table bounds.

2.4. Hybrid BML/Flamelet Technique

The hybrid BML/Flamelet model differ from the FGM approach in the source term closure. In the Hybrid BML/Flamelet model the source term in the progress variable transport equation is closed using a BML type model. The approach assumes that chemical reactions in premixed turbulent flames occur in a thin surface, which is represented as a sheet separating unburnt mixture from burnt gas. This is due to the high velocity of chemical reactions. The formulation involves introducing a progress variable field, which represents the state of the mixture as burnt or unburnt, with a value of $c^* = 0$ for completely unburnt mixture and $c^* = 1$ for completely burnt mixture. Typically it is defined as a normalized temperature.

A premixed flame has a constant equivalence ratio, while in a partially premixed flame, the equivalence ratio can vary spatially, leading to a change in the laminar flame speed², combustion products, and density, which are now functions of the local equivalence ratio ϕ . This dependence can be expressed through a mixture fraction relation, as it is linked to the equivalence ratio through the following expression

$$Z = \frac{\phi Z_{st}}{1 - Z_{st}(1 - \phi)} \quad (2.18)$$

where Z_{st} is the stoichiometric mixture fraction. Therefore the aforementioned physical variables can be still tabulated as function of the mixture fraction.

The governing equations considered by the solver are the same governing equations as the FGM case [Eq.1.17, Eq.1.18, Eq.2.7, Eq.2.8, Eq.2.13]. However, in this approach thermochemical quantities are retrieved from a linear interpolation using two different pre-integrated table. For example, the computation of the density is formulated as follows

$$\bar{\rho} = (1 - c^*)\bar{\rho}(\tilde{Z}, \widetilde{Z''^2})_{mix} + c^*\bar{\rho}(\tilde{Z}, \widetilde{Z''^2})_{fl} \quad (2.19)$$

where $\bar{\rho}(\tilde{Z}, \widetilde{Z''^2})_{fl}$ is a Flamelet table computed for a strain rate $a = 100\frac{1}{s}$. Considering also the turbulence presence, the table has a dependence also on $\widetilde{Z''^2}$.

²In reality, the laminar burning velocities are determined via a polynomial equation which is modeled by fitting experimental data. This method is preferred because it is accurate near the flammability limits and does not require the presence of the laminar flame speed in a table. Furthermore, parabolic equations are available for laminar flame speed modeling in the case fuel-air mixture is not provided in FINE/Open.

Instead, $\bar{\rho}(\tilde{Z}, \widetilde{Z''^2})_{mix}$ is a mixing table computed from a non-premixed counterflow diffusion flame. It represents the pure mixing between fuel and oxidizer before the occurrence of combustion.

In conclusion, the Hybrid BML/Flamelet technique combines elements of both premixed and non-premixed combustion models. It utilizes the formulation and computation of the progress variable, which is a hallmark of premixed combustion models, but also incorporates the use of tabulated thermochemical properties, such as those obtained through Flamelet model, which are typical of non-premixed combustion models. This combination allows for a different but complete representation of the partially-premixed combustion with respect to the FGM model. The primary benefit of employing this model is the acceleration of combustion table computation and the reduction in the table's file size.

2.5. Table Generation - TabGen/Chemistry

TabGen/Chemistry is the available tool in FINE/Open for the generation and integration of combustion look-up tables which uses the CHEM1D solver from TU Eindhoven. It offers the generation of both equilibrium and Flamelet tables, as well as Flamelet libraries, for non-premixed combustion. For partially-premixed combustion, it is possible to generate tables for the Hybrid BML/Flamelet technique and the FGM model.

However, it should be noted that this tool does not account for compressibility effects, as the Flamelets are computed under constant pressure. The FGM tables are based on counter-flow diffusion Flamelets, and differential diffusion effects are not included. Additionally, when dealing with high heat loss conditions, the chemistry is assumed to be frozen.

The tables used in this thesis serve as the basis for testing the various combustion models presented earlier. In order to build the necessary tables the steering (input) file for TabGen/Chemistry must be properly configured. The specific type of table must be specified, along with other important parameters such as the chemical mechanism, pressure level, mole fraction composition of the fuel and oxidizer streams, and the inlet temperature values of both streams. It should be noted that the same combustion model can be utilized with different tables based on the values of other parameters, such as strain rate.

When it comes to non-premixed combustion, two types of Flamelet tables can be generated using TabGen/Chemistry. The first option is to create a table with two Flamelets, one for a strain rate of $100\frac{1}{s}$ and another for a strain rate of $101\frac{1}{s}$. The second option is to generate a Flamelet library, which is a table that contains Flamelets for multiple different strain rates such as 20, 30, ..., 90, 100, 125, 150, ..., 475, $500\frac{1}{s}$. The creation of a

Flamelet table is specified by the command `<tabletype type=Flamelet>` in the steering file, while the creation of a Flamelet library is specified using the keyword `<tabletype type=Flameletlibrary>`.

Considering partially-premixed combustion, the concept behind the FGM method is to construct a manifold utilizing a collection of Flamelets. To generate the FGM tables, a library of non-premixed or premixed Flamelets can be utilized. In FineOPEN there are three possible types of non-premixed look-up tables that can be generated. The first option is to create a table based on an unsteady non-premixed counter-flow diffusion Flamelet. This type can be created by incorporating the command `<tabletype type=fgm_nonpremixed>` into the steering file. The second option is to combine this table with a Flamelet library, hence the table is based on a set of steady counter-flow diffusion Flamelets and one unsteady Flamelet. This can be done using the command `<tabletype type=fgm_nonpremixed_wflamlib>`. The third option is similar to the first one, but it also takes into account auto-ignition effects. The command to use is `<tabletype type=fgm_nonpremixed_ignition>`. Alternatively in order to create a table based on a library of premixed Flamelets the command to be used is `<tabletype type=fgm_premixed>`. In this case is possible to specifically set the lower and upper flammability limits related to the mixture fraction. In the case of the Hybrid BML/Flamelet technique, the table is a combination of a mixing table and a Flamelet table, calculated for a strain rate of $100\frac{1}{s}$. The required command to generate this table is `<tabletype type=hybrid>`.

The example in figure 2.3 showcases the process of producing a pre-integrated Flamelet table for non-premixed combustion of methane and air. The specific conditions considered are: absolute pressure equal to $2e6$ Pa, air temperature is 623 K, while methane temperature is 368 K. Therefore the Flamelet is computed in isobaric condition for a pressure level equal to 20 bar where the fuel and oxidizer inlet temperature are the ones previously mentioned. The GRI-Mech 3.0 is the chemical mechanism implemented. This mechanism is optimized for modeling the combustion of natural gas and methane, with a specific focus on the formation of nitrogen oxides and reburn chemistry. It encompasses 325 elementary chemical reactions and corresponding rate coefficient expressions, as well as thermochemical parameters for the 53 species involved in the reactions. It must be highlighted that this mechanism is the one considered in all the tables used. More information about the chemical mechanism and how it was developed can be found in [29].

It is important to note that the generation of non-premixed FGM tables using the TabGen/Chemistry tool is not feasible due to convergence issues. After consultations with FINE/Open developers, it was established that achieving quenching conditions is chal-

```
<tabgenchem>
  <tabletype type=Flamelet/>
  <CHEM\_MECHANISM file=gri30.chm/>
  <Pressure value=2.0E5/>
  <stream name=fuel>
    <Composition unit=mole>
      <Species>CH4=1</Species>
    </Composition>
    <Temperature value=368./>
  </stream>
  <stream name=oxidizer>
    <Composition unit=mole>
      <Species>O2=0.21</Species>
      <Species>N2=0.79</Species>
    </Composition>
    <Temperature value=623./>
  </stream>
</tabgenchem>
```

Figure 2.3: Example of steering file

lenging owing to the presence of pure oxygen as an oxidizer. In contrast, generating non-premixed FGM tables using air as an oxidizer is easier due to the lower quenching limit. Consequently, premixed FGM tables are employed despite the non-premixed nature of the combustion case. Nevertheless, this inconsistency does not significantly impact the outcomes since the limitation given by the flammability limits is overcome thanks to an extrapolation technique that allows the states between pure mixing and flammability limits to be attained.

3 | Case Settings

In this chapter, the configuration of each computed case is discussed. Initially, the architecture of each case, which refers to how convergence is achieved, is described. Subsequently, the similarities between all the cases are highlighted, such as the mathematical models utilized in all the simulations. Following that, each case - Flamelet, FGM, and Hybrid - is described, highlighting the specific boundary conditions implemented, the generic and numerical parameters required by the solver, and the specific combustion table used. Regarding the Flamelet simulation computed with FLUENT, the set up can be found in appendix B. Additionally, the possible alternatives that can be utilized are also discussed. In the next chapter the results will be compared and analysed with respect to a DNS simulation provided by the TUM Space Propulsion Chair.

The case configuration consists in a 2D combustive shear layer between a pure methane and pure oxygen stream. Before simulating the combustion case a convergence study of the mesh should be done. Performing a mesh independence study involves systematically varying the mesh refinement and checking the convergence of the solution to ensure that specific variables are not significantly affected by the grid size. It is not just about showing that a particular mesh works, but also determining the appropriate mesh resolution for capturing the relevant gradients and features of the problem. Once the appropriate mesh resolution is determined, it can be applied to other meshes with similar grid characteristics without the need for further mesh independence studies. In this thesis the mesh used is a section of the one used in [20], hence it has the same grid characteristics. Therefore it is reasonable to assume that the mesh is appropriate for the computed case.

Each case consists of 5 simulations that are interrelated. Specifically, each simulation serves as the initial solution for the subsequent one. The first simulation is an inert case, referred to as the NoComb case in the following discussions. Afterward, there are 4 combustion cases, namely Comb1, Comb2, Comb3, CombProfile.

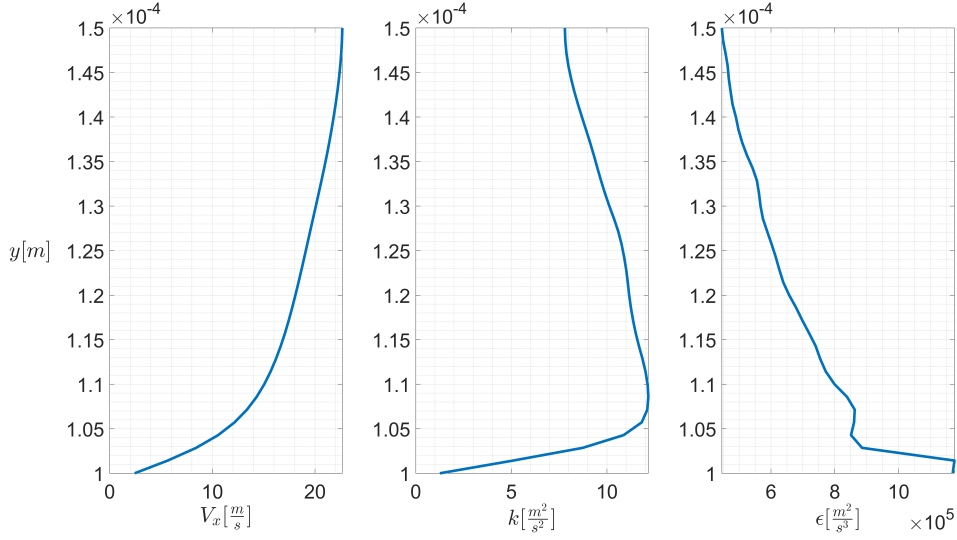


Figure 3.1: Fuel Boundary conditions for CombProfile simulation.

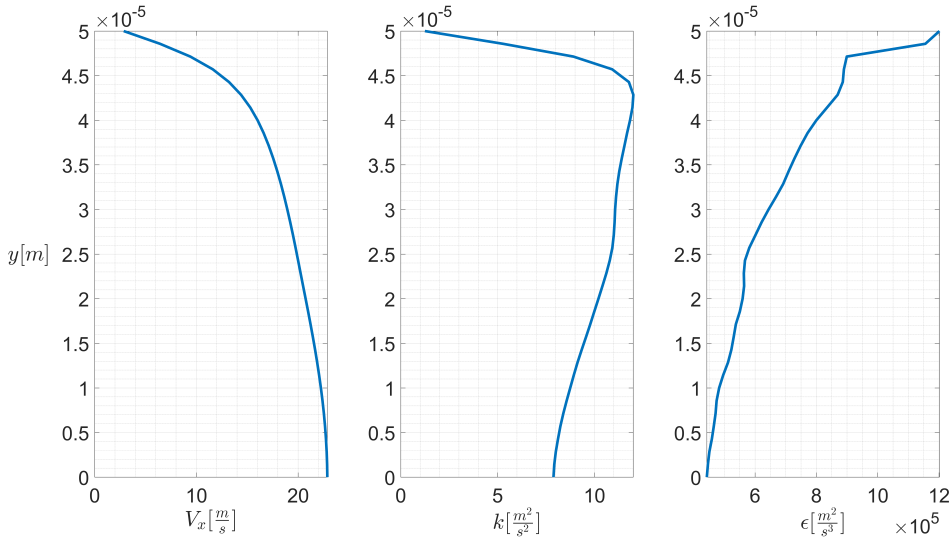


Figure 3.2: Oxidizer Boundary conditions for CombProfile simulation.

In these simulations the boundary conditions are gradually increased to eventually match the DNS boundary conditions in the final simulation - CombProfile. The DNS boundary conditions for the fuel and oxidizer inlet are respectively depicted in figure 3.1 and 3.2. It can be seen that Comb3 boundary conditions are similar to the average values of the DNS profiles. The variables considered are the axial velocity component V_x , the turbulent kinetic energy k and the turbulent dissipation ϵ . The y-coordinate corresponds to the height of the fuel and oxidizer inlets in the mesh. The aforementioned variable profiles are obtained through linear interpolation of the values associated with the nearest cells

to the inlet, taking into account the size of DNS cells.

In all three cases, the outlet and solid walls boundary conditions are the same across all simulations. The outlet static pressure is set to 20 bar and the backflow control option is selected, as recommended in the user guide.

For the solid walls - both lateral, upper and lower - the selected option is mirror conditions. This means that the solver applies a zero normal gradient to all the CFD variables on the surface. The wall postip has been set with Navier-Stokes temperature imposed conditions. This means that the velocity relative to the wall is zero, pressure is extrapolated from the first interior cell and temperature is set to 300 K on this surface. The complete overview of the domain and the related boundary conditions are shown in figure 3.3 and reported in appendix A in table A.1. The inlet boundary conditions will be reported in the following sections since they are different depending on the combustion model applied.

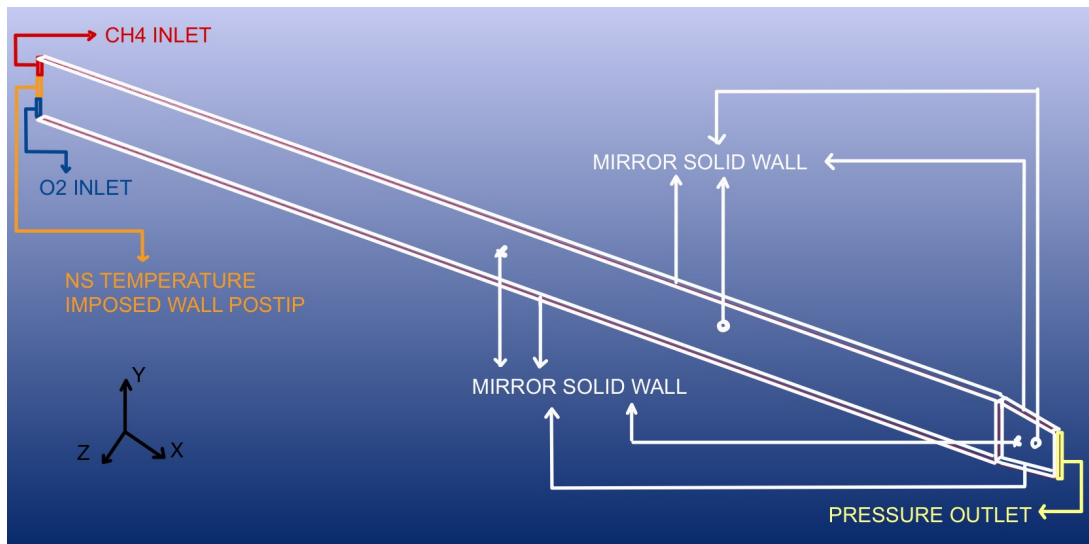


Figure 3.3: Mesh boundary conditions.

As previously stated, the first simulation, NoComb, represents an inert flow. In this simulation, the fluid under consideration is perfect air, with the same reference values and properties for all three major cases. These settings are reported in appendix A in figure A.2. In all combustion simulations the fluid is automatically considered as reactive. Only a limited number of values can be specified by the user in this scenario. The majority of thermochemical properties are retrieved from the combustion lookup tables. The specified parameters are reported in appendix A in figure A.1.

The turbulence model used in both the inert and combustion simulations is the $k-\epsilon$ Low Re Yang-Shih model. This model was extensively described in the subsection 2.1. This model was chosen instead of the $k-\omega$ due to the low Reynolds number conditions of the

flow. Furthermore the $k-\omega$ model includes the enhanced wall treatment approach which is not needed in this case. Moreover the contribution of gravity forces is not considered. Due to the low mach number of the streams, the low speed flow option is included. This enables the solver to use a preconditioning procedure which helps in reducing¹the computational time. The preconditioning approach involves modifying the time derivatives of the transport equations in a way that decreases the stiffness of the eigenvalue problem. This is achieved by multiplying the time derivatives with a preconditioning matrix. The method is applicable to steady-state simulations solved by time-marching algorithms, as the time derivatives have no physical meaning and can be modified without altering the final solution.

Two preconditioning techniques are available on FINE/Open, namely Hakimi and Merkle. The latter is selected due to its robustness and its efficiency at all Mach, Reynolds and Strouhal numbers. More informations about the precoditioning theory are available in section 6.2 of [16].

In the FINE/Open solver the multigrid strategy is a key feature and is highly recommended [17]. The advantage of this method is that it effectively reduces low-frequency errors that cannot be eliminated by explicit schemes. This results in faster convergence and more efficient simulations. The multigrid method involves transferring the problem to coarser grids, where an approximation to the solution correction is obtained, and then transferring the correction back to the finer grid. The explicit Runge-Kutta scheme is used as a smoother to damp high frequency errors, and the method is adapted to the treatment of the non-linear equations through the Full Approximation Storage approach, which is explained in Sec. 6.1.3 of [16]. For all the simulations the number of grid levels used in the multigrid strategy is set equal to 4.

The multigrid strategy involves interpolations from coarser grids to finer grids, which can result in high discontinuities and cause numerical instabilities. To prevent these issues, the Correction damping feature is activated for all the simulations in order to smooth the interpolation results and ensure the robustness of the multigrid method.

Exclusively in the NoComb simulation, the Coarse Grid Initialization feature is also selected. This option is related to the Full Multigrid method [Sec. 6.1.4 of [16]] and it is used to generate a suitable initial solution. It works by starting an iteration process on the coarsest grid. The solution on that level will not be transferred to the next grid until it has converged to a specified accuracy. Once the solution has been interpolated to the next finer grid, it is used as the initial solution for further iterations on that grid level. The process is repeated recursively until the finest grid is reached. The Coarse Grid Initialization option is not available for the subsequent simulations because each initial

solution is the final result of the previous simulation. Anyhow an initial solution for the NoComb simulation must be provided. The values - considered constant in all the domain - are reported in Tab.3.1.

$P[Pa]$	$T[K]$	$V_x[\frac{m}{s}]$	$V_y[\frac{m}{s}]$	$V_z[\frac{m}{s}]$	$k[m^2/s^2]$	$\epsilon[m^2/s^3]$
2e6	293	30	0	0	50	1e4

Table 3.1: Initial solution NoComb computation.

The numerical parameters still need to be defined, however they slightly vary between cases, therefore they are described in the specific sections.

In conclusion, the combustion look-up tables also need to be defined. Since they vary depending on the chosen combustion model and the level of refinement, their details are covered in the specific sections of each case.

3.1. Flamelet Set Up

The inlet boundary conditions are specified in table 3.2. The y and z components of velocity are consistently set to zero. With regards to the mixture fraction, the inlet value for methane is fixed at 1 and the inlet value for oxygen is fixed at 0. Note that the inlet temperature is needed only for the inert case because when the combustion model is activated, the temperature is retrieved from the combustion look up tables without the need of solving the related transport equation.

The next step is to specify the numerical parameters and options [Tab.3.3]. The CPU booster option accelerate convergence, which results in a significant decrease in computational time. Since the solver is explicit, this feature - based on enhancing implicitness²- is the only one allowing to select a CFL number greater than 1. Anyhow the suggested CFL number for combustion simulations is 1.5, which it was used for all the simulation without the CPU booster feature. Moreover, when the CPU booster feature is selected the density relaxation factor (ρ rel. factor) is set equal to 0.1 instead of 0.01 which is the default value. Another constraint related CPU booster is that only the Merkle preconditioning scheme is available.

The number of iterations and the convergence criteria are the result of a trial and error

¹This is required because the flow velocity is small compared to the speed of sound and the solution becomes more sensitive to small changes in the velocity and density fields, increasing the effort for the time marching compressible codes to converge.

Inlet CH_4	NoComb	Comb1	Comb2	Comb3	CombProfile
$V_x[\frac{m}{s}]$	10	1	2	20	Fig.3.1
$T[K]$	300	/	/	/	/
$k[\frac{m^2}{s^2}]$	5	5	5	10	Fig.3.1
$\epsilon[\frac{m^2}{s^3}]$	1e5	1e5	1e5	1e5	Fig.3.1
Inlet O_2	NoComb	Comb1	Comb2	Comb3	CombProfile
$V_x[\frac{m}{s}]$	20	2	4	20	Fig.3.2
$T[K]$	300	/	/	/	/
$k[\frac{m^2}{s^2}]$	5	5	5	10	Fig.3.2
$\epsilon[\frac{m^2}{s^3}]$	1e5	1e5	1e5	1e5	Fig.3.2

Table 3.2: Inlet Boundary Conditions Flamelet case.

process. These values are related in order to let the solver get to convergence from the inlet and outlet mass flow rates matching point of view. In the particular instance of Comb1, the simulation was terminated at approximately the 800th iteration due to an unfeasible value of the global density residual. However, it is noteworthy that the inlet and outlet mass flow rates were deemed satisfactory. Furthermore, the temperature trend was analyzed prior to utilizing this simulation as the initial solution for Comb2. The results indicated that the combustion process was nearly fully developed, thereby confirming the adequacy of this computation for its intended purpose. The effectiveness of this outcome was subsequently corroborated by the successful convergence of Comb2 without any complications. All the other parameters not mentioned are kept with their default value as stated in section 8.1.2 of [17].

	NoComb	Comb1	Comb2	Comb3	CombProfile
CPU booster	ON	ON	OFF	OFF	OFF
CFL	100	4	1.5	1.5	1.5
Iterations	4e3	1e3	2e3	1.5e3	1.5e3
ρ rel. factor	0.1	0.1	0.01	0.01	0.01
Conv. crit.	-10	-8	-6	-6	-6

Table 3.3: General and Numerical parameters Flamelet case.

²No further informations can be attained from FINE/Open developers.

The last step is to provide the combustion look-up table to the solver. In the Flamelet case the parameters required by the steering file are reported in table 3.4. The number of points considered in specific variable direction are $\#\tilde{Z}$, $\#\widetilde{Z}''^2$, $\#a$ respectively for mixture fraction, mixture fraction variance and strain rate. This means that in this specific case, the integration procedure created 77 tables for each value of strain rate. In each table, the mixture fraction field is decomposed by 177 nodes. The resolution can be modified by specifying the related option in the steering file (section 21.3 of [17]).

Type	$P[Pa]$	$T_{CH_4}[K]$	$T_{O_2}[K]$	$\#\tilde{Z}$	$\#\widetilde{Z}''^2$	$\#a[\frac{1}{s}]$
Flameletlibrary	2e6	300	300	177	77	25

Table 3.4: Combustion table parameters Flamelet case.

3.2. FGM Set Up

As stated for the Flamelet case the table 3.5 does not include the y and z components of velocity as they are consistently set to zero. With regards to the mixture fraction, the inlet value for methane is fixed at 1 and the inlet value for oxygen is fixed at 0. Nevertheless, table 3.5 includes the inlet values for the progress variable Y which were set after a trial and error process. Note that an inlet value for the progress variable equal to zero would not provide a reasonable solution.

As stated in the previous subsection 3.1, the numerical parameters must be specified. Refer to the previous subsection for the explanation of the parameters. Note that in this case [Tab.3.6] only the number of iterations of Comb1 are different with respect to the Flamelet case. As in the Flamelet case, the Comb1 computation was terminated due to an unfeasible value of the global density residual at approximately the 2000th iteration. The error between the inlet and outlet mass flow rates is around 30%, anyhow the temperature trend was checked and the computation was considered adequate for its purpose. Also in this case the successful convergence of Comb2 verified the effectiveness of the previous computation. All the other parameters can be found in section 8.1.3 of [17].

Regarding the combustion look-up table, the FGM model requires the progress variable \tilde{Y} instead of the strain rate a . As stated for the Flamelet case, $\#\tilde{Z}$, $\#\widetilde{Z}''^2$ and $\#\tilde{Y}$ are the number of points in the related variable direction [Tab.3.7]. The resolution can be modified by specifying the proper option in the steering file.

As described in subsection 2.3, an interpolation is required for states with mixture fraction

Inlet CH_4	NoComb	Comb1	Comb2	Comb3	CombProfile
$V_x[m/s]$	10	1	2	20	Fig.3.1
$T[K]$	300	/	/	/	/
$k[m^2/s^2]$	5	5	5	10	Fig.3.1
$\epsilon[m^2/s^3]$	1e5	1e5	1e5	1e5	Fig.3.1
$Y[mol/kg]$	/	0.9	0.9	0.9	0.9
Inlet O_2	NoComb	Comb1	Comb2	Comb3	CombProfile
$V_x[m/s]$	20	2	4	20	Fig.3.2
$T[K]$	300	/	/	/	/
$k[m^2/s^2]$	5	5	5	10	Fig.3.2
$\epsilon[m^2/s^3]$	1e5	1e5	1e5	1e5	Fig.3.2
$Y[mol/kg]$	/	0.9	0.9	0.9	0.9

Table 3.5: Inlet Boundary Conditions FGM case.

	NoComb	Comb1	Comb2	Comb3	CombProfile
CPU booster	ON	ON	OFF	OFF	OFF
CFL	100	3	1.5	1.5	1.5
Iterations	4e3	3e3	2e3	1.5e3	1.5e3
ρ rel. factor	0.1	0.1	0.01	0.01	0.01
Conv. crit.	-10	-8	-6	-6	-6

Table 3.6: General and Numerical parameters FGM case.

Type	$P[Pa]$	$T_{CH_4}[K]$	$T_{O_2}[K]$	$\# \tilde{Z}$	$\# \widetilde{Z}''^2$	$\# \tilde{Y}$
fgm_premixed	2e6	293	293	201	51	201

Table 3.7: Combustion table parameters FGM case.

values that fall below Z_l or exceed Z_u . Hence, it may be advantageous to adjust these values to increase the number of states that are automatically incorporated into the table. Obviously they must also be physically consistent with the fuel-oxidizer couple. In this table the values chosen are 0.2 for the lean flammability limit equivalence ratio and 2 for the rich one. The mapping between equivalence ratios and mixture fractions Z_l and Z_u is described by equation 2.18.

3.3. Hybrid BML/Flamelet Set up

As stated for the other two cases, the table 3.8 does not include the y and z components of velocity as they are consistently set to zero. With regards to the mixture fraction, the inlet value for methane is fixed at 1 and the inlet value for oxygen is fixed at 0. Nevertheless, table 3.8 includes the inlet values for the progress variable Y - set after a trial and error process - such as the FGM case. In this case an inlet value for the normalized progress variable is required. After a trial and error process this value was set for all the computations.

Inlet CH_4	NoComb	Comb1	Comb2	Comb3	CombProfile
$V_x[m/s]$	10	1	2	20	Fig.3.1
$T[K]$	300	/	/	/	/
$k[m^2/s^2]$	5	5	5	10	Fig.3.1
$\epsilon[m^2/s^3]$	1e5	1e5	1e5	1e5	Fig.3.1
$\tilde{Y}[-]$	/	0.3	0.3	1	1
Inlet O_2	NoComb	Comb1	Comb2	Comb3	CombProfile
$V_x[m/s]$	20	2	4	20	Fig.3.2
$T[K]$	300	/	/	/	/
$k[m^2/s^2]$	5	5	5	10	Fig.3.2
$\epsilon[m^2/s^3]$	1e5	1e5	1e5	1e5	Fig.3.2
$\tilde{Y}[-]$	/	0.3	0.3	1	1

Table 3.8: Inlet Boundary Conditions Hybrid BML/Flamelet case.

Regarding the numerical parameters, in this case the CFL number is higher for Comb1 with respect to Flamelet and FGM cases [Tab.3.9]. Nevertheless an higher number of iterations is needed to get Comb1 simulation converging. This counter intuitive result can

be explained by the fact that the combustion table is not as resolved as in the previous simulations. Comb1 computation reaches mass flow rates convergence, leading to a lower number of iterations for the subsequent computation Comb2. However, Comb3 requires more iterations with respect to the same computations for the previous cases. Regarding the other parameters refer to section 8.1.4 of [17].

	NoComb	Comb1	Comb2	Comb3	CombProfile
CPU booster	ON	ON	OFF	OFF	OFF
CFL	100	50	1.5	1.5	1.5
Iterations	4e3	4e3	1.5e3	2e3	1e3
ρ rel. factor	0.1	0.1	0.01	0.01	0.01
Conv. crit.	-10	-8	-6	-6	-6

Table 3.9: General and Numerical parameters Hybrid case.

Regarding the combustion look-up table, the Hybrid model requires the progress variable \tilde{Y} instead of the strain rate a . In this case, only 2 progress variable values are considered [Tab.3.10]. This is due to the fact that thermochemical variables are retrieved with an interpolation considering 2 tables. Therefore, the progress variable dependence is not embedded in the tables but it is directly explicited in equation 2.19. The resolution for mixture fraction and its variance can be modified by specifying the proper option in the steering file.

Type	$P[Pa]$	$T_{CH_4}[K]$	$T_{O_2}[K]$	# \tilde{Z}	# $\widetilde{Z''^2}$	# \tilde{Y}
hybrid	2e6	293	293	177	77	2

Table 3.10: Combustion table parameters Hybrid case.

Moreover, due to the partially-premixed conditions the laminar flame speed as function of the equivalence ratio must be specified. Since the fuel-oxidizer couple considered is not included in the software, none of the polynomial models comprehended can be used. The only available option is to consider a parabolic function from experimental data. In this thesis the parabola is computed by fitting in a least-square sense the experimental data attained in section 2.5.2 of [15].

4 | Results and Critical analysis

This chapter will present and analyze the simulation outcomes. Initially, an explanation will be presented regarding the post-processing of DNS data to facilitate a comparison with RANS results, given the inherent dissimilarities between the two methodologies. After that, a comparison will be given between the FINE/Open and FLUENT Flamelet cases and the DNS results, providing a brief overview of the computations. Subsequently, the rationale behind the exclusion of FLUENT results will be elucidated. The succeeding sections will focus on the scrutiny of the outcomes of each FINE/Open combustion model to ascertain their consistency with the mathematical modeling, followed by a comparison with the DNS results.

4.1. DNS post-processing

As previously mentioned, DNS computations involve direct calculation of the entire turbulent energy spectrum. This means that transport equations are solved for the overall instantaneous variables, therefore including the fluctuations due to the turbulent behavior. On the other hand, RANS simulations solve transport equations only for averaged quantities. Therefore a direct comparison between DNS and RANS results would still be possible but not so useful.

To visualize the outcomes of the different approaches, isolines of the physical variables are utilized. The concept behind DNS post-processing is to obtain averaged quantities to compare DNS variable trends with RANS isolines. In this thesis, DNS isolines are obtained in a specific way. Firstly, an isolevel is established for each variable by visually examining RANS contours to identify an isolevel that is present in the entire field. For instance, a temperature isolevel of 1500 K is chosen since it was visible in the whole computed field. Then, the average cell location where the threshold is reached is computed. Starting from the lower wall, each cell is examined going upward to confirm whether the threshold is reached or not. The process is stopped once the isolevel is overcome, and the cell location where the threshold is achieved is stored. Additionally, this technique is employed for each time step of the DNS simulation. Hence, the final cell location computed for

each axial position is averaged over all the time steps¹ of the DNS computation. This routine is conducted for each axial position - column of cells - composing the DNS mesh, beginning from the inlet and progressing to the outlet. Furthermore, the same procedure is repeated beginning from the upper wall and going downward to calculate the other half of the desired isoline. However, it should be noted that for specific variables, the isolevel selected may result in ambiguous cell locations in limited parts of the mesh, due to the highly fluctuating behavior of the flow induced by the turbulence chemistry interaction.

4.2. FINE/Open vs FLUENT Flamelet cases

This section presents a comparison between the FINE/Open and FLUENT Flamelet cases with the DNS results. The objective is to elucidate why the FLUENT results are excluded from subsequent sections. The rationale is presented by analyzing the temperature isolines of both software packages.

Figure 4.1 displays the temperature field of the DNS results at the final time step, along with the isolines for FINE/Open, FLUENT, and DNS at 1500 K.

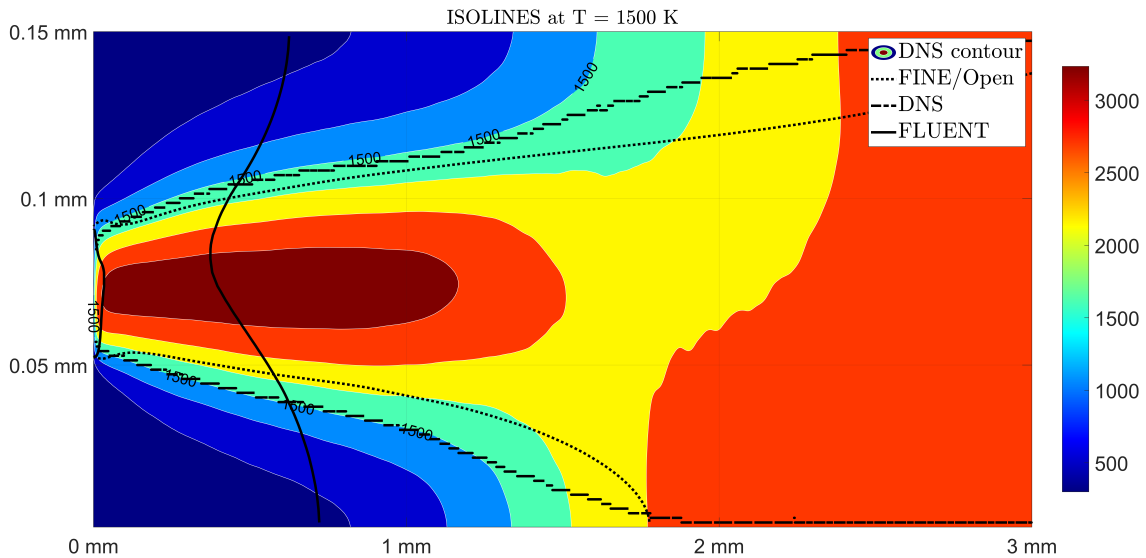


Figure 4.1: FINE/Open vs FLUENT temperature isolines.

¹DNS simulations inherently involve unsteady physics, and therefore, variable fields are computed for each time step. However, the entire DNS computation is simulating a steady combustion case despite the presence of unsteady physics phenomena. As a result, the variable fields cannot be deemed steady. This is why isolines are utilized for comparison purposes.

It is evident from the figure that the DNS isoline closely follows the actual isoline of the DNS field. In the figure the DNS contour shown is the one related to the latest time step which is the one in which the convergence was considered to be achieved. As a consequence, due to the averaging process, the computed DNS isoline is not perfectly matching the contour isoline, even though the resemblance is evident. However, beyond the axial position of 1.5 mm , the computed isoline deviates from the actual field due to the highly fluctuating behavior of turbulence. In reality, the temperature exceeds the isolevel for $x > 1.5\text{ mm}$, but the isoline position may not coincide with the upper and lower walls since the temperature threshold was reached in previous time steps. Moreover, for $x > 2\text{ mm}$, the lower isoline overlaps with the lower wall.

With regards to the FINE/Open isoline, it is evident that it quite resembles the DNS isoline. More precisely, the upper line almost coincides with the DNS isoline for $x < 1.5\text{ mm}$, while the lower line accurately predicts the position ($x \approx 2\text{ mm}$) at which the DNS isoline starts to be located on the lower wall. However, a detailed discussion of the FINE/Open results will be presented in the subsequent section.

The FLUENT isoline exhibits a big contrast when compared to the DNS and FINE/Open results. This observation is further substantiated by Figure 4.2, where the complete temperature fields of FINE/Open and FLUENT are presented.

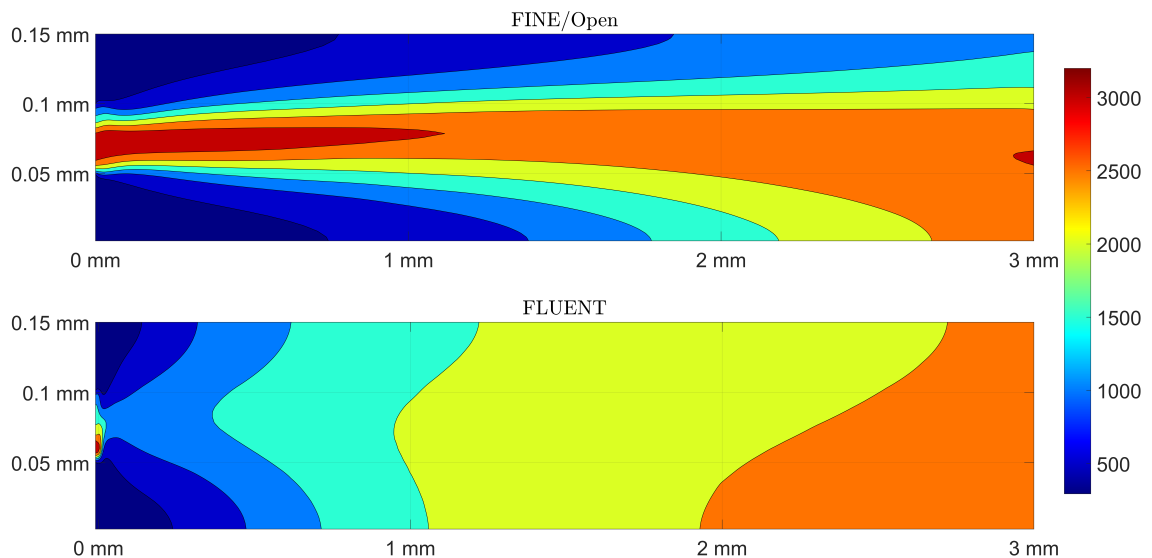


Figure 4.2: FINE/Open vs FLUENT temperature fields.

It is evident that the temperature field in FLUENT exhibits less variability in the vertical direction when compared to FINE/Open. This can be attributed to the Flamelet model

tabulation, which results in the temperature field being strictly dependent on the mixture fraction and its variance². Figure 4.3 illustrates that the mixture fraction trend in FLUENT exhibits a more rapid evolution in the axial direction as compared to FINE/Open, indicating that the fuel and oxidizer streams are more mixed. Consequently, there exists a significantly large region ($x > 1 \text{ mm}$) in FLUENT where the mixture fraction is confined between 0.2 and 0.4, whereas in FINE/Open, for example at $x = 2 \text{ mm}$, the mixture fraction varies from 0 to 0.7. The temperature field in FLUENT mirrors this condition by exhibiting a more uniform progression, characterized by an almost constant vertical profile with a small increase in absolute value along the axial direction.

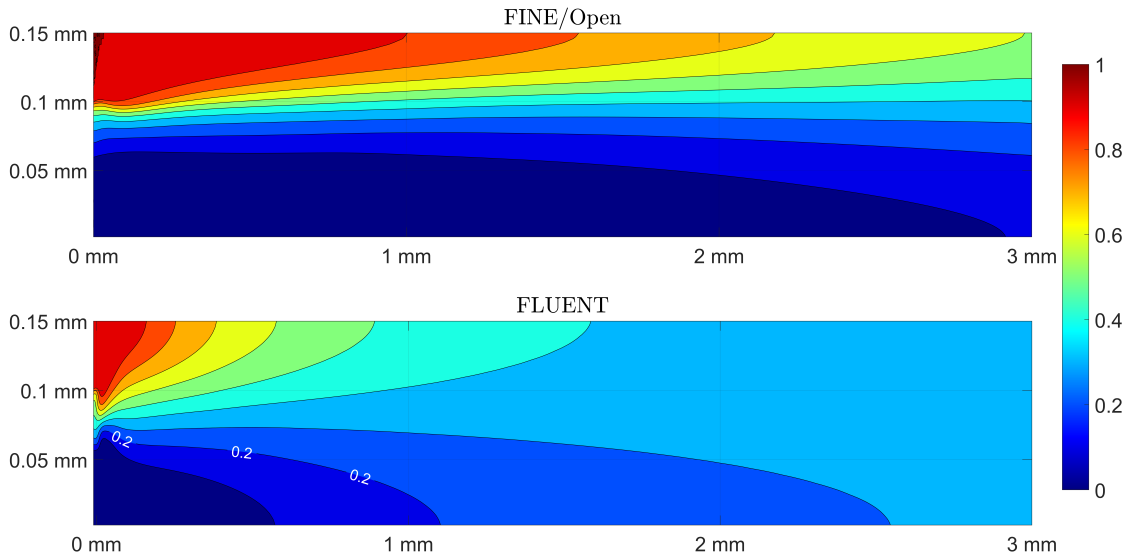


Figure 4.3: FINE/Open vs FLUENT mixture fraction fields.

Before investigating the enhanced mixing, it is crucial to highlight that the temperature field in FLUENT attains significantly low values at the stoichiometric mixture fraction. Specifically, the isoline corresponding to $Z = 0.2$ vanishes at approximately $x = 1 \text{ mm}$, and the maximum temperature achieved before this location is about 1500 K . This is due to a greater mixture fraction variance in FLUENT in comparison to FINE/Open. As a matter of fact, temperatures corresponding to $Z = 0.2$ in FINE/Open are considerably higher. A comparison between mixture fraction variance fields is presented in figure A.3.

The process of mixing is governed by the transport equation of mixture fraction, and the accurate modeling of this equation is essential for an accurate representation of the

²The influence of the stoichiometric scalar dissipation rate [Eq.1.37] is not considered, as its behavior is found to be quite analogous in both software simulations.

process. The equations for mixture fraction in FINE/Open and FLUENT, given by Equation 2.7 and Equation 2.11, respectively, differ only in the modeling of the diffusivity coefficient³. A comparison of the diffusion coefficients used by FINE/Open and FLUENT, as shown in Figure 4.4, reveals that FLUENT employs higher values throughout the field, resulting in a more widespread mixture fraction field.

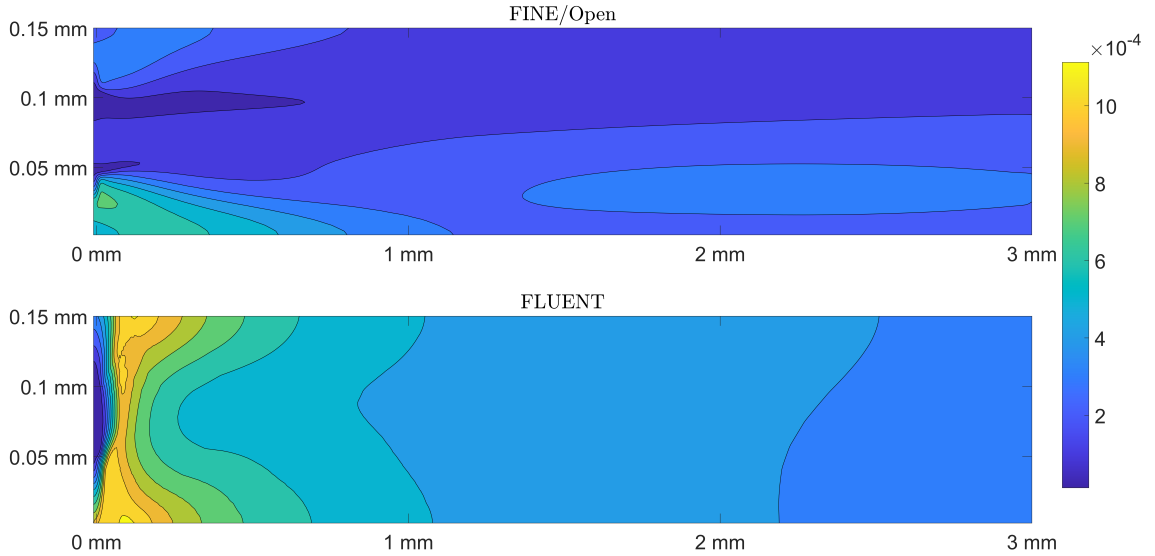


Figure 4.4: FINE/Open vs FLUENT effective diffusivity coefficient fields.

Examining the specific modeling of the coefficient, it was found that the turbulent contribution of the diffusivity coefficient D_t in FLUENT is greater than the overall diffusivity coefficient in FINE/Open. This discrepancy is attributable to the k and ϵ fields, as D_t is proportional to the turbulent eddy viscosity μ_t . Thus, in FLUENT, a higher k field [Fig.A.4] combined with a comparable ϵ field [Fig.A.5], from an order of magnitude perspective, culminated in a higher μ_t value and consequently a higher D_t value. A further discussion could be carried out regarding the turbulence model used. It could be argued that in light of the comparison with DNS data, the k - ϵ model implemented in FINE/Open provides a more realistic estimation. This assertion will also be corroborated in the subsequent section. The reason for this might be attributed to the incorporation of the Yang-Shih and Yap correction terms in Equation 2.2. Therefore, to achieve more realistic outcomes in FLUENT, a different turbulence model selection could prove beneficial. However, to ensure a consistent comparison between the software, it was imperative to employ the same turbulence model.

In conclusion, the results obtained from FLUENT are not taken into consideration in the

subsequent sections due to the aforementioned rationale, which resulted in significantly divergent outcomes from DNS [Fig.4.1].

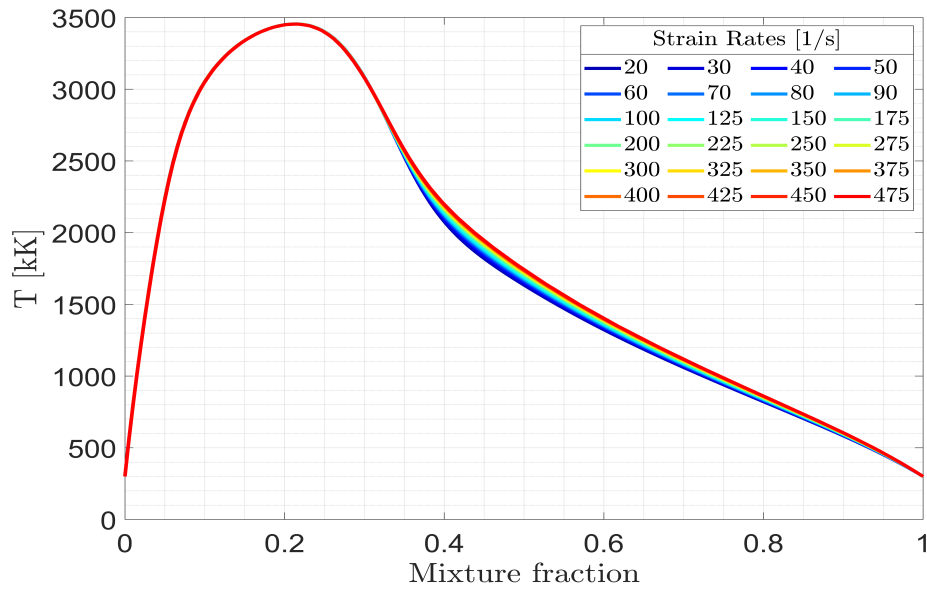
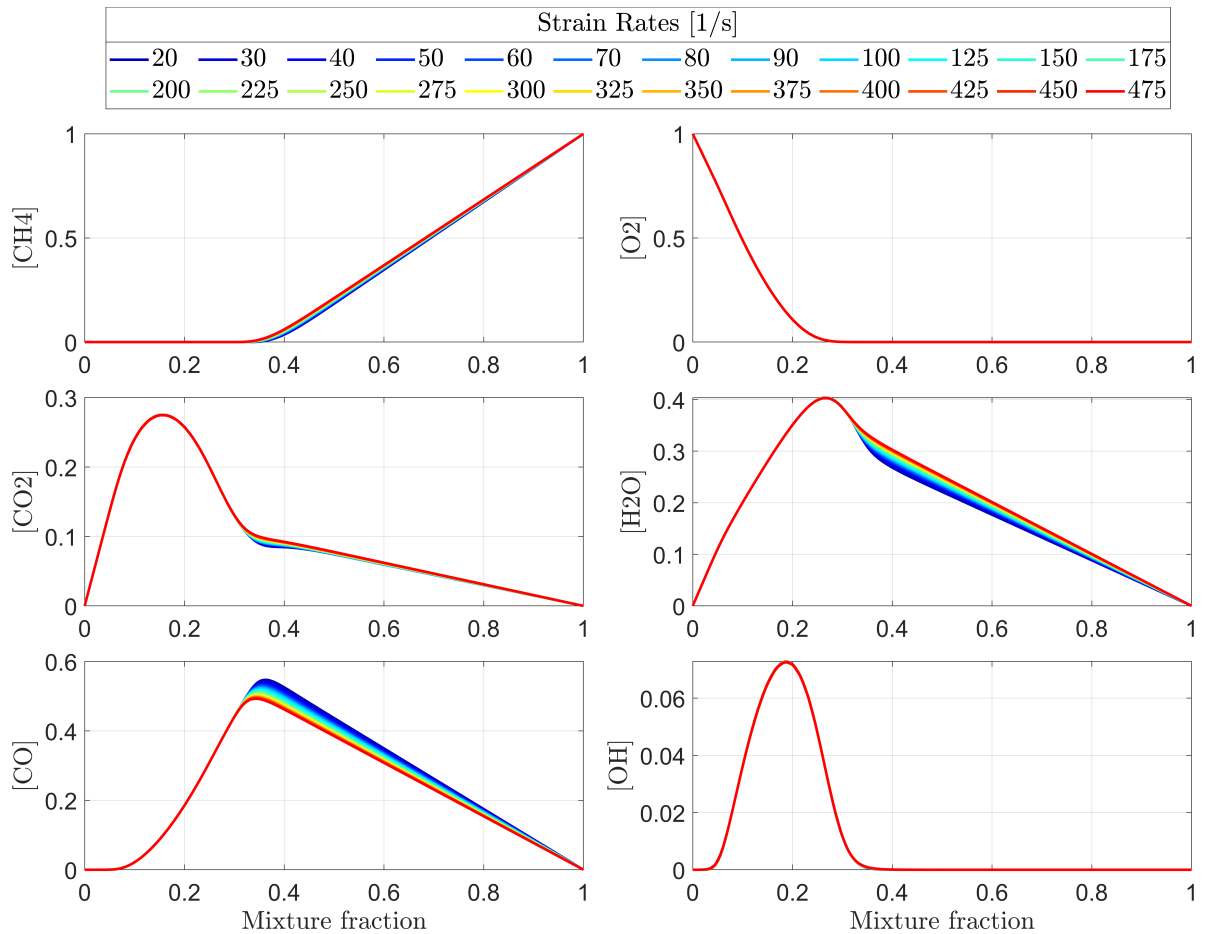
4.3. Flamelet results

This section aims to present and examine the results obtained from the FINE/Open Flamelet model. Firstly, a summary of the laminar Flamelet tables computed with TabGen/Chemistry will be presented. Subsequently, the consistency of the outcomes concerning the Flamelet model will be discussed. Finally, a comparison with DNS data will be provided.

Figure 4.5 depicts the temperature profiles computed in the Flamelet library as a function of the mixture fraction and parameterized concerning the strain rate for a constant pressure level of $2e6 Pa$. It is apparent that the maximum temperature is attained at $Z \approx 0.2$, which corresponds to the stoichiometric condition. In cases of pure oxidizer ($Z = 0$) and pure fuel conditions ($Z = 1$), there are no chemical reactions, and thus the temperature remains unchanged at $300 K$. Examining the variation of the strain rate value, it can be observed that for the range of strain rates considered, the temperature profile is largely unaffected when $Z < 0.3$. In the remaining region, temperature values tend to increase for higher values of a , resulting in flatter profiles. Although not discernible from this figure, the maximum temperature slightly decreases with higher strain rates. The quality of this table can be verified by comparing the results with those of [18].

Figure 4.6 shows the mass fraction profiles for the main species involved in the chemical reaction. It is expected that an increase in the scalar dissipation would result in a larger effective diffusivity, allowing CH_4 molecules to enter oxidizer-rich domains ($Z < 0.2$) at larger a values. This behavior is reflected in the mass fraction of CH_4 , which increases for higher dissipation values. The concentrations of other species should also reflect this trend. This is due to the fact that less methane reacts, resulting in less mass being available for the formation of products and intermediate species. The mass fractions of CO clearly decreases as the strain rate becomes larger for the whole mixture fraction range. The observed behavior of CO_2 and H_2O remains valid for mixture fractions below 0.3, and its effect would be even more noticeable if the range of strain rates considered during the generation of laminar Flamelet tables reached the quenching limit. Additionally, the behavior is also present for mixture fractions above 0.3, particularly when the strain rate is higher than approximately $1e5 \frac{1}{s}$. The validity of this behavior was confirmed by examining the Flamelet tables generated using FLUENT and in [18].

³ S_m has no contribution and S_{user} is set to zero in the FLUENT simulation.

Figure 4.5: Temperature laminar Flamelet library at $P = 2e6 Pa$.Figure 4.6: Species mass fraction laminar Flamelet library at $P = 2e6 Pa$.

It must be highlighted that the tables reported are for the laminar case, therefore the integration with the Z -PDF, to include the turbulence chemistry interaction, is not included. However, these tables can be used to check the consistency of the Flamelet results due to a really low mixture fraction variance field, as it can be seen in figure A.3. Operatively, it means that Z -PDFs resemble gaussian distributions centered in the corresponding mixture fraction values. Hence, the shape of the laminar profile is not affected. In order to verify the consistency of the temperature field with the Flamelet tables vertical profiles of temperature, mixture fraction and strain rate are shown for different axial positions in figure 4.7. All the profiles are normalized with respect to the maximum value attained for each variable, which are reported in table 4.1.

	$x = 1 \text{ mm}$	$x = 1.5 \text{ mm}$	$x = 2 \text{ mm}$	$x = 2.5 \text{ mm}$
Strain rate [1/s]	10180	9238	7785	6300
Temperature [K]	3031	2945	2942	2961

Table 4.1: Maximum profile values for the Flamelet case.

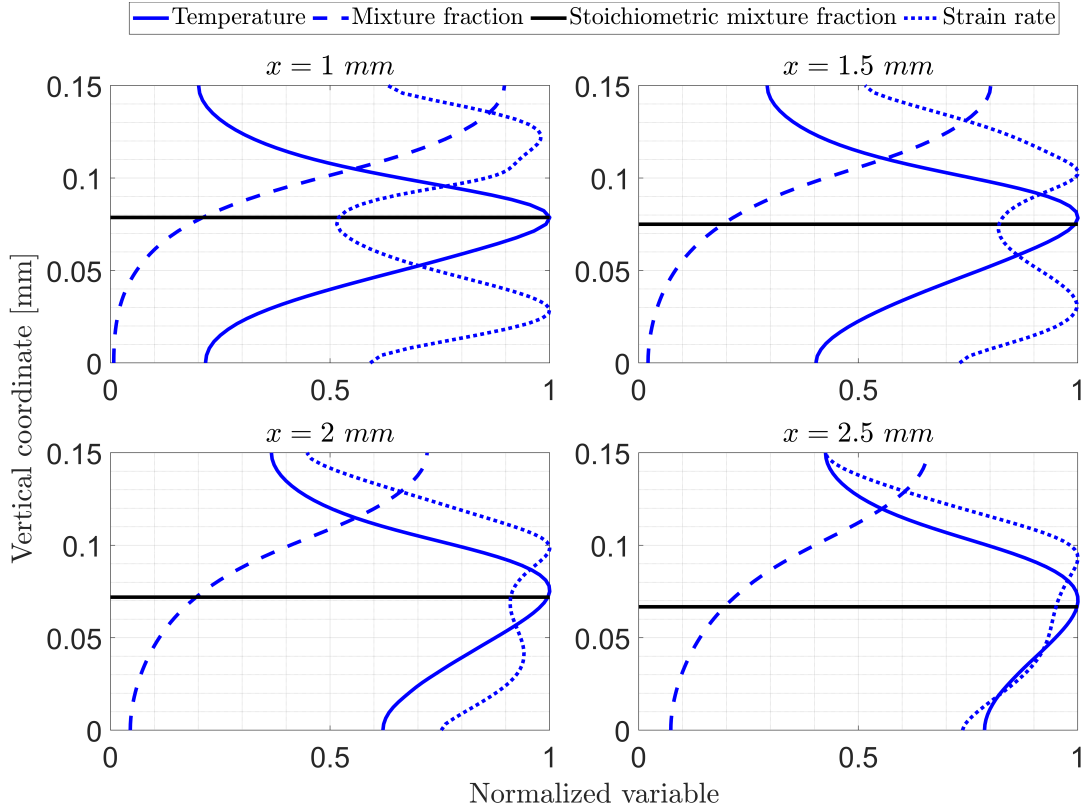


Figure 4.7: Flamelet vertical profiles for different axial positions.

The temperature profiles in the system were observed to peak at a mixture fraction of around 0.2, which is in line with expectations. In general, the effect of the strain rate increment consists in increasing the transport of heat and intermediate species away from the flame, leading to a reduction of the flame temperature. However, it was determined that the strain rate in the examined profiles exceeded $500 \frac{1}{s}$, meaning that only the temperature table computed for $a = 500 \frac{1}{s}$ was used in the software, due to its zero-order interpolation implementation. If the strain rate field had been lower than this value, small temperature increases would have been observed in the proximity of stoichiometric conditions, while fuel-rich conditions would have seen a slight temperature decrease. . In conclusion, it can be stated that the combustion process develops in the axial direction, with the temperature profile flattening out as a result of increased mixing, as evidenced by the flattening of the mixture fraction profile.

It is important to note that the use of the Slavinskaya chemical mechanism [28] instead of GRI-Mech 3.0 in FINE/Open may lead to slightly different predictions in the species mass fractions fields, which could affect the comparison with DNS results.

The comparison between FINE/Open and DNS mass fraction profiles of CH₄, O₂, CO₂, H₂O, CO, and OH is presented for different axial positions in figure 4.8. FINE/Open mixture fraction profile is also plotted and its consistency with respect to the mass fraction tables was verified [Fig. 4.6]. The difference in species profiles shapes between FINE/Open and DNS results is a direct consequence of the mixture fraction dependence.

By a first visual examination, it can be observed that as the flow goes through the outlet, FINE/Open results become less accurate compared to DNS. At the first axial position $x = 1 \text{ mm}$, the Flamelet model predicts all the species profiles quite well. However, from $x = 1.5 \text{ mm}$, FINE/Open and DNS results start to diverge. Looking at the DNS CH₄ and O₂ profiles, it is evident that methane is present with higher mass fraction in the oxygen stream and vice versa. This means that the mixing process in DNS is more developed, leading to more uniform profiles of intermediates and products along the vertical direction because the reaction is taking place in a wider region. This observation is applicable to $x = 2 \text{ mm}$ and $x = 2.5 \text{ mm}$, where the consumption of reactants and the flattening of products and intermediates profiles is even more evident. However, also Flamelet profiles flatten as they evolve in the axial direction, but the overall mixing is not comparable with DNS. This is particularly evident for the H₂O profile. In conclusion, to obtain better matching with DNS results, it can be stated that the mixture fraction profile in FINE/Open should decrease more rapidly. Therefore the mixture fraction transport equation is underestimating the mixing process in the Flamelet simulation.

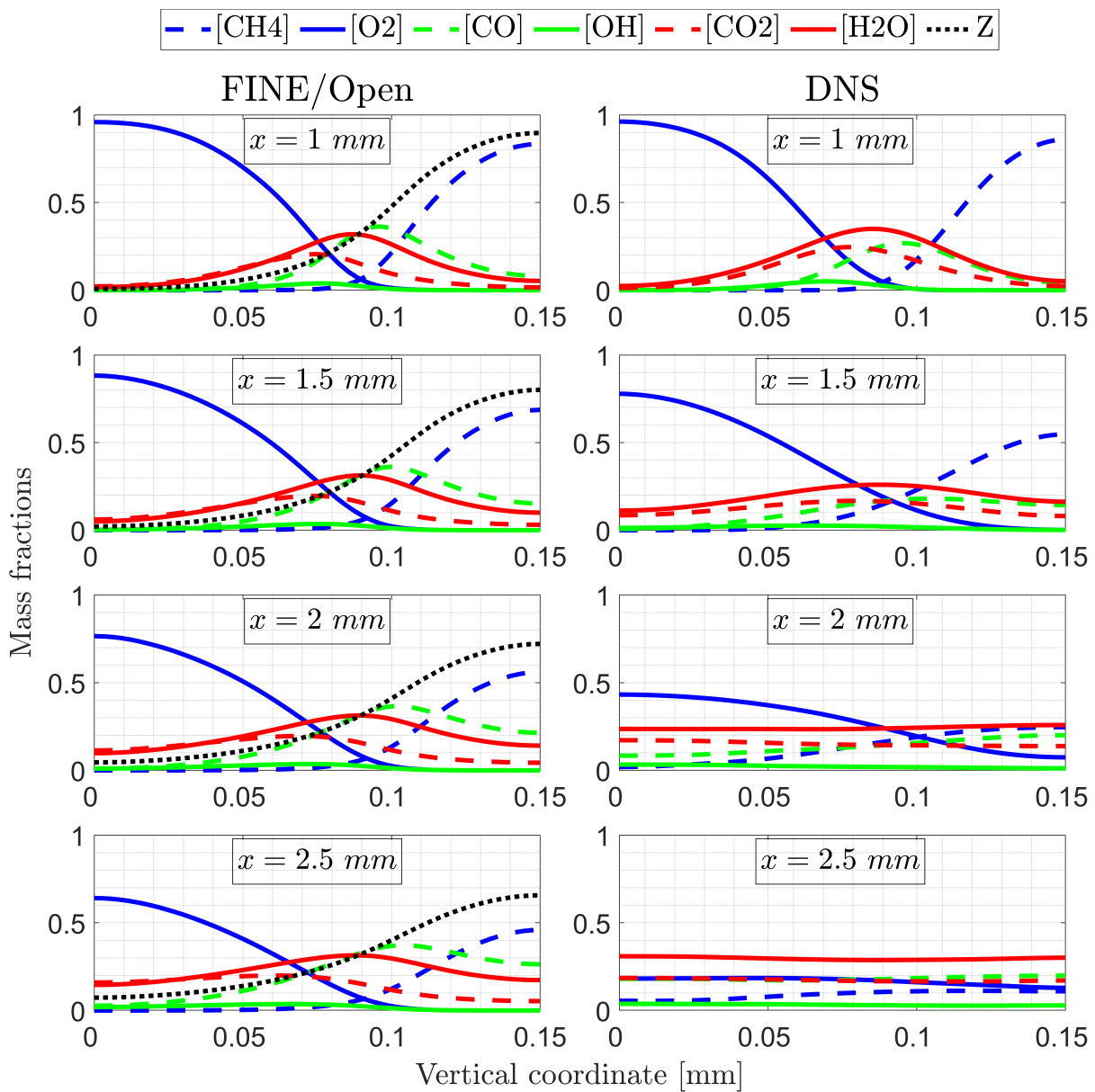


Figure 4.8: Flamelet mass fractions profiles for different axial positions.

The comparison between Flamelet temperature and mass fractions fields and DNS isolines is presented in the following analysis. Figure 4.9 illustrates the temperature field along with the superimposed DNS isoline computed at a temperature of 1500 K. A strong agreement between the upper isoline of the DNS and the Flamelet model can be observed up to an axial position of $x = 1.2 \text{ mm}$, whereas for the lower isoline, the discrepancy is higher despite its ability to accurately replicate the location where the level is exceeded on the lower wall. The DNS isoline for both its upper and lower parts is found to be closer to the upper and lower wall, respectively, compared to the Flamelet isoline. For each axial position, vertical coordinates below the upper isoline and above the lower isoline are associated with temperatures higher than the isolevel under consideration in the DNS. Therefore, the Flamelet computation exhibits less developed combustion process in the vertical direction, and this is attributed to the lower estimation of the mixing process in FINE/Open, as discussed earlier.

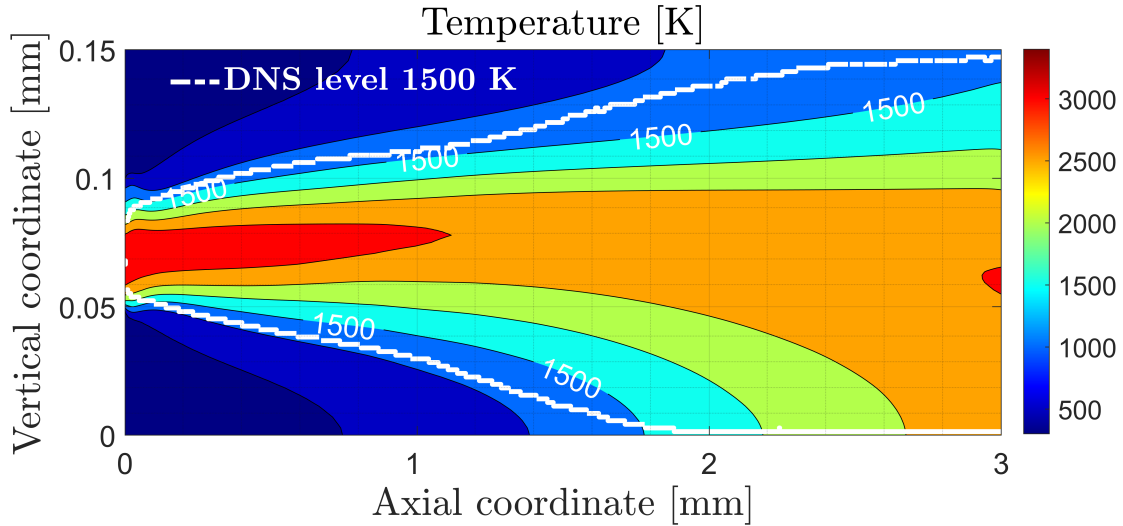


Figure 4.9: Flamelet temperature field.

The mass fraction fields of CH₄, O₂, and H₂O computed with FINE/Open are presented in Figure 4.10. The DNS isolines for CH₄ and O₂ show a good match with the Flamelet computation until $x \approx 1.5 \text{ mm}$, after which they start to significantly diverge. This divergence is not a mistake in the Flamelet computation but rather a consequence of the method used to calculate DNS isolines, as explained in Section 4.1. The mass fraction profiles of CH₄ and O₂ are both below 0.5 for $x = 2 \text{ mm}$ and $x = 2.5 \text{ mm}$ [Fig. 4.8]. However, despite this, the DNS approach can still be considered valid. This is because the DNS approach accounts for turbulence fluctuations, and it is possible that for some specific time steps, the isolevel was reached despite the final lower mass fraction values. The H₂O mass fraction field shows that the chosen isolevel of 0.15 is exceeded at each axial

position [Fig. 4.8], indicating that the DNS isoline matches well with the Flamelet isoline throughout the field. Additionally, both parts of the DNS isolines for H₂O are closer to the walls than the Flamelet isolines, which is consistent with the previous analysis of the temperature field. Since H₂O is one of the main combustion products, it is expected that lower mass fractions would be computed in the Flamelet simulation due to a less developed combustion process in the vertical direction compared to DNS. Figure 4.11 displays the CO₂ field along with OH and CO fields.

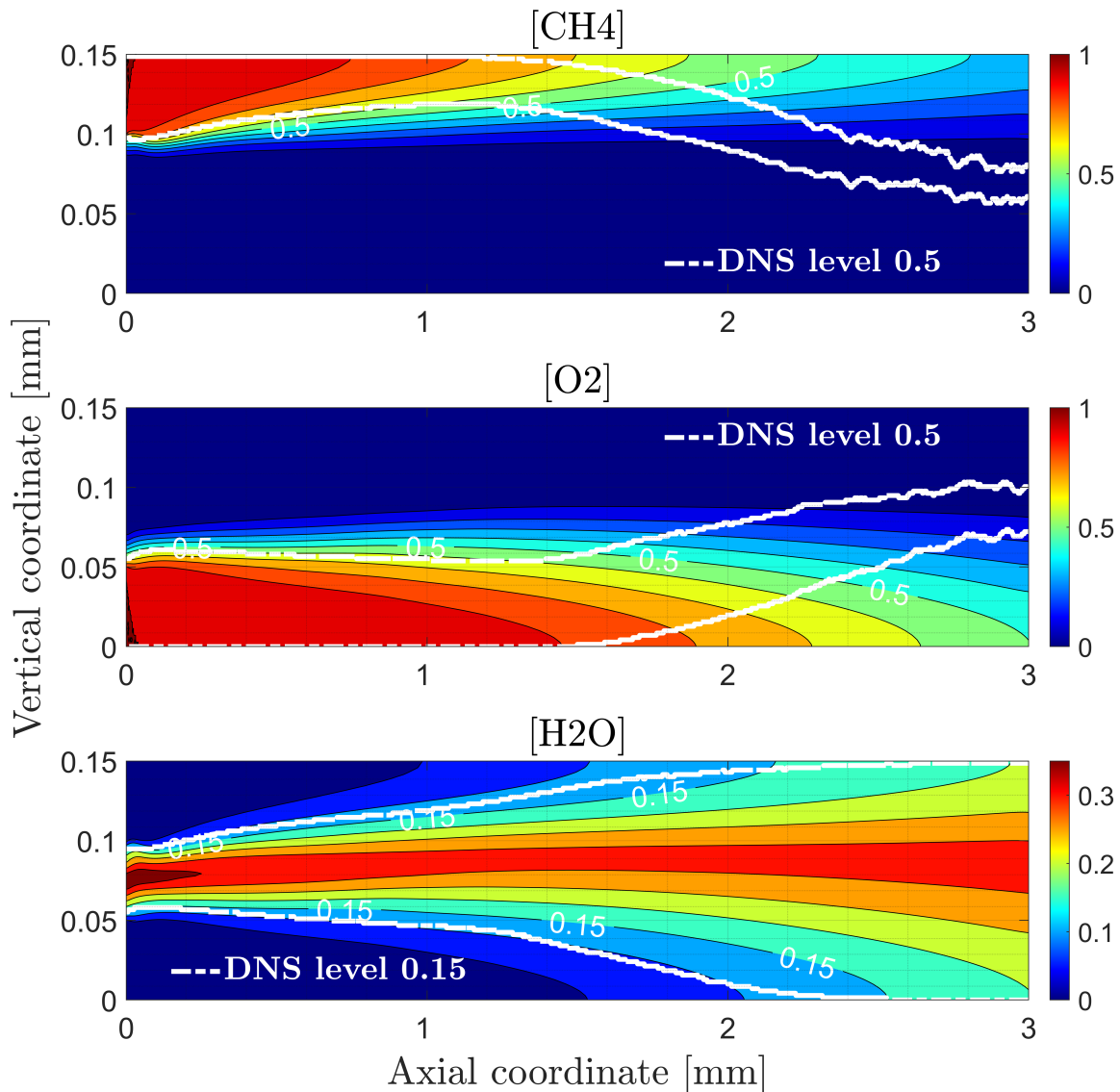


Figure 4.10: Flamelet mass fraction fields.

Concerning CO₂, it can be observed that the upper DNS isoline can be explained with

the same justification presented for H₂O. However, the lower part is inconsistent, and a possible explanation for this discrepancy could be the implementation of different chemical mechanisms in the two simulations. This indicates that the CO₂ mass fraction is being described differently in the Flamelet table compared to the finite rate approach utilized in DNS. The appearance of reaction intermediates can be used to evaluate the fidelity of the Flamelet tables as they are more sensitive than the products, indicating whether the chemical evolution is calculated similarly to DNS. However, discrepancies with the DNS simulation can also be related to the diffusion phenomenon, making it difficult to distinguish the actual cause.

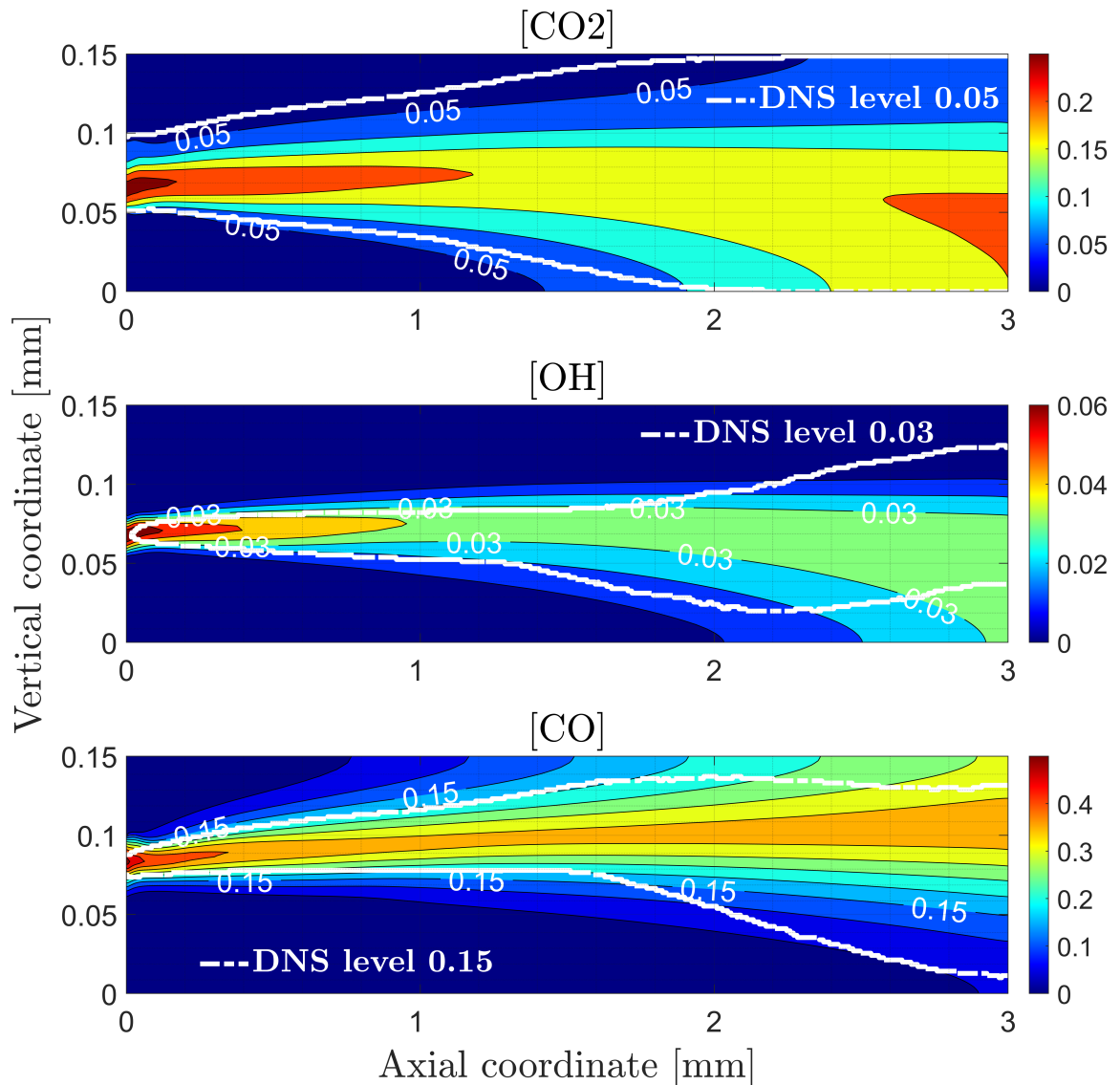


Figure 4.11: Flamelet mass fraction fields.

For CO, a good agreement is observed for $x < 1.5 \text{ mm}$, but a significant divergence is observed beyond that point, which can be attributed to the heightened turbulence fluctuations in the flow. Regarding the OH field, a good matching is achieved for the upper isoline for $x < 1.8 \text{ mm}$, while an increasing divergence is observed for the lower isoline. The small molecular weight of this intermediate makes it more sensitive to diffusion, and the diffusivity assumption in the Flamelet approach may be too stringent for this species. In the subsequent chapter, a rigorous method, involving the analysis of numerous additional species, will be detailed for a further examination.

4.4. FGM results

The objective of this section is to present and analyze the results obtained using the FINE/Open FGM model. Initially, the laminar table for temperature generated using TabGen/Chemistry will be introduced. Subsequently, the accuracy of the results obtained with the FGM model will be evaluated. Finally, a comparison with the DNS data will be presented.

Figure 4.12 depicts the temperature FGM table for null mixture fraction variance. The maximum temperature value is observed at approximately $Z = 0.2$ for each value of normalized progress variable \tilde{Y} , which is expected. For $\tilde{Y} = 0$, the temperature remains constant for each value of mixture fraction, while for $\tilde{Y} = 1$, the temperature value is the highest for each value of Z . Similar to the Flamelet case, the mixture fraction variance field has low values, implying that the turbulent FGM table considered in this computation is comparable to the laminar one.

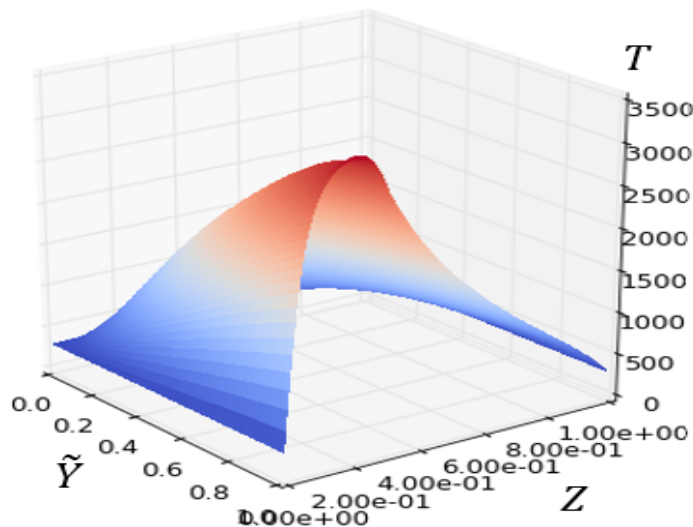


Figure 4.12: FGM temperature table.

Figure 4.13 illustrates vertical profiles of temperature, mixture fraction, strain rate, and normalized progress variable to assess the consistency with the applied FGM table. Table 4.2 reports the maximum values used to normalize the profiles. The progress variable profiles are normalized using equation 2.16 where $Y_{min}(Z) = 0.9 \frac{mol}{Kg}$ and $Y_{max}(Z) = 26.4 \frac{mol}{Kg}$. Notably, in this approach, the strain rate dependence is incorporated into the progress variable using a remapping technique. However, the strain rate profiles are still presented to demonstrate their relationship with the temperature profile.

	$x = 1 \text{ mm}$	$x = 1.5 \text{ mm}$	$x = 2 \text{ mm}$	$x = 2.5 \text{ mm}$
Strain rate [1/s]	10748	9703	7981	6489
Temperature [K]	2983	2907	2913	2942

Table 4.2: Maximum profile values for the FGM case.

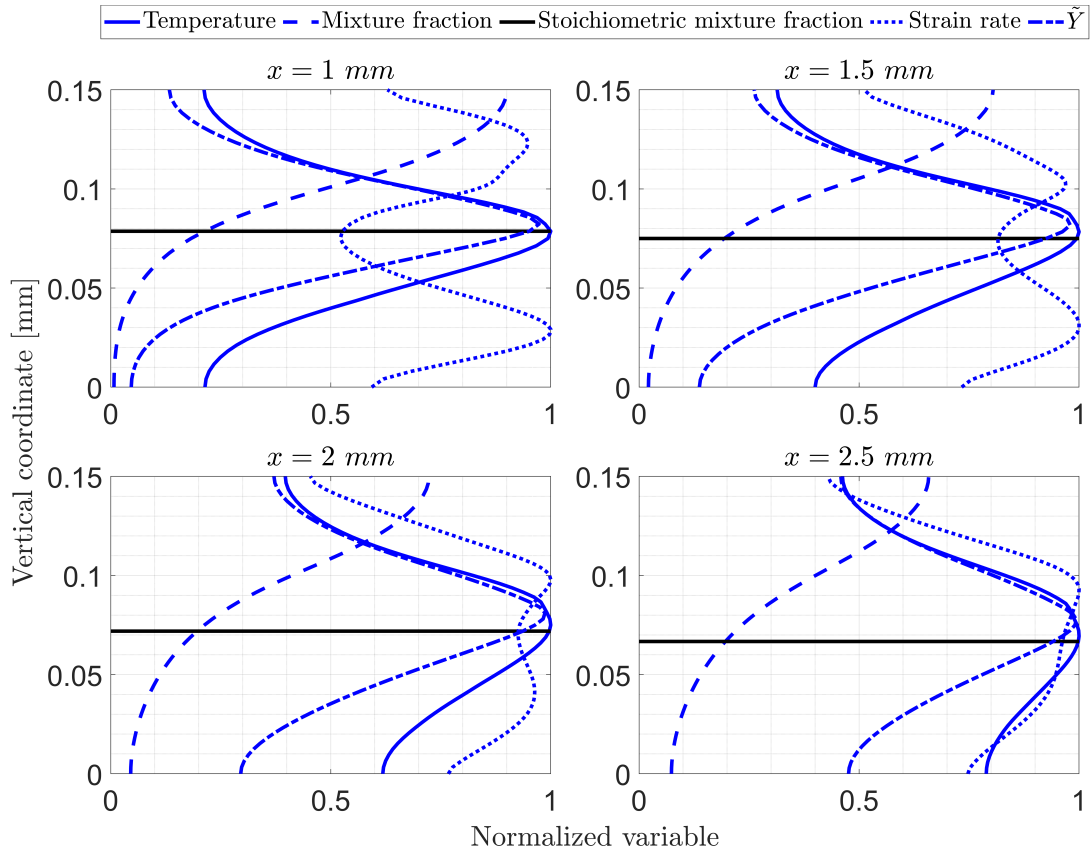


Figure 4.13: FGM vertical profiles for different axial positions.

The temperature profile follows the expected trend, with a maximum at the stoichiometric mixture fraction and the maximum value of the progress variable. Additionally, it

is observed that the temperature and the progress variable profiles flatten out as they approach the outlet. This behavior is attributed to the vertical development of the combustion process as it progresses towards the outlet.

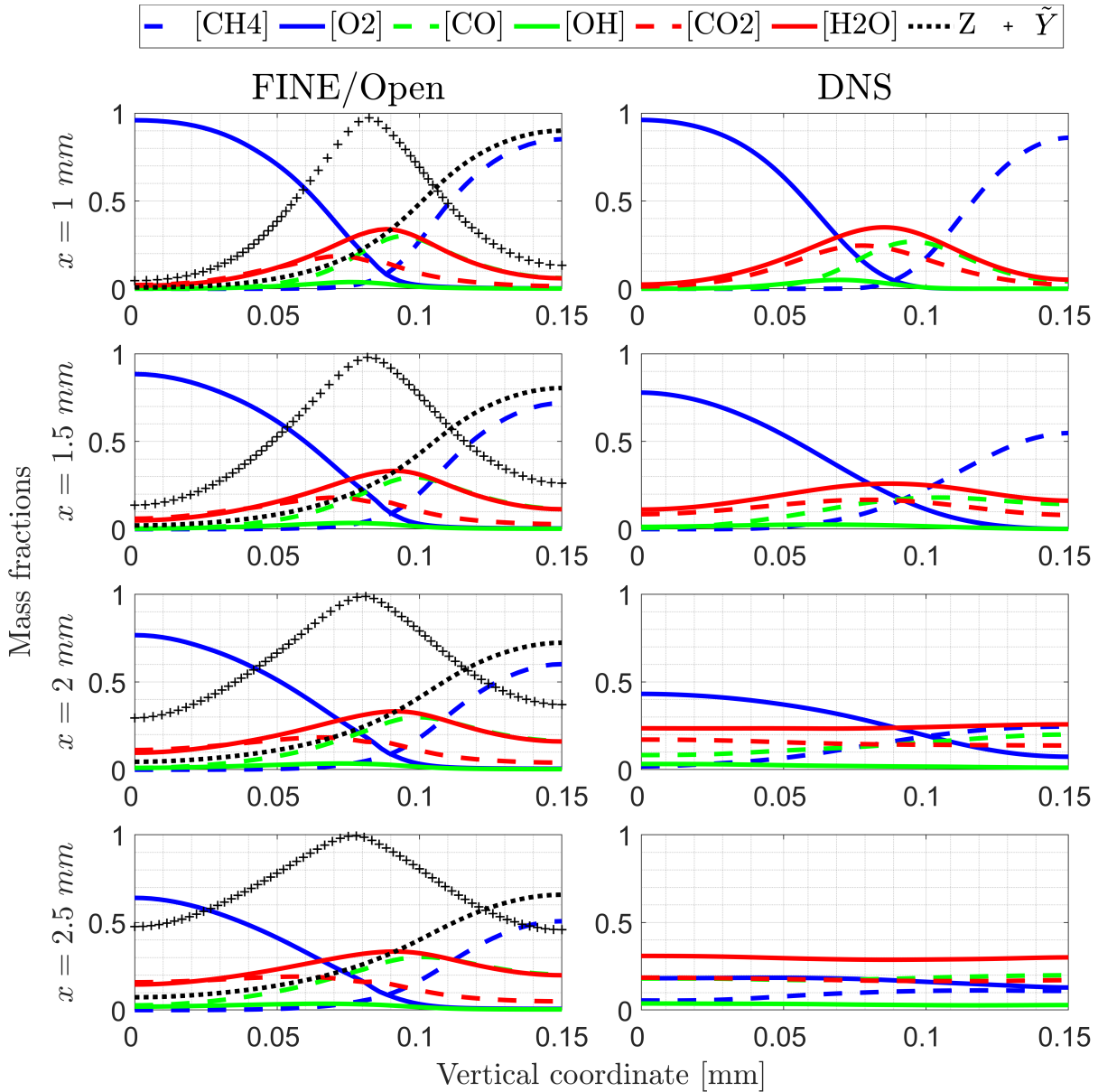


Figure 4.14: FGM mass fractions profiles for different axial positions.

The main species' mass fraction profiles at different axial positions are compared with the DNS simulation in Figure 4.14, similar to the Flamelet analysis. In addition, normalized progress variable profiles are plotted for the FINE/Open representation. The maximum of the progress variable is expected to be within a vertical coordinate range limited by the maximum of CO and CO₂ mass fraction profiles. This condition is confirmed in

Figure 4.14. Moreover it can be seen that the integral of the normalized progress variable increases going towards the outlet. This is due to the fact that CO and CO₂ mass fractions are increasing as combustion is developing. Regarding the comparison with DNS results, similar to the Flamelet case, it can be observed that the mixing process is underestimated in FINE/Open as it progresses towards the outlet. Consequently, the products and intermediates of the reaction exhibit less uniform profiles along the vertical coordinate. Based on this brief analysis, it can be concluded that the addition of the progress variable transport equation does not provide a better estimation for the mixing process.

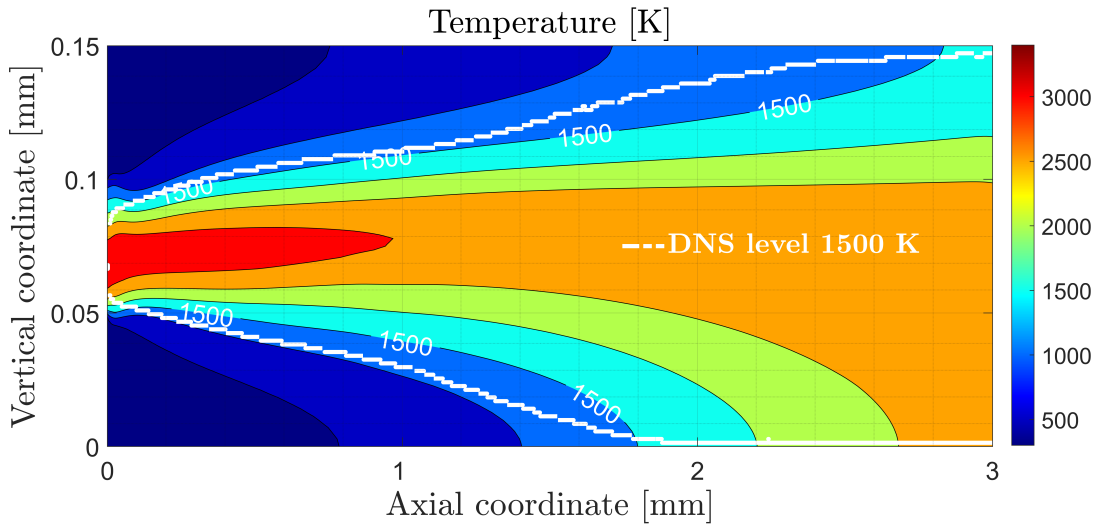


Figure 4.15: FGM temperature field.

The FGM temperature field is shown in Figure 4.15, along with DNS isolines computed for a temperature of 1500 K. The temperature field appears to be quite similar to the Flamelet one, but there are some differences. The FGM isoline corresponding to a temperature of 3000 K extinguishes before $x = 1$ mm, whereas the Flamelet isoline does not. Additionally, the FGM temperature does not reach the same level as the Flamelet simulation in proximity to the outlet. These differences can be attributed to the dependence of the temperature FGM tables on the progress variable. There is good agreement between the upper DNS isoline and the FGM simulation for $x < 1.2$ mm, but a poorer matching is observed for the lower isoline. Anyhow, as in the Flamelet case, the position on the lower wall in which the level is overcome is well estimated. The motivation of the different behavior of FGM with respect to DNS is the underestimation of mixing. It can be observed from figure 4.16 that the FGM simulation shows good agreement with the DNS for the reactants fields. Specifically, for CH₄, the lower DNS isoline begins to diverge at $x = 1.1$ mm, while for O₂, the upper isoline begins to diverge at $x = 1.2$ mm.

As the simulation progresses towards the outlet, the DNS isolines exhibit a completely different behavior due to the turbulent fluctuations of the DNS computation. For H₂O, a good agreement is achieved for the upper isoline, while the lower DNS isoline is closer to the lower wall, indicating a higher mass fraction with respect to the FGM simulation. This can be attributed to the higher development of the combustion process, leading to higher concentrations of products. Overall, the FGM simulation shows an improvement in the H₂O estimation compared to the Flamelet simulation, with a better matching with the upper isoline and a higher overall field.

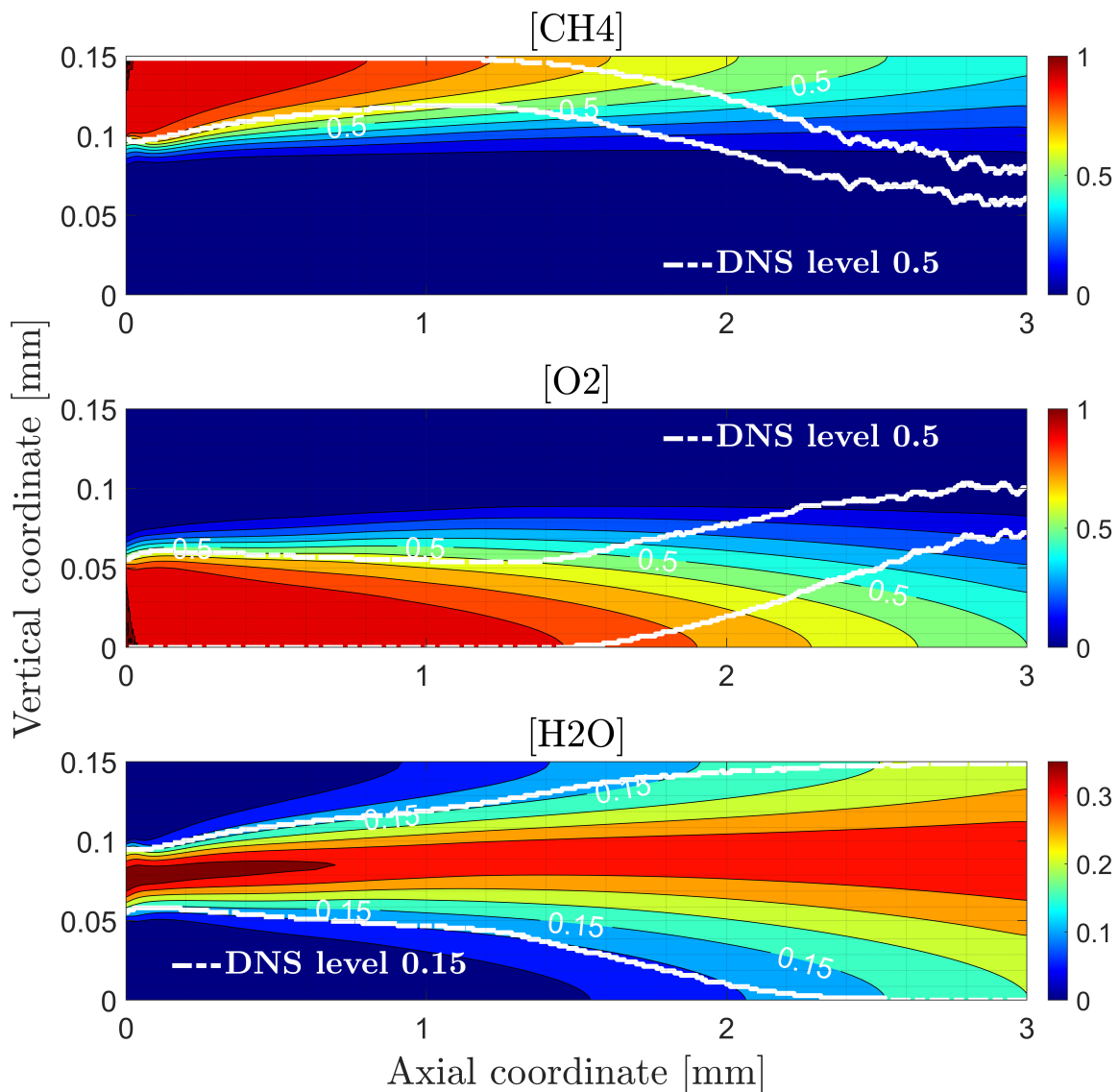


Figure 4.16: FGM mass fraction fields.

Regarding the CO₂ field, the explanation given for the H₂O can still be considered valid in relation to the upper DNS isoline. For the lower isoline, a good matching is attained for $x < 1 \text{ mm}$, even though the FGM isoline is always located closer to the lower wall. This behavior is in contrast with the previous explanation of the H₂O field. Therefore, this mismatch could be due to the different modeling of the chemical reaction in the two simulations.

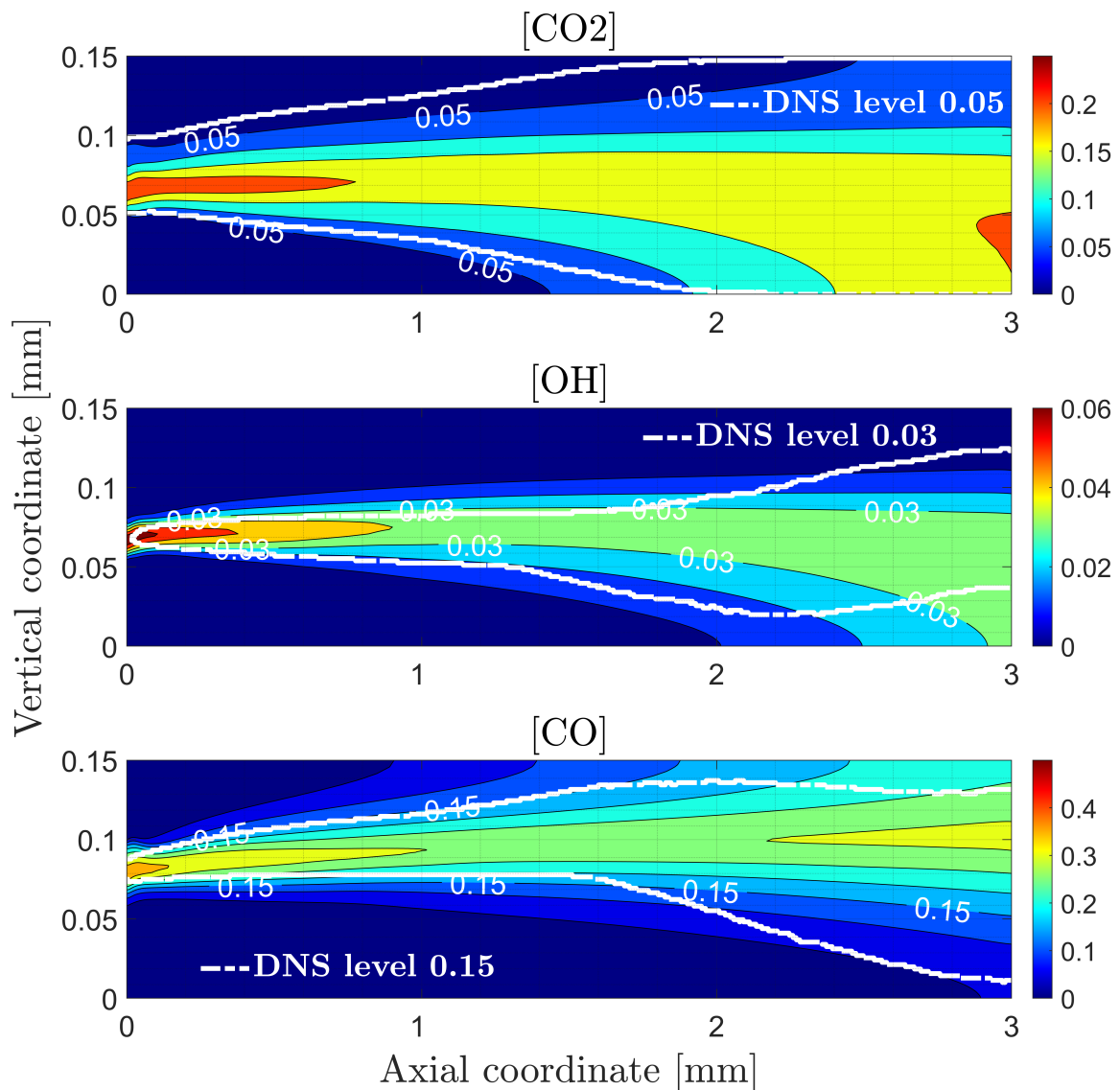


Figure 4.17: FGM mass fraction fields.

The comparison between FGM and DNS simulations reveals that the upper isoline of OH agrees well between the two methods until $x = 1.8 \text{ mm}$, whereas a growing discrepancy is observed for the lower isoline as the distance from the inlet increases. The reason for

this can be attributed to the assumption of equal diffusivities for all species in the FGM method, which is not accounted for in DNS. Conversely, there is no enhancement in the OH field using the FGM method when compared to the Flamelet simulation. In contrast, the CO estimation is significantly improved with the FGM method, with the upper DNS isoline in good agreement with the FGM one up to $x = 1.6 \text{ mm}$ and a satisfactory matching for the lower isoline for $x < 1.6 \text{ mm}$. This can be attributed to the specific modeling of the progress variable with the transport equation. Furthermore, the CO₂ field exhibits a slightly better estimation compared to the Flamelet simulation. Overall, the FGM method does not offer significant improvement in the temperature field, while it provides a better estimation of CO and H₂O.

4.5. Hybrid results

Before presenting the results of the computation using the Hybrid model, an important consideration needs to be addressed. In this model, the transport equation for the progress variable is solved for the normalized variable \tilde{Y} , which takes on a value of 0 for completely unburnt mixtures and 1 for completely burnt mixtures. In the computations using Comb3 and CombProfile, as shown in Table 3.8, \tilde{Y} was set to 1, indicating that the flow entering the inlet was already burnt. Several attempts were made to change this setting for a more consistent computation, but no solutions were found, indicating that the model itself requires further improvement⁴. Consequently, the entire normalized progress variable field is equal to 1, and for the computation of thermochemical quantities using equation 2.19, the contribution given by the mixing table is completely neglected.

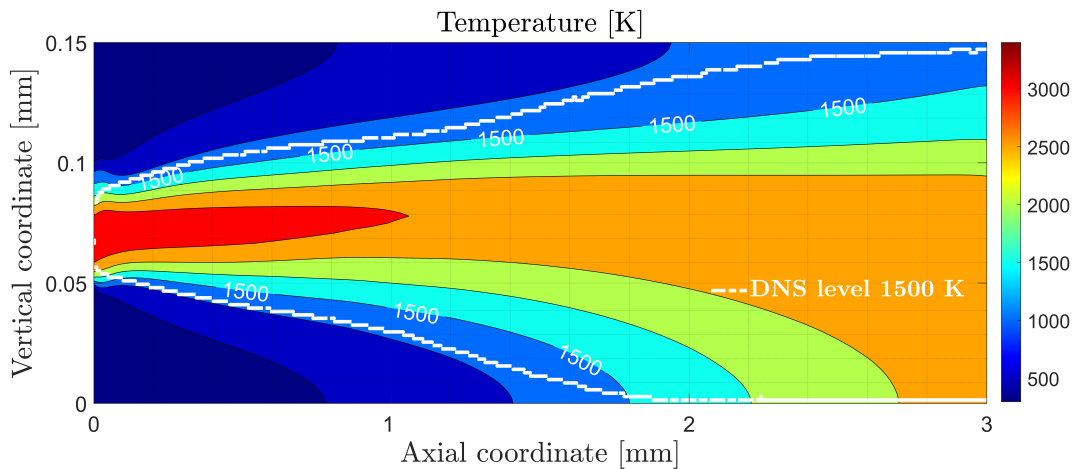


Figure 4.18: Hybrid temperature field.

⁴After a meeting with the software developers, it was concluded that further developments are needed for the Hybrid model.

Therefore the results obtained from the Hybrid model are based on the Flamelet table computed for a strain rate of $a = 100 \frac{1}{s}$, since the model did not allow for a better estimation of the normalized progress variable. Although the Flamelet library used for the Flamelet simulation included strain rates up to $500 \frac{1}{s}$, the results obtained with the Hybrid model were found to be almost equal to those obtained with the Flamelet model. This was demonstrated in previous figures, where the temperature and species mass fraction profiles were almost identical for both strain rates. To display the similarity with the Flamelet case the results obtained with the Hybrid model, are depicted in figures 4.18, 4.19 and 4.20.

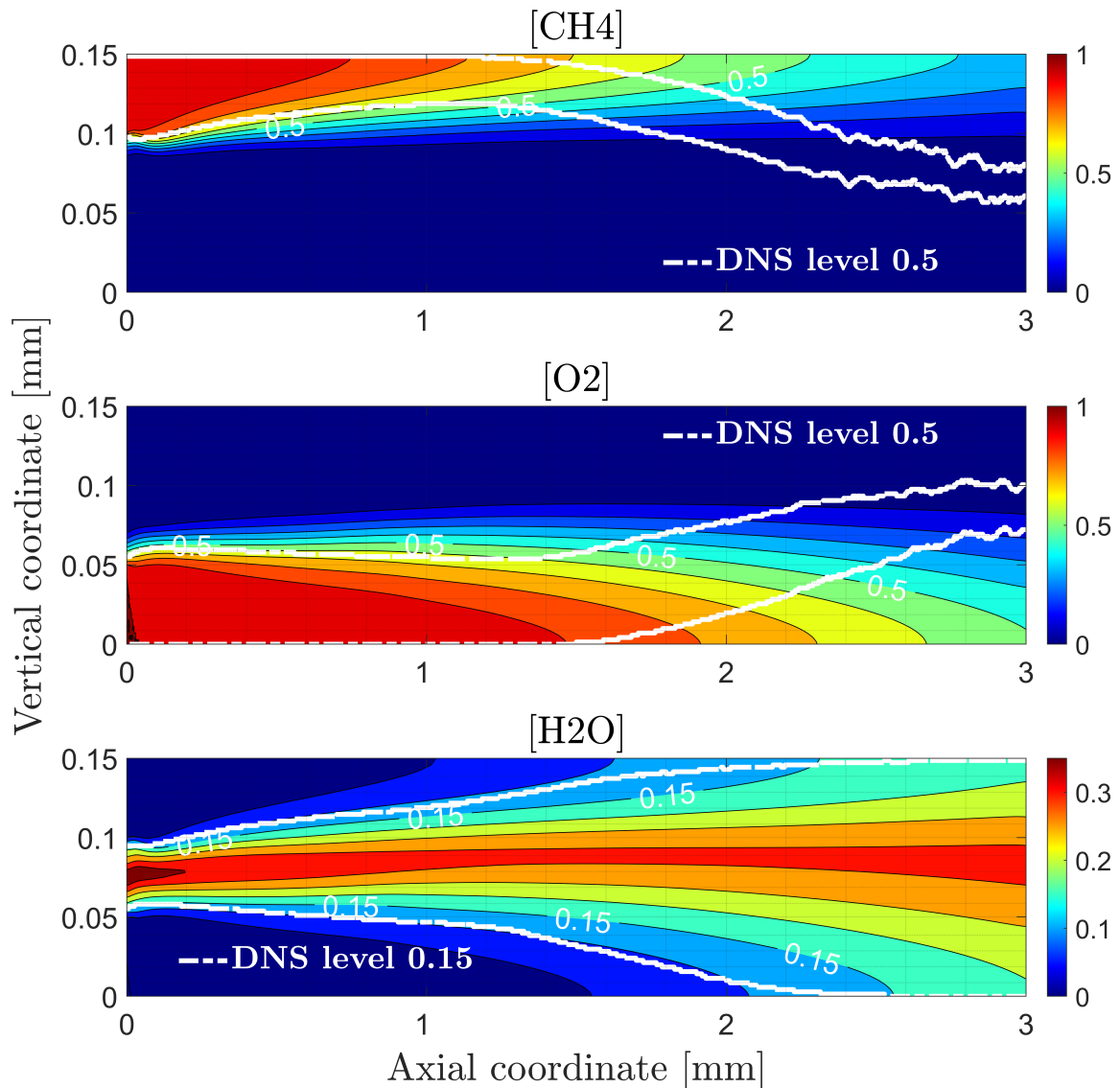


Figure 4.19: Hybrid mass fraction fields.

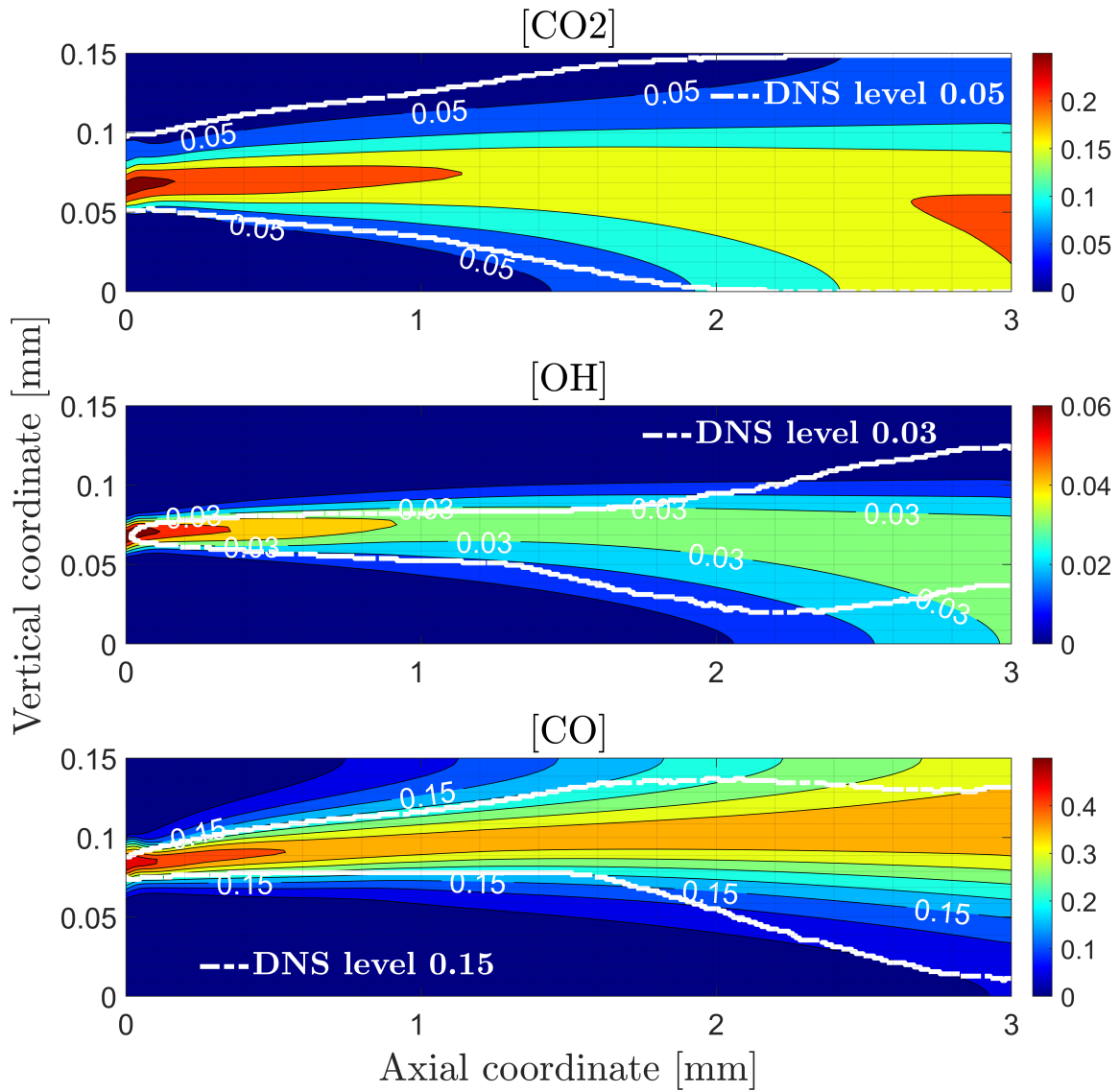


Figure 4.20: Hybrid mass fraction fields.

5 | Conclusion

The efficient modeling of methane combustion reactions is complicated due to the complex reaction mechanism involved. Finite rate chemistry modeling, although it can incorporate a large number of species, is not always precise. The Flamelet model, utilized in commercial software, overcomes this limitation by calculating the mixture fraction, variance, and strain rate in the flow field, and then interpolating the tabulated values of species' mass fractions as a function of these quantities. This reduces the turbulent combustion problem to a mixing problem, resulting in faster computational speeds. Including the strain rate in the model enables the simulation of non-equilibrium effects, which is critical for hydrocarbon combustion since chemical processes cannot be assumed to be infinitely fast.

In this study, the Flamelet combustion models available in the FINE/Open framework were employed to simulate a methane/oxygen diffusion flame. The FGM method was found to provide a better estimation of species mass fraction fields than the Flamelet simulation, while no significant improvements were observed in the temperature field. The FGM model differs from the Flamelet model by including a reaction progress variable, thus extending the mathematical model implemented. All three models were found to provide consistent results with respect to the DNS computation used for comparison. However, it is important to note that important assumptions are made during the formulation of Flamelet models, such as the equal diffusivity assumption of all chemical species and the similarity between the thermal and composition fields embedded in the unity Lewis number assumption. Despite these differences, the Flamelet model, and particularly the FGM method, can be a valuable tool for providing fast and accurate estimates of combustion fields, particularly in situations where detailed DNS simulations are not feasible due to computational limitations.

To determine whether discrepancies between computed results and DNS are due to chemical reaction modeling or the unity Lewis number assumption, two post-processing analyses can be performed.

For evaluating the accuracy of the Flamelet tables computation, a comparison can be

made between the deviation of chemical species with low and high concentration from DNS fields. Species with low mass fraction fields are more sensitive to the thermophysical condition during reaction, indicating the precision of the chemical path modeled. Higher discrepancy in low concentration species such as O or H compared to high concentration species implies the need to improve chemical modeling embedded in table generation tools. It is noteworthy that species selected for comparison should have comparable molecular weights.

Regarding the diffusion phenomenon directly linked to unity Lewis number assumption, species with lower molecular weight are more affected. Thus, a comparison between mass fraction fields of low and high molecular weight species with DNS results can demonstrate the assumption's validity in this specific case. For instance, H and H₂ could be compared with CO. In this case the species selected for comparison should have comparable mass fraction fields.

It should be noted that the above analysis requires computation of DNS isolines for multiple levels, resulting in a significant computational effort, especially if extended to many more chemical species. Moreover, an interpolation technique is necessary to retrieve DNS profiles after computing different isolevel positions, leading to possible inaccuracies. Additionally, the FGM simulation only considers mass fraction fields of CH₄, O₂, H₂O, CO₂, OH and CO as TabGen/Chemistry generates FGM tables with only those chemical species.

To enhance the accuracy of the Flamelet model, there are two possible developments. The first one involves applying the non-adiabatic extension to the Flamelet model, as discussed in Section 1.4.2. This would introduce enthalpy-level dependence in the chemical species profiles and could potentially lead to improved representation of the chemical evolution. This reasoning could be extended to other thermochemical properties, however, this would increase the computational time required for pre-tabulation.

The second approach involves incorporating differential diffusion effects using the model proposed by Pitsch and Peters [24]. This could improve the accuracy of the estimation of low molecular weight species. While the unity Lewis number assumption is generally accurate for methane combustion, incorporating differential diffusion effects could lead to more precise results in the case of hydrogen combustion.

Bibliography

- [1] S. Adami. Introduction to turbulent flows lecture notes. Chair of Aerodynamics and Fluid Mechanics of Technical University of Munich, 2020.
- [2] K. C. Altimira. *Non-premixed Laminar and Turbulent Flames by means of Flamelet Modelling Approaches*. PhD thesis, Centre Tecnològic de Transferència de Calor Departament de Màquines i Motors Tèrmics Universitat Politècnica de Catalunya, 2005.
- [3] ANSYS. *ANSYS Fluent 2020 R2 Theory Guide*. ANSYS Inc., 2020.
- [4] J. Bauer, V. Bykov, and U. Maas. Implementation of ILDM's based on a representation in generalized coordinates. In *Conference proceedings*. European Conference on Computational Fluid Dynamics, Delft University of Technology, 2006.
- [5] R. Bilger. The structure of turbulent nonpremixed flames. *Symposium (International) on Combustion*, 22(1):475–488, 1989. ISSN 0082-0784.
- [6] K. Bray, P. Domingo, and L. Vervisch. Role of the progress variable in models for partially premixed turbulent combustion. *Combustion and Flame*, 141(4):431–437, 2005. ISSN 0010-2180.
- [7] H. Burkhardt, A. Herberitz, J. Klevanski, and M. Sippel. Kerosene vs methane: A propellant tradeoff for reusable liquid booster stages. *Journal of Spacecraft and Rockets - J SPACECRAFT ROCKET*, 41:762–769, 09 2004. doi: 10.2514/1.2672.
- [8] E. Effelsberg and N. Peters. A composite model for the conserved scalar pdf. *Combustion and Flame*, 50:351–360, 1983. ISSN 0010-2180. doi: [https://doi.org/10.1016/0010-2180\(83\)90075-5](https://doi.org/10.1016/0010-2180(83)90075-5).
- [9] T. Fiala. *Radiation from High Pressure Hydrogen-Oxygen Flames and its Use in Assessing Rocket Combustion Instability*. PhD thesis, Technische Universität München Institut für Energietechnik, 2015.
- [10] B. Ivancic, H. Riedmann, and M. Frey. Validation of turbulent combustion models for

the 3d-simulations of liquid H₂/O₂ rocket combustors. *Space Propulsion Conference*, 2012.

- [11] C. K. Law. *Combustion Physics*. Cambridge: Cambridge University Press, 2006.
- [12] D. Lee, S. Thakur, J. Wright, M. Ihme, and W. Shyy. Characterization of flow field structure and species composition in a shear coaxial rocket GH₂/GO₂ injector: Modeling of wall heat losses. *47th AIAA/ASME/SAE/ASEE Joint Propulsion Conference and Exhibit 2011*, 07 2011. doi: 10.2514/6.2011-6125.
- [13] J. Lin, J. West, R. Williams, P. Tucker, and J. Chenoweth. *CFD Code Validation of Wall Heat Fluxes for a GO₂/GH₂ Single Element Combustor*. doi: 10.2514/6.2005-4524.
- [14] B. Marracino and D. Lentini. Radiation modelling in non-luminous nonpremixed turbulent flames. *Combustion Science and Technology*, 128(1-6):23–48, 1997. doi: 10.1080/00102209708935703.
- [15] D. Martinez. A flame control method for direct numerical simulations of reacting flows in rocket engines. Master’s thesis, Technical University of Munich, 2021.
- [16] NUMECA. *THEORY GUIDE - FINE/Open with OpenLabs 11.1*. NUMECA, 2022.
- [17] NUMECA. *USER GUIDE - FINE/Open with OpenLabs 11.1*. NUMECA, 2022.
- [18] N. Perakis. *Flamelet Modeling and Simulation of CH₄/O₂ Rocket Thrust Chambers*. PhD thesis, Technical University of Munich, 2016.
- [19] N. Perakis, C. Roth, and O. J. Haidn. Development of a non-adiabatic flamelet model for reacting flows with heat loss. In *Space Propulsion Conference*, volume 2018, 2018.
- [20] N. Perakis, D. Rahn, O. J. Haidn, and D. Eiringhaus. Heat transfer and combustion simulation of seven-element O₂/CH₄ rocket combustor. *Journal of Propulsion and Power*, 35(6):1080–1097, 2019.
- [21] N. Peters. Laminar diffusion flamelet models in non-premixed turbulent combustion. *Progress in Energy and Combustion Science*, 10(3):319–339, 1984. ISSN 0360-1285. doi: [https://doi.org/10.1016/0360-1285\(84\)90114-X](https://doi.org/10.1016/0360-1285(84)90114-X).
- [22] N. Peters. Laminar flamelet concepts in turbulent combustion. *Symposium (International) on Combustion*, 21(1):1231–1250, 1988. ISSN 0082-0784. doi: [https://doi.org/10.1016/S0082-0784\(88\)80355-2](https://doi.org/10.1016/S0082-0784(88)80355-2). Twenty-First Symposium (International on Combustion).

- [23] N. Peters. *Turbulent Combustion*. Cambridge Monographs on Mechanics. Cambridge University Press, 2000. doi: 10.1017/CBO9780511612701.
- [24] H. Pitsch and N. Peters. A consistent flamelet formulation for non-premixed combustion considering differential diffusion effects. *Combustion and Flame*, 114(1):26–40, 1998. ISSN 0010-2180. doi: [https://doi.org/10.1016/S0010-2180\(97\)00278-2](https://doi.org/10.1016/S0010-2180(97)00278-2).
- [25] T. Poinso and D. Veynante. *Theoretical and numerical combustion*. RT Edwards, Inc., 2012.
- [26] F. Proch and A. Kempf. Modeling heat loss effects in the large eddy simulation of a model gas turbine combustor with premixed flamelet generated manifolds. *Proceedings of the Combustion Institute*, 35(3):3337–3345, 2015. ISSN 1540-7489. doi: <https://doi.org/10.1016/j.proci.2014.07.036>.
- [27] W. Ramaekers. *Development of flamelet generated manifolds for partially-premixed flame simulations*. PhD thesis, Technische Universiteit Eindhoven, 2011.
- [28] N. Slavinskaya, M. Abbasi, J.-H. Starcke, A. Mirzayeva, and O. J. Haidn. *Skeletal Mechanism of the Methane Oxidation for Space Propulsion Applications*. doi: 10.2514/6.2016-4781.
- [29] G. Smith. Gri-mech 3.0 web site. http://www.me.berkeley.edu/gri_mech/, 1999.
- [30] J. A. van Oijen and L. P. H. de Goey. Modelling of premixed laminar flames using flamelet-generated manifolds. *Combustion Science and Technology*, 161(1):113–137, 2000.
- [31] J. A. van Oijen and L. P. H. de Goey. A numerical study of confined triple flames using a flamelet-generated manifold. *Combustion Theory and Modelling*, 8(1):141, jan 2004. doi: 10.1088/1364-7830/8/1/008.
- [32] H. Wu and M. Ihme. Modeling of wall heat transfer and flame/wall interaction: A flamelet model with heat-loss effects. *9th U.S. National Combustion Meeting*, 2015.

A | Appendix A

Wall	Variable	Value
NS Temperature imposed wall postip	Temperature	300 K
Pressure outlet	Pressure	20 bar
Mirror solid wall	All variables	$\nabla_n(\cdot) = 0$
CH4 inlet	Tab.3.2,3.5,3.8	Tab.3.2,3.5,3.8
O2 inlet	Tab.3.2,3.5,3.8	Tab.3.2,3.5,3.8

Table A.1: Mesh boundary conditions.

Fluid Properties		
Fluid name	:	Reactive fluid
Reference pressure	:	2001325.0 [Pa]
Reference temperature	:	498.15 [K]
Heat conduction law	:	Prandtl
Prandtl number	:	0.72
Schmidt Number	:	0.7

Figure A.1: Fluid model parameters for combustion simulations.

Fluid Properties		
Fluid name	:	AIR(Perfect)
Fluid type	:	Perfect Gas
Reference pressure	:	2001325.0 [Pa]
Reference temperature	:	300.0 [K]
Cp	:	1006.0 [J/(kg K)]
Gamma	:	1.4
Heat conduction law	:	Prandtl
Prandtl number	:	0.708
Viscosity law	:	Sutherland law
Kinematic viscosity	:	1.57e-005 [m ² /s]
At temperature	:	293.111 [K]
At density	:	1.2 [kg/m ³]
Sutherland temperature	:	110.555 [K]
Density	:	23.2095 [kg/m ³]

Figure A.2: Fluid model parameters for NoComb simulation.

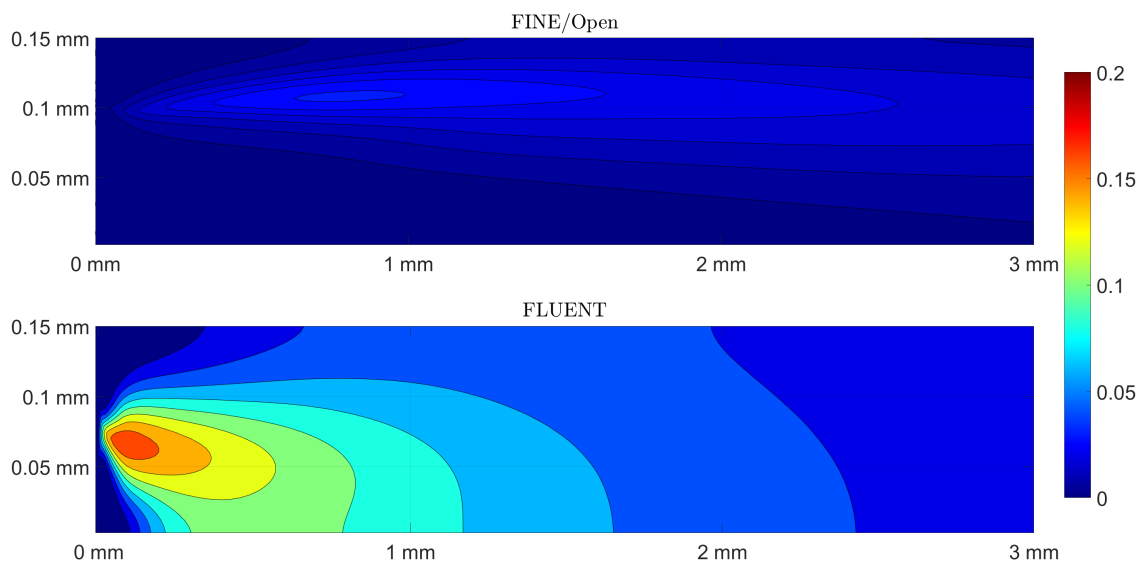


Figure A.3: FINE/Open vs FLUENT mixture fraction variance fields.

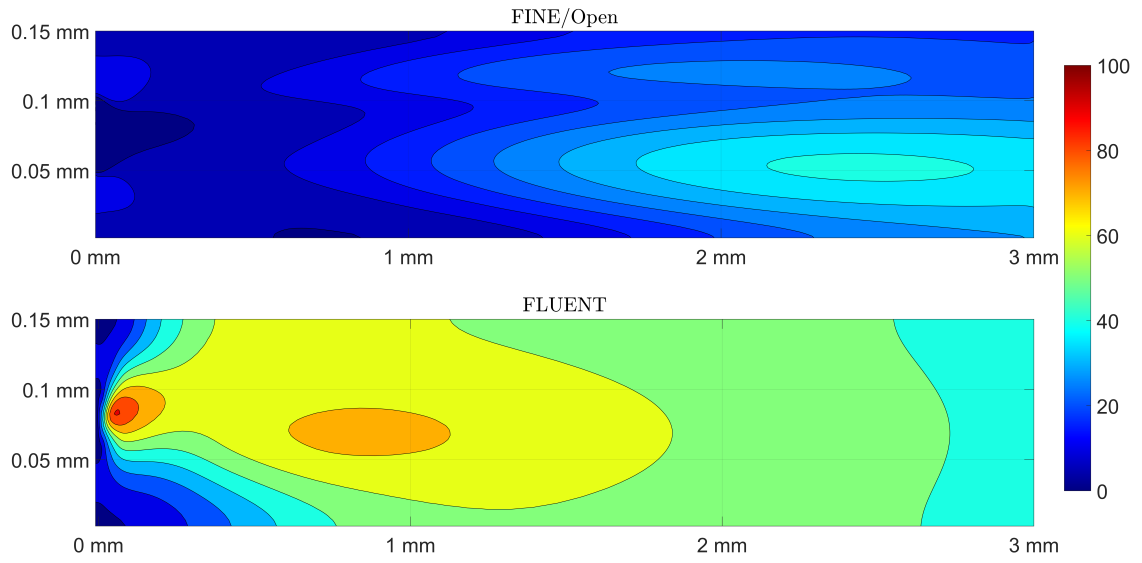


Figure A.4: FINE/Open vs FLUENT turbulent kinetic energy fields.

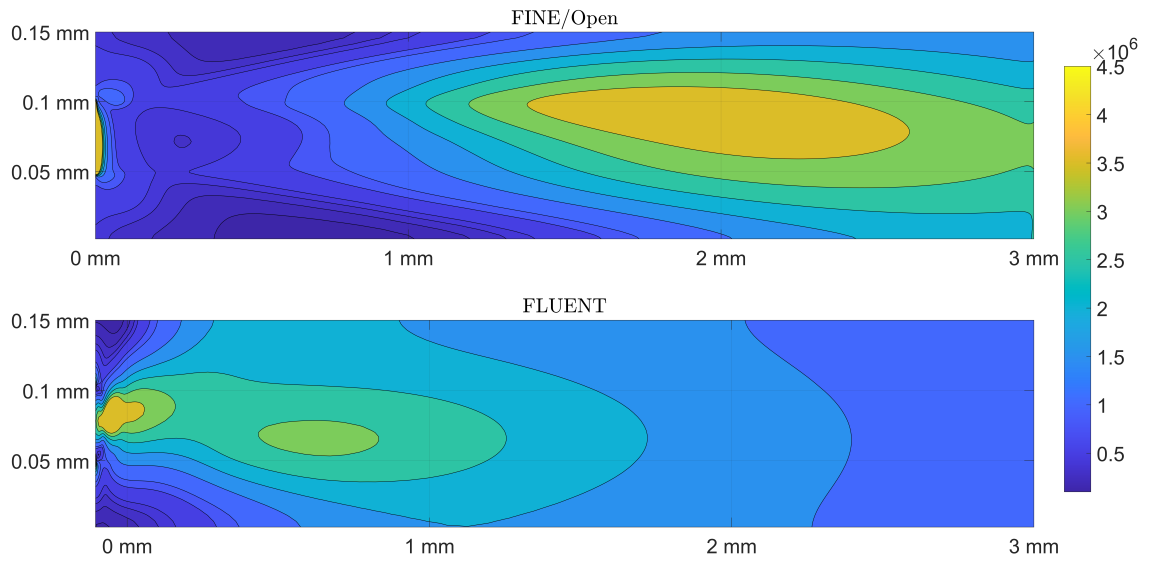


Figure A.5: FINE/Open vs FLUENT turbulent dissipation rate fields.

B | Appendix B

Viscous Model
×

Model

Inviscid
 Laminar
 Spalart-Allmaras (1 eqn)
 k-epsilon (2 eqn)
 k-omega (2 eqn)
 Transition k-k-omega (3 eqn)
 Transition SST (4 eqn)
 Reynolds Stress (5 eqn)
 Scale-Adaptive Simulation (SAS)
 Detached Eddy Simulation (DES)

k-epsilon Model

Standard
 RNG
 Realizable

Near-Wall Treatment

Standard Wall Functions
 Scalable Wall Functions
 Non-Equilibrium Wall Functions
 Enhanced Wall Treatment
 Menter-Lechner
 User-Defined Wall Functions

Enhanced Wall Treatment Options

Pressure Gradient Effects

Options

Curvature Correction
 Production Kato-Launder
 Production Limiter

Model Constants

Cmu

C1-Epsilon

C2-Epsilon

TKE Prandtl Number

TDR Prandtl Number

PDF Schmidt Number

User-Defined Functions

Turbulent Viscosity

Prandtl and Schmidt Numbers

TKE Prandtl Number

TDR Prandtl Number

Turbulent Schmidt Number

Figure B.1: Turbulence settings FLUENT.

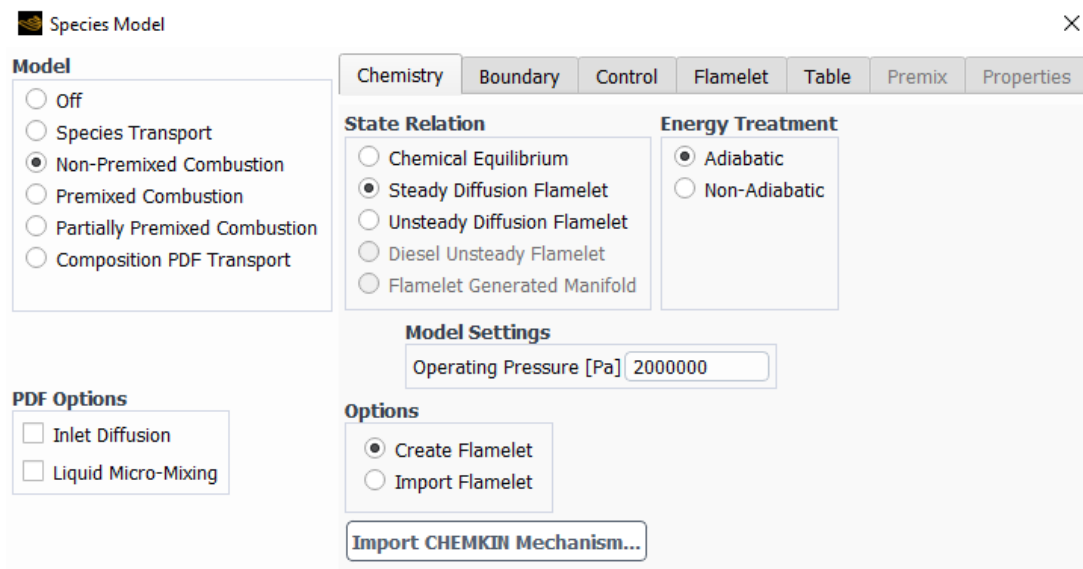


Figure B.2: Combustion settings FLUENT.

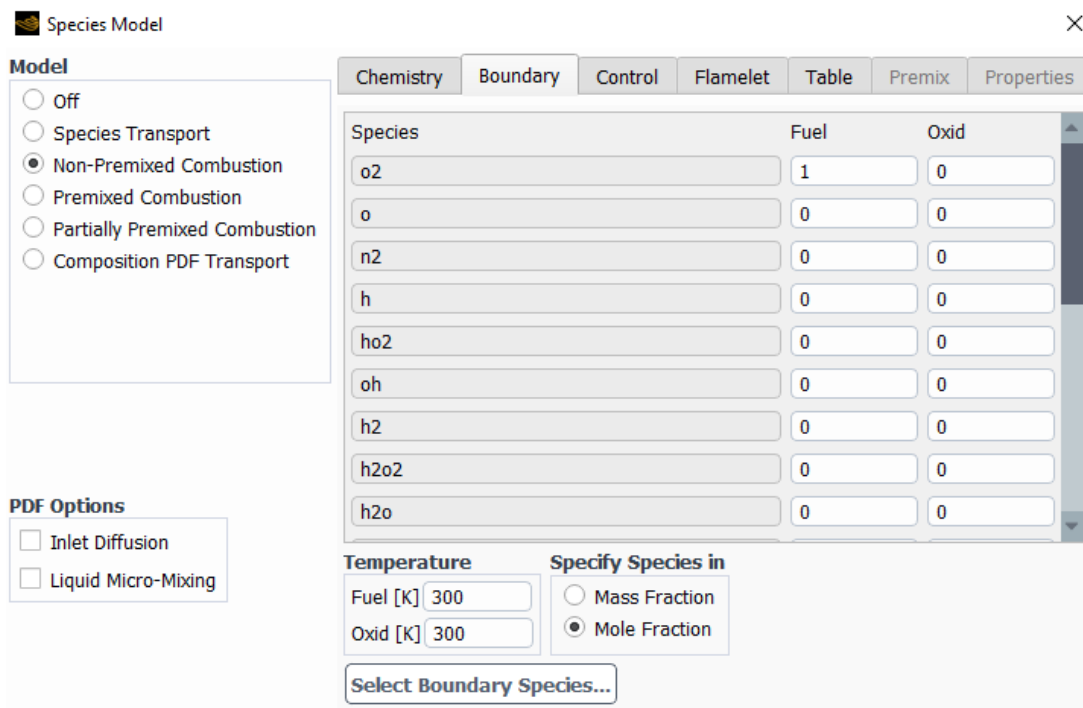



Figure B.3: Combustion settings FLUENT.

Due to an internal bug of FLUENT GUI mole fractions of fuel and oxidizer must be switched, as it is shown in figure B.3.

Solution Methods 

Pressure-Velocity Coupling

Scheme
Coupled

Flux Type
Rhie-Chow: distance based Auto Select

Spatial Discretization

Gradient
Least Squares Cell Based

Pressure
Second Order

Momentum
Second Order Upwind

Turbulent Kinetic Energy
Second Order Upwind

Turbulent Dissipation Rate
Second Order Upwind

Mean Mixture Fraction
Second Order Upwind

Mixture Fraction Variance
Second Order Upwind

Pseudo Time Method
Global Time Step

Figure B.4: Solution scheme settings FLUENT.

List of Figures

1.1	Flamelet approach for non-premixed turbulent flames [25].	13
1.2	Counter-flow diffusion flame configuration.	14
1.3	Graphical description of the PDF [3].	19
2.1	Flamelet model solver implementation [25].	25
2.2	Flamelet model implementation steps [25].	26
2.3	Example of steering file	34
3.1	Fuel Boundary conditions for CombProfile simulation.	36
3.2	Oxidizer Boundary conditions for CombProfile simulation.	36
3.3	Mesh boundary conditions.	37
4.1	FINE/Open vs FLUENT temperature isolines.	46
4.2	FINE/Open vs FLUENT temperature fields.	47
4.3	FINE/Open vs FLUENT mixture fraction fields.	48
4.4	FINE/Open vs FLUENT effective diffusivity coefficient fields.	49
4.5	Temperature laminar Flamelet library at $P = 2e6 Pa$	51
4.6	Species mass fraction laminar Flamelet library at $P = 2e6 Pa$	51
4.7	Flamelet vertical profiles for different axial positions.	52
4.8	Flamelet mass fractions profiles for different axial positions.	54
4.9	Flamelet temperature field.	55
4.10	Flamelet mass fraction fields.	56
4.11	Flamelet mass fraction fields.	57
4.12	FGM temperature table.	58
4.13	FGM vertical profiles for different axial positions.	59
4.14	FGM mass fractions profiles for different axial positions.	60
4.15	FGM temperature field.	61
4.16	FGM mass fraction fields.	62
4.17	FGM mass fraction fields.	63
4.18	Hybrid temperature field.	64
4.19	Hybrid mass fraction fields.	65

4.20 Hybrid mass fraction fields.	66
A.1 Fluid model parameters for combustion simulations.	73
A.2 Fluid model parameters for NoComb simulation.	74
A.3 FINE/Open vs FLUENT mixture fraction variance fields.	74
A.4 FINE/Open vs FLUENT turbulent kinetic energy fields.	75
A.5 FINE/Open vs FLUENT turbulent dissipation rate fields.	75
B.1 Turbulence settings FLUENT.	77
B.2 Combustion settings FLUENT.	78
B.3 Combustion settings FLUENT.	78
B.4 Solution scheme settings FLUENT.	79

List of Tables

3.1	Initial solution NoComb computation.	39
3.2	Inlet Boundary Conditions Flamelet case.	40
3.3	General and Numerical parameters Flamelet case.	40
3.4	Combustion table parameters Flamelet case.	41
3.5	Inlet Boundary Conditions FGM case.	42
3.6	General and Numerical parameters FGM case.	42
3.7	Combustion table parameters FGM case.	42
3.8	Inlet Boundary Conditions Hybrid BML/Flamelet case.	43
3.9	General and Numerical parameters Hybrid case.	44
3.10	Combustion table parameters Hybrid case.	44
4.1	Maximum profile values for the Flamelet case.	52
4.2	Maximum profile values for the FGM case.	59
A.1	Mesh boundary conditions.	73

Acknowledgements

First of all, my greatest thanks go to my parents who gave me the opportunity to take this path in the best possible conditions. The thesis is dedicated to them who always believed in me more than I did and who always supported me in the most difficult moments during this journey.

A special thanks goes to Prof. Maggi that gave me the opportunity to make an experience abroad in which I developed this thesis. I also thank Andrej Sternin and Matthias Schramm for the support and readiness they have had to me during the six months spent at TUM.

Finally, I thank all my friends who have been close to me over the years and with whom I have shared my difficulties. Thanks to you, I have been able to get through the hardest moments.

